Stride parameter estimation by fusing Radio and Inertial sensing data

Uthvag Sakthivelu
Biomedical Signals and Systems
University of Twente
Enschede, Netherlands
u.sakthivelu@student.utwente.nl

Abstract*—The quantitative analysis of human gait is crucial for medical rehabilitation, allowing the diagnosis and remediation of existing or potential injuries and diseases. Contemporary clinical grade gait analysis is predominantly based in laboratory environments, thereby increasing the setup and operational costs while decreasing the range of analyzable motions. In this work, a completely on-body minimal sensing setup in tandem with Extended Kalman Filter (EKF) comprising Ultra-wide band (UWB) sensors and Inertial Measurement Units (IMU) is developed for the analysis of lower limb stride parameters. This paper also delves into the characterization of the UWB sensors at sub-50 cm distances and the incorporation of the angle of arrival (AoA) for gait analysis. Among 5 different filter configurations tested on a dataset comprising 250 steps from 4 subjects, the best performing model based on the calculated errors, resulted in the estimation of stride parameters with the following errors: step length 2.9$\pm$2%, step width 2.9$\pm$2.3%, stride length- right foot 3.5$\pm$3% stride length- left foot 4.1$\pm$3.1%, an overall RMSE (error in the estimated distance between the feet throughout the trial) 2.9$\pm$2.2% and a Pearson correlation coefficient of 0.89. A longer trial with a curved path (1 subject and 120 steps) of approx 8 m resulted in results similar to the shorter walk. Overall, for both trials, the stride parameters are estimated with an average normalized RMSE of 3.1%. In addition, the incorporation of UWB based ranging sensors' model resulted in a minimization of the drift observed in the range estimates. The inclusion of AoA measurements, resulted in a minor improvement in the stride parameter estimation.

***Index Terms*—Ultra-Wide Band, IMU, Gait analysis, Sensor fusion**

I. Introduction

A. The need for portable gait analysis

Human gait is defined as the range of cyclical motions a human goes through while locomoting. Human gait, being intrinsically linked with a majority of human activities (Eg: walking, sports, travel etc.), is a major factor in determining the overall health and quality of life of the individual. Any detriment/alteration in the gait can have far-reaching repercussions[1] which would require prolonged rehabilitative measures or corrective surgical treatments. The analysis of the gait would be a proactive measure in preventing cumulative damage caused by bad gait, and it also presents an opportunity to evaluate the current health of the limbs. However, the average human being has minimal access to personnel or devices which would analyze their gait due to the cost, size or complexity of such avenues. A solution would be to use a low-cost, minimal sensing on-body gait analysis system, which can not only make gait analysis accessible to the general population, but also be able to quantify it. A quantitative approach to gait analysis is required since it would enable the detection and assessment of minor, seemingly innocuous changes to the gait. For very similar reasons, the quantitative analysis of human gait is gaining prevalence rapidly, especially in the field of healthcare. This increase can be attributed to the improvements in the quality and accuracy of injury diagnostics and rehabilitation routines which follow the quantitative assessment of such conditions[2]. Current quantitative gait analysis systems are usually the traditional clinical grade gait analysis setups which are constrained to a controlled laboratory environment. In addition, the clinical systems involve devices which are usually costly (Ex: Xsens Link), non-portable (Ex: Vicon), complex and would need multiple sensors/subsystems to operate[3]. A portable sensor setup for gait analysis eliminates the need for such installations by replacing it with on-body sensors such as IMUs, Electromyogram [4], force sensors [5] or thin fold-able platforms [6][7] depending on the bio-mechanical parameter being investigated. This paper focuses on walking and its related parameters.

B. Clinical relevance of accurate human stride analysis

Walking can be assessed via the quantification and evaluation of its stride parameters. Among the walking parameters, the step length and step width are used as metrics for assessing new algorithms due to the ease in extraction as well as its medical relevance. The stride parameters have been linked with the quality of life as well as the mortality of the patients and is of major concern in geriatric patients[8][1]. Parameters like stride width and stride length are vital as they are indicators of a person's fall risk[9][10].

A more in depth example would be the significance of the aforementioned stride parameters for the assessment of Parkinsons Disease(PD) and its treatments[11]. For healthy subjects of height 175 cm, the stride length and step width are in the order of 70-90 cm and 10-15 cm respectively [12]. Stride length estimation with just the zero velocity update (ZUPT), using foot and shank mounted IMUs exhibited an accuracy of approx. 5.9% and 9.4% respectively, translating to around 7

cm for the stride length[13]. In both these cases, a variation in the estimated stride length would not impact the overall assessment much. However, in case of patients suffering from Parkinson's Disease, a major type of gait exhibited is festination (shuffling). Traditionally, the analysis of this motion is qualitatively assessed via various rating scales, commonly using the Unified Parkinson's Disease Rating (UPDRS -III) [14]. According to the UPDRS Lower Extremity ratings, the patients are classified into three categories - low, middle and high depending on the exhibited bradykinesia, rigidity of neck and lower extremities, tremor in the lower extremities, agility of the legs, posture, gait, overall postural stability and the stability while rising from a chair. While shuffling, Parkinson patients move their feet in small steps, characterized by low foot clearance and smaller stride lengths. These steps exhibit a stride length of 1.2 m,1.1 m and 1.05 m [15] for patients classified under the low, medium and high UPDRS categories respectively. In addition, the foot clearance for non-Parkinsonian patients was found to be around 14.8cms while for PD patients, it was 10.3 cm [15].

Empirical evaluation of Parkinsons would benefit from a setup which can distinguish different stages based on the stride and step parameters.

C. Portable gait analysis- sensor options

The portable sensing options commercially available include sensors such as IMUs, EMG sensors, force sensors, LIDAR, ultrasound and RF sensors. For stride parameter estimation, EMG and force sensors have a disadvantage of providing indirect parameters such as force, flexion and impact which have to be processed via a complex human bio-mechanical model which relates the extracted variables to the position and angles[7]. The conversion of indirectly related variables like force into position exacerbates the underlying sensor and model inaccuracies and compounds the errors further. IMUs, on the other hand, provide the acceleration from its accelerometers and the angular velocity from its gyroscopes, and both quantities can be related to gait parameters such as joint angles and position using a simpler, and therefore less error-prone models [16]. Sensing methodologies such as LIDAR and radar, while immune to drift, are influenced by the environmental conditions present Among the options presented, the IMU has the most potential for providing a comprehensive spatio-temporal analysis of the human gait due to the size and portability of the device and robustness of its measurements [17] [16].

A recent development due to advances in the miniaturization and the development of smart devices is the utilization of radio sensors for measurement of distances. The current state-of-the-art radio based sensors are very small and low power making them a viable option for portable setups.

From the analysis of the available sensing options, we can conclude that the IMU and radio based sensors have a large potential for portable gait analysis systems.

D. Issues using standalone IMUs or Radio sensors for gait analysis

The standalone utilization of IMU's to find the position by means of integrating the acceleration is prone to error accumulation over time, and despite methods for minimizing the integration error such as the zero velocity update algorithm (ZUPT) [18], the problem still persists. Due to the position of the IMU being calculated by means of strap down integration, involving the calculation of the position via the accelerometer while using the orientation estimates from the gyroscopes as well. Since, the calculation of the free acceleration (acceleration sans the gravity component) and its frame is a function of the orientation, any errors in the orientation would magnify the position errors. In addition, apart from the drift in position, there is an additional drift in orientation. The source of drift in orientation is twofold - The integration of the angular velocity for the orientation leads to a drift, and in the second case, if a magnetometer is included in the IMU, any magnetic field disturbances would result in a corresponding variation as well. Since the stride parameter estimation requires the IMUs on each foot to compute their orientation w.r.t to the global frame, a drift in the orientation estimates of each IMU would aggregate the error in the computed stride parameters. If the frame of each IMU differs, it would be starkly reflected in the stride width and step length parameters, which depend on the differences in the X, Y and Z position of each IMU in the global frame. Any difference in the rotation estimates (sensor to global frame) would skew the global X, Y and Z coordinates, leading to errors.

The drift issue with IMU's has been analyzed in literature quite extensively and to rectify it, there have been multiple attempts at rectification by fusion of the IMU data with data from other body mounted sensors to provide better accuracies in their estimations. The main requirement for the add-on sensors is the capability to provide the parameters (directly or its derivative) needed to estimate the stride based gait parameters, namely - position and its derivatives. The IMU, despite being precise over short durations of time, cannot be used for the long term gait tracking and monitoring without complicated constraints/models (Ex: Xsens MVN's Biomechanical constraints).

The radio based sensors, on the contrary, have better long term performance but a poor accuracy when compared to the IMU's. The improved long term performance is attributed to the fact that most radio based sensors are capable of measuring the distance directly instead of deriving it from related quantities like IMU's. These sensors, despite measuring the distance as a direct quantity, provide an accuracy in the order of meters, and would be unsuitable for applications such as the ones elaborated above. Thus, among the on-body sensor options, the IMU's are capable of providing the precision required for stride parameter estimation.

A recent development in the field of radio based ranging (the act of gauging the distance between a base station and a transceiver) is the emergence of UWB based ranging sensors.

The UWB technologies spectrum occupies the frequencies from 3.1GHz to 10.6GHz, split into fourteen 500MHz bands. The large bandwidth, along with the regulated transmission power, enables the UWB technology's coexistence with other wireless devices with minimal interference.

Contemporary commercial devices utilizing the UWB promise better localization due to the innate properties of their bandwidth and method of transmission (sharp pulses). The availability of a large bandwidth is conducive for the transmission of short and sharp pulses. UWB technology's precision is provided by the transmission of short sub-nanosecond pulses, enabling a precise estimation of the time delay. A better time delay resolution corresponds to an increase in the time of flight's (TOF) estimation, which again corresponds to better distance calculation. This work uses DecaWave's off the shelf UWB kits to provide the ranging estimates. The kit specifies a ranging accuracy within 10 cm, while offering a relatively higher immunity to noise sources like multi-path and cross talk.

The short term precision of the IMU's and the relative imperviousness of the radio based ranging devices to drift complement each other, and would be ideal for fusion using sensor fusion techniques.

E. Contemporary work

Conventional sensor fusion approaches towards gait analysis involved the fusion of the inbuilt gyroscope and the accelerometer, which has been investigated extensively in literature, with stride length estimation accuracy of 2.9% [19].

To improve the accuracy further, external ranging sources were incorporated. The distance measurements provided by the ranging sources (ultrasound[20], radio waves[21][22], LIDAR, Bluetooth, etc.) were fused with the position estimates from the IMU resulting in better accuracy.

The fusion of radio information acquired via discreet and a phone's inbuilt Wi-Fi antennas and the IMUs provided a stride length accuracy of 3% [21]. This method, rather than exploiting the ranging capabilities of Wi-Fi, uses the Channel State Information (CSI), which enables the utilization of super-resolution methods to detect the distance traversed[23]. Although this method promises good accuracies, it is not viable since it currently uses a fixed base station for operation. This method has potential to be used for a portable system if the fixed base station is replaced with a suitable body mounted one if possible.

The most accurate work uncovered while surveying, for the fusion of IMU with another wearable sensor's data for stride length estimation, is the utilization of ultrasound sensors. The accuracy mentioned was 1.7 cm for the stride length and 1.2 cm for the stride width [20]. The main evident advantage of UWB over ultrasound is the relative imperviousness to environmental fluctuations and noise. The transmission speed of sound is dependent on atmospheric factors such as weather, temperature, humidity etc. A rule of thumb for sound's transmissions speed's variation in air, is a 2% variation with every 10° rise in temperature. In contrast, electromagnetic waves are unperturbed by any variations in air. In addition, ultrasound has a penchant for diffraction and attenuation when faced with Non-Line of Sight (NLOS) conditions, leading to further inaccuracies and error sources. Radio based sensors, while still sensitive to line of sight (LOS) conditions, perform relatively better in NLOS conditions than ultrasound in the case of foot mounted sensors.

From our previous section, it is apparent that the fusion of UWB based ranging devices and IMU's would provide optimal results for the estimation of stride parameters. Although UWB sensors and IMU's have been fused a priori for mechatronic devices[22], most forays in gait analysis used IMU's for analysis of the motion and used UWB sensors as a localization mechanism to find the position of the person in the prescribed environment. The byproduct of such methods would be the estimation of stride length, which aids in pedestrian dead reckoning (PDR). In addition, most such methods used the fixed base station approach for the incorporation of the UWB sensor[24][25][26][27][28]. The most recent forays on UWB and IMU sensor fusion using an on-body setup for gait analysis involved the usage of the range data exclusively [29]. The incorporation of UWB based ranging and the IMU based localization in [29] did not avail any sensor fusion techniques, which are traditionally used to combine sensor measurements.

In addition to the incorporation of UWB ranging estimates, there is a significant potential for the incorporation of the angle of arrival (AoA) estimates of the UWB. The AoA is the angle at which a signal from the transmitter impinges on the receiver. In a two-dimensional Cartesian frame with a transceiver at a point A, and a transceiver at point B of a right angle triangles hypotenuse, the range measured would be the hypotenuse, whereas the angle of arrival would be the angle between the hypotenuse and side with the receiver (figure 41).

From the survey of the state-of-the-art technologies for on-body stride parameter estimation, the potential sources of improvement identified are (to the best of the authors' knowledge)

- Development of a portable and completely body mounted device which is relatively immune to environmental factors like temperature, magnetic field etc.
- Characterization and utilization of UWB based devices for sub 50 cm distances.
- Incorporation of UWB sensors in the lower limb for gait analysis using sensor fusion techniques.
- Utilization of angle of arrival (AoA) in lower limb gait analysis.
- Real-time gait analysis.(semi-realtime analysis was performed in[19])

F. Our contribution(s)

Our main contribution and goal of this paper would be the development of fusion algorithms incorporating IMUs and UWB based ranging sensors and an on-body minimal sensing system for gait analysis. The project encompasses the first four identified gaps in the contemporary work done.

Of the abovementioned contributions, the inclusion of AoA estimates is in a filter (alongside the range measurements) has not been previously for gait analysis. The exploration of localization enhancement using the AoA would ascertain if AoA incorporation is beneficial for the accuracy of the stride parameters being investigated. We hypothesize that due to the narrowing down of the uncertainty from a 3D sphere in case of using ranging to a 3D wedge in case of AoA + ranging measurements, there would be an increase in the stride parameters being investigated (depicted in figure 2 and figure 3).

The work carried out is focused on translating the fusion of UWB sensor's and the IMU's data from mechatronic and fixed base station based applications to on-body gait analysis. Due to the organic nature of human gait, it is (expected) harder to predict than movements of mechatronic devices, with variables such as duck feet, swaggered gait and other non-idealities in the field. In addition, apart from the sensor fusion aspect, the project also involves the development of the on-body hardware for the gait analysis system.

To quantify the effectiveness of our system in analyzing gait, our work investigates parameters pertinent for the estimation of the relative foot position, namely - the walking stride length, step width and step length. In addition, to investigate the drift compensation aspect of the system, we include 2 additional parameters - the overall RMSE and the pearson correlation. This leads us to the research objective which is the development of the sensor fusion algorithms and the hardware for a portable stride parameter estimation system using IMUs and UWB based ranging sensors. This can be further broken down into two parts :

1) Design and evaluation of a sensor fusion algorithm incorporating UWB sensors ranging data to estimate the stride parameters.
2) Design and evaluation of a sensor fusion algorithm incorporating UWB sensors ranging and AoA data to estimate the stride parameters.

II. Methodology

The methodology section describes the design specifications and procedures carried out in this work. The section is split up and grouped into subsections which describe the algorithm, the experimental setup and validation protocols used.

Methodology- Sensor models and characterization

In this section, the groundwork involving sensor characterization and process modelling required for devising a filter for the fusion of UWB data and IMU is sketched. In order to incorporate the UWB sensors and IMUs, a thorough evaluation of the sensors and their performance is required in-order to model the sensor's behaviour, and incorporate them into our system. The sensors to be fused are the Xsens DOT IMUs (Xsens B.V, Enschede, Netherlands) and the DecaWave UWB PDOA (Decawave Inc. Dublin, Ireland.) beta kit. The testing and modeling of the sensors is expounded on in the following section.

A. Xsens DOT

The Xsens DOT is an IMU sensor consisting of a tri-axial accelerometer and a tri-axial gyroscope sampled at 60Hz. The sensor models for the accelerometer and the gyroscope are expounded on in the following sections.

1) Accelerometer model: The sensor's accelerometer output is modelled as the acceleration experienced by the sensor including gravity and an additive gaussian noise [30]. The sensor's acceleration measured is given by:

$$y^s_{acc} = a^s - g^s + w_{acc} \tag{1}$$

where,

y^s_{acc} - accelerometer reading in the sensor frame.
a^s - acceleration of the sensor (sans the gravitational component).
w_{acc} - Gaussian noise.

2) Gyroscope model: The gyroscope is modelled as the sum of the angular velocity in the sensor frame, a slowly varying gyroscope bias, and some Gaussian noise [30].

$$y^s_{gyr} = \omega^s + b^s + w_g \tag{2}$$

where,

y^s_g - gyroscope reading in the sensor frame.
ω^s - angular velocity in the sensor frame.
b^s - gyroscope bias in the sensor frame.
w_g - Gaussian noise.

B. UWB kit

The UWB kit consists of a DecaWave Phase difference of Arrival (PDOA) beta kit, which consists of a base station analogue called the node and another peripheral transceiver called the tag. The devices operate at a central frequency of 6.5GHz with a bandwidth of 500MHz [31].

The UWB kit provides two types of data pertinent to localisation:

1) Range data - The distance between the node and the tag.
2) Angle of Arrival (AoA) - The angle of incidence of the signal impinging from the tag onto the node. Details on how it is acquired can be found in the Appendix VI -Angle of arrival and Localization.

A short description of the two types of data and their models is mentioned in the subsequent sections.

The node serves as the base station from which the results from the distance and AoA measurement operations are transmitted. The node initializes the polling or the transmission to the tag, and the tag, upon reception, sends a message to the node in return. The data and the signal being transmitted are used for the ranging and AoA modes.

Apart from the aforementioned data, the UWB sensors also can provide/ are equipped with:

1) The tag has an integrated three-dimensional accelerometer and the data acquired is processed internally in the node using a Kalman filter.
2) The Channel Impulse response(CIR) of the channels between the node and the tag. The CIR is an indicator for the channel's health and quality of transmissions and is used purely for diagnostic purposes in our setup.
3) The Received Signal Strength (RSS) of the signal emitted by the tag.

The node and the tag are mounted on the right and left feet respectively, along the direction in which the feet point7. The details are provided in the experimental setup section of the methodology.

1) Ranging data : The ranging data is the distance between the tag and the node, which in our case translates to the distance between the feet. In terms of position, it is the norm of the difference in the position between the feet in three dimensions.

In the paper, the terms ranging and distance between the node and the tag are used interchangeably, since the distance finding operation is called ranging.

The method for ranging is an asymmetric Two Way Ranging (TWR) which involves the transmission of data with a time stamp of transmission from the node to the tag initially, followed by a reply from the tag with the time stamps for the tags reception and transmission allowing us to calculate the time of flight (tof) [32]. The asymmetric TWR implemented in the DecaWave kit dampens the influence of the clock drift between two devices [33][34], and hence we are ignoring any such errors in our model. A detailed description on TWR and other ranging methods can be found in the cited DecaWave manual.

The ranging model of the UWB kit can be formulated as:

$$r = c * t_{doa} - rb + w_r \tag{3}$$

where,

r - the range (distance) measured by the UWB kit.
c - speed of light in air.
t_{doa} - time of flight (time difference of arrival).
rb - range bias.
wr - gaussian noise (assumption). [35]

For ranging, according to DecaWaves manual, the device is capable of accuracies in the order of 10 cm.

Although DecaWave provides a detailed performance report on the UWB kit [33][36], it lacks the documentation and evaluation of the performance being conducted at distances less than 50 cm (Which is the range within which most of the stride parameters fall).In addition, most of the UWB systems designed and the existing implementations and literature usually operate at distances larger than 1 m. Hence, we will be assessing and characterizing the UWB kit at distances less than 50 cm as a part of this report (Appendix VII - Bias evaluation and compensation in the UWB kit).

Specifics of the hardware / Embedded software / data parsing involved is mentioned in the Appendix section (Appendix II- DecaWave PDOA kit repurposing).

2) AoA data: Angle of arrival (AoA) is the angle of incidence of a transmitted signal. The AoA is measured with respect to the plane of the receiver. In our case, since the node and tag are mounted on the feet, the AoA provides information relevant to the relative orientation of the feet in the nodes azimuthal plane. We postulate that incorporation of AoA would enable us to localize the position of the feet better than using just the ranging data. Due to the array configuration in the node (linear array), the AoA measured is in 2D, with the 2D plane being the plane of the node, which in our case is the orientation of the foot.

The node module consists of two DW1000 chips connected to two UWB antennae with a spacing of 2.08 cm [36]. The presence of two antennae separated by a distance smaller than $\lambda/2$ (half the wavelength) enables the measurement of the phase difference between the received signals. Due to the separation, it is expected that the signal from the tag is received by the two antennae at different phases. This difference in phase can be utilized to find the path difference of signals, which in turn can be used to estimate the AoA. An elaboration on the AoA concept is provided in the appendix (Appendix VI -Angle of Arrival and Localization).

The DecaWave kit provides us with the phase difference of arrival, from which the AoA is calculated by the following formula[37][38] (derived in Appendix VI, eq 85):

$$AoA = sin^{-1}((pdoa + pb + w_p) * \frac{c * pi}{2 * 180 * f * dist}) \tag{4}$$

where,

AoA - Angle of arrival (radians).
pdoa - phase difference of arrival truncated [-180 to +180] (degree).
pb - is the bias in the phase measurements.
w_p - noise in phase measurements (considered to be gaussian).
c - speed of light.
f - central frequency (6.5GHz).
dist - distance between the antenna elements (m).

The error in the phase measurements (azimuthal) as stated by DecaWaves manual is 5° [36]. Nuances regarding the hardware / Embedded software/ data parsing involved is mentioned in the Appendix section (Appendix VI -Angle of Arrival and Localization).

3) Comparison of the AoA mode and ranging mode : This section briefs on providing an intuition behind the utilization of the AoA data and the range data. Another 2D representation of the uncertainties are provided in Appendix IX as figures 41 and 42 for the sake of clarity and cross-referring.

As shown and described in the figure 2, the distance measured being the norm of the 3D position differences would

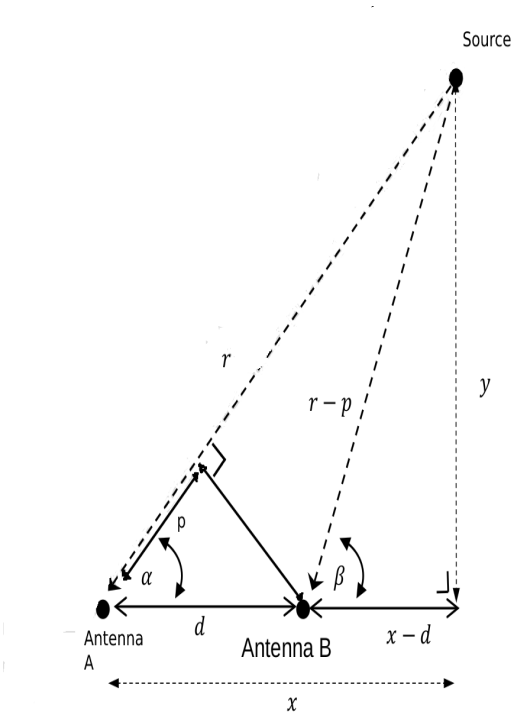

Fig. 1. The Angle of Arrival based decomposition of the range into X and Y coordinates from the DecaWave manual [36]. The equation and the concepts are detailed in Appendix VI

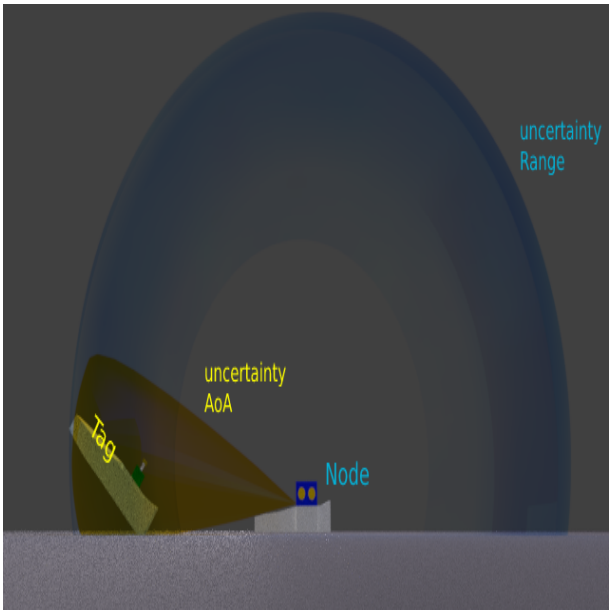

Fig. 2. Side view/cross-section: A 3D representation of measured range uncertainty (transparent blue annular sphere) and the AoA uncertainty (transparent yellow cone with a curved base) from the side. The combination of the AoA and range measurements is the volume where both uncertainties intersect.

result in an uncertainty being modelled as an annular sphere, with the thickness of the sphere representing the noise in the measurements and the sphere itself indicating that the position of the left foot with the tag could occupy any point in the annular sphere. This method when combined with the IMUs would provide improved measurements due to the overall uncertainty being curtailed to the volumes where the IMU and UWB range uncertainties intersect, leading to a reduction in the drift.

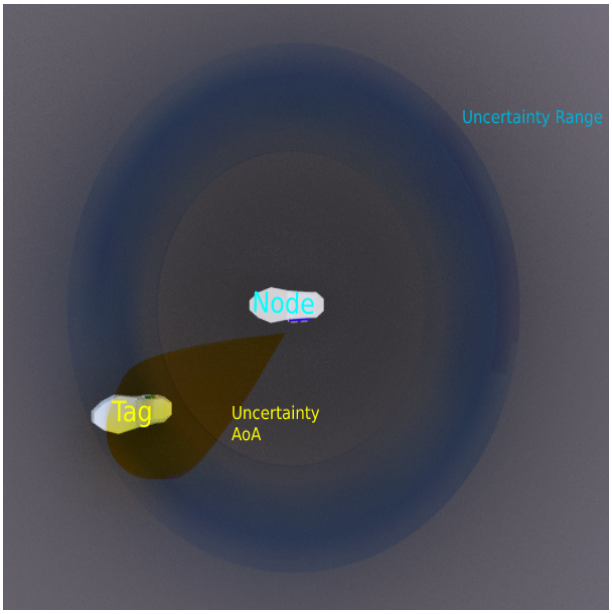

Fig. 3. Top view/cross-section: A 3D representation of measured range uncertainty (transparent blue annular sphere) and the AoA uncertainty (transparent yellow wedge with a curved base) from the top. A combination of the AoA and angle would result in the localization of the feet in a two dimensional plane, while the 3rd dimension's uncertainty would extend to a distance depicted by the height of the cone.

In cases where angle of arrival is used alongside the range measurement, the previously mentioned uncertainty sphere for the range is now restricted by the AoA. This results in a wedge shaped uncertainty in the azimuthal plane, and a circular uncertainty pertaining to the elevation (Z axis) combining to produce a curved cylinder with tapered ends. Although ideally, since the elevation angle is unknown, the uncertainty in the elevation angle should extend from +90° to -90° in the elevation. Due to the performance of the DecaWave kit at finding the azimuthal AoA at different elevation angles, the uncertainty in the elevation AoA is restrained to a narrower range (+20° to -20°). The performance of the azimuthal AoA with a variation in the elevation angle is discussed in later sections. The difference in the uncertainty of the range measurements and the range with AoA measurements is expected to increase the overall accuracy in the estimation of the position of the feet and minimize the drift from the IMU estimates.

C. Biases and errors in the UWB kit

The data from the UWB kit, namely the AoA and the range data, cannot be directly used in the filter due to the biases and

errors in the system. The error in the measurements are due to various sources, from physics based constraints to the errors which occur due to a persons gait. The results acquired by the fusion of this data by the filters mentioned in the sensor fusion section resulted in subpar results. Inorder to efficiently utilize the results from the UWB kit, the characterization and modelling of the underlying processes were performed. More details on this can be found in the Appendix section (Appendix VII - Bias evaluation and compensation). In brief, an overview of the errors are listed

- Range bias error - An error in the range measurements which is compensated using an infilter model (a state variable) and an external model.
- AoA error - Errors in the AoA measurements due to the human gait, due to the AoA estimation algorithm used, and due to physics based constraints. These errors are solved by thresholding and ignoring the erroneous AoA values or taking the errors into account in the filter.
- AoA bias - The AoA measured by the UWB kit is in 2D. In 3D scenarios, as experienced by the tag and node, there is an additional elevation angle present. This elevation angle causes a bias in the measured AoA. This is tackled in two ways: compensating the bias using the state variables to account for it, or by using thresholds to ignore the erroneous values.

METHODOLOGIES -SENSOR FUSION

The Kalman Filter (KF) [39] is an estimation technique which is used to fuse the measurements of multiple sensors for estimation of related variables. This is performed via the utilization of the uncertainties in the individual sensor's measurements and the model. In the typical Kalman filter, the probabilities are assumed to be Gaussian [40].

Figure:4 depicts the rudimentary structure of the EKF outlining the general steps involved in the fusion of the UWB and IMU data. This is similar to the structure of the EKF in [20].

The Extended Kalman Filter (EKF)[41] is, as suggested by the name, extends the KF to non-linear systems by Taylor series' linearization [23]. In our case, we intend to fuse the ranging updates provided by the DecaWave UWB kit, with the position updates provided by the IMUs from the accelerometer data. These will be fused to determine a set of fused state variables.

An Error State EKF (ES-EKF) has been used to propagate the position of both feet[42][43][20]. The error states in our case are the Orientation error and the Gyroscope bias error[44][45][46][45]. The rotation in the sensor frame and gyroscope measurements compensated for the bias are propagated externally and are corrected during the measurement update.

Incorporation of the UWB data into the filter is via the measurement update stage. The measured range from the UWB sensors is used to update the position of the left and right feet. The AoA is used to update the position using the angle calculated from the position of the feet in the sensors frame.

To operate on a common time frame, the sampling frequency at which the filter operates is 240Hz and all the sensors measurements are coordinated with respect to the common time frame. The variables mentioned in this section, unless explicitly stated so otherwise, are in the global frame.
Notations used in the filter :

- Frames of references: The frame of reference for all state variables, unless explicitly stated so otherwise, are in the global frame. In case a particular frame is referred to, it is mentioned as a superscript. Ex a^s represents the sensor frame, a^g represents the global frame.
- Rotations:The rotations and its propagation is described for both quaternion and rotation matrices. The rotation from one frame to the other is described by the following notation:$R_{destinationframe,currentframe}$. For example R_{gs} encodes a rotation from the sensor frame to the global frame.
- Axial subscripts: For three-dimensional operations, the conventional x, y, z notation is followed. The axis in which a variable operates is depicted in the subscript Ex: a^g_x depicts the variable 'a' in the x-axis and in the global frame.
- Foot subscripts: The involvement of both the feet and their relative positions necessitates the utilization of subscripts to distinguish between them. In cases with multiple subscripts, the first subscript depicts the foot. Example: a^g_{lx} describes the variable 'a' of the left foot in the global x-axis.
- Estimates: Estimates are denoted by the hat operator $\widehat{a}$.
- Priors: The priors (estimates before being corrected by the measurement update) is depicted by a overhead minus sign a^-.
- Multiplication: a * operation indicates conventional multiplication, whereas a $\times$ operator indicates matrix multiplication.

The state variables are

1) Position -left foot x,y,z (p_{lx},p_{ly},p_{lz}).
2) Position -right foot x,y,z (p_{rx},p_{ry},p_{rz}).
3) Velocity -left foot x,y,z (v_{lx},v_{ly},v_{lz}).
4) Velocity -right foot x,y,z (v_{rx},v_{ry},v_{rz}).
5) Orientation error -left foot x,y,z (θ_{lx},θ_{ly},θ_{lz}).
6) Orientation error -right foot x,y,z (θ_{rx},θ_{ry},θ_{rz}).
7) Gyroscope bias error -left foot x,y,z (be_{lx},be_{ly},be_{lz}).
8) Gyroscope bias error -right foot x,y,z (be_{rx},be_{ry},be_{rz}).
9) Range bias (rb).

Condensing the axial subscripts, the state vector x therefore is

$$x = [p_l, p_r, v_l, v_r, \theta_l, \theta_r, be_l, be_r, rb].T \tag{5}$$

The input variables are:

1) Acceleration -left foot x,y,z (a_{lx},a_{ly},a_{lz}).
2) Acceleration -right foot x,y,z (a_{rx},a_{ry},a_{rz}).

The measurement updates are:

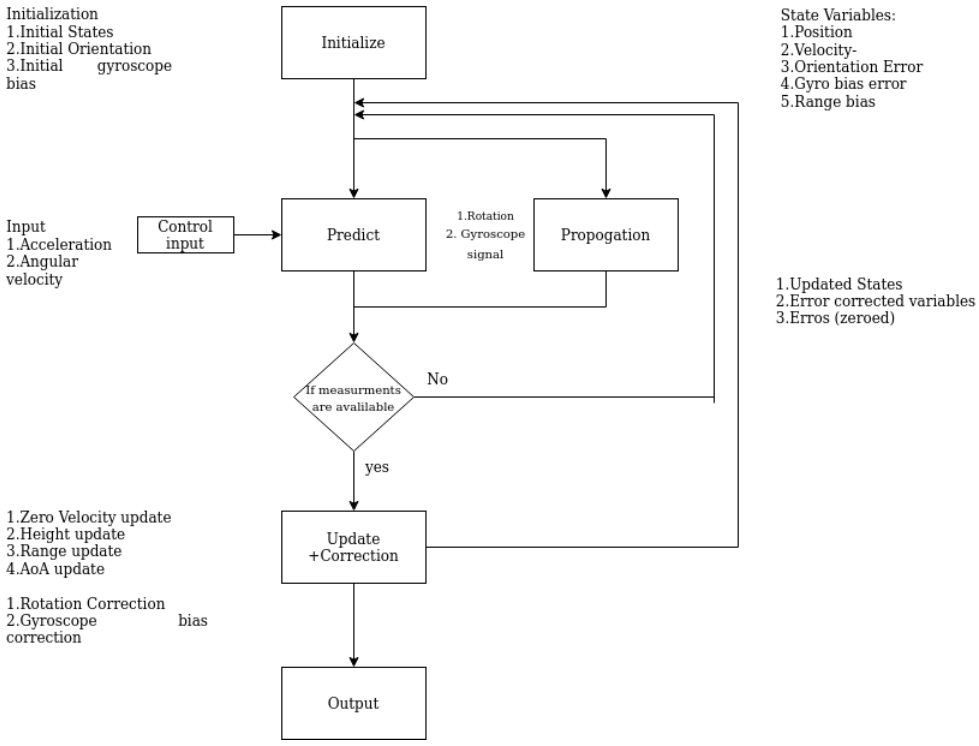

Fig. 4. The flowchart depicts the overall flow of the Error State - Extended Kalman Filter that has been developed. The position, velocity, orientation, range bias and gyroscope related values are acquired from the IMU and the UWB provides the AoA and range measurements.Here, the UWB sensors measurements are incorporated via the measurement updates) .

1) Zero Velocity + height updates - The zero velocity update is performed in the foot flat position of the gait cycle. During this position, the velocity is set to 0 and the height is set to the height of the sensor from the ground in the stance position.
2) UWB ranging updates - Due to the different sampling rate, whenever the UWB range is available, the position is updated.
3) Angle of arrival update - Whenever the AoA is available, it can be used to update the position state vectors.

The filter is described in detail below.

D. Initialization

The initialization of the filter comprises the initial conditions of the filter - namely the starting values for the state variables, the externally propagated variables and the noise and state co-variances.

the initial state variables are initialized as follows:

1) Position - The position of the feet are set to the preset initial positions in the sensor frame. This is then further rotated to the global frame using the rotation R_{gs} which is the rotation from the sensor frame to the global frame. The distance between the feet is set using the preset values, but the bias compensated range from the UWB sensors have also been used without issues.
2) Velocity - The velocity is set to 0.
3) Orientation error - The orientation error is set to 0.
4) Gyroscope bias error - The bias error is set to 0.

The external variables are:

1) gyroscope bias (b) - The mean gyroscope signal during the first 1 second of the double stance position is considered to be the bias.
2) R_{gs} - The orientation of the feet with respect to a global frame. In our case, using the magnetometer data exclusively for the initialization and the accelerometer data, the initial orientations (and only the initial orientations) are set in the East(X) North(Y) Up(Z) frame. Due to the propensity of the filter with range updates to correct the heading [20], any minor distortions in the orientation due to magnetic field issues would be corrected by the filter due to the relation between the position and orientation error(elaborated in the following sections).

E. Prediction and Propagation

The standard EKF prediction equations by which the state variables are propagated are given as:

$$\hat{x}_{n+1}^{-} = F_n \times \hat{x}_n + B \times u_n \tag{6}$$

$$\hat{P}_{n+1}^{-} = ((F_n \times \hat{P}_n) \times F^T) + Q_n \tag{7}$$

where,

x - state vector.

P - process co-variance.

B - control matrix.
u - control input.
Q - process noise.
n - time instance.

With an Error State EKF, additional parameters have to be propagated alongside the state variables. In our case, it is the gyroscope bias and sensor orientation.

Note: In the prediction and propagation section, for the sake of clarity and brevity, the equations described are for one foot. The foot subscripts are omitted, and the same equations are reformulated w.r.t the other foot while implementing.

1) Gyroscope propagation: In order to calculate orientation R_{gs} accurately, any error in the gyroscope measurements should be rectified. The gyroscope is affected by the gyroscope bias, which in turn is modelled as a first order Markov process driven by white gausian noise[46][30]. The bias is formulated as:

$$b_{n+1} = b_n + w_{b,n} \tag{8}$$

Giving us the gyroscope bias prediction as:

$$\hat{b}^-_{n+1} = \hat{b}_n \tag{9}$$

Since an error state model is used for the gyroscope bias, the gyroscope bias error state is defined as the difference between the true bias and the estimated bias, given by:

$$be_n = b_{true,n} - \widehat{b_n} \tag{10}$$

Therefore by substitution:

$$be_{n+1} = be_n - w_{b,n} \tag{11}$$

Hence the gyroscope measurements are propagated as:

$$y^s_{gyr,n+1} = y^s_{gyr,n} + \widehat{b_n} \tag{12}$$

where,

b_n is the bias in the gyroscope at time instance n.
be_n is the gyroscope bias error at time n.
$y^s_{gyr,n}$ is the angular velocity measurement in the sensor frame.

2) Orientation and orientation error propagation: The rotation is propagated on the basis on infinitesimal rotations[45][47]. The changes in orientation from one frame to another is considered as very small, and hence commutative. By using this concept, the Rotation matrix is propagated as:

$$Rgs_{n+1} = Rgs_n \times (I_3 + \widetilde{\omega^s}) * dt \tag{13}$$

Or the quaternions as [45][48]

$$Qgs_{n+1} = Qgs_n \times (I_4 + \widetilde{\omega^s}) * dt/2 \tag{14}$$

where,

Rgs - orientation of the sensor in a particular frame w.r.t the global in terms of rotation matrices.
Qgs - orientation of the sensor in a particular frame w.r.t the global in terms of quaternions.
I_a - Identity matrix of size a.
ω^s - is the gyroscope readings (angular velocity) in the sensor frame.
$\widetilde{\omega^s}$ - is the skew symmetric matrix of ω^s.
dt - is the sampling time.

The skew symmetric matrix operator on a variable is given as:

$$\widetilde{\omega}^s = \begin{bmatrix} 0 & -\omega^s_z & \omega^s_y \\ -\omega^s_z & 0 & -\omega^s_x \\ -\omega^s_y & \omega^s_x & 0 \end{bmatrix} \tag{15}$$

The skew symmetric matrix operator in case of quaternions:

$$\widetilde{\omega}^s = \begin{bmatrix} 0 & \omega^s_x & \omega^s_y & \omega^s_z \\ -\omega^s_x & 0 & -\omega^s_z & \omega^s_y \\ -\omega^s_y & \omega^s_z & 0 & -\omega^s_x \\ -\omega^s_z & -\omega^s_y & \omega^s_x & 0 \end{bmatrix} \tag{16}$$

The orientation error is propagated as an infinitesimal rotation, and hence it is propagated using the same concept as the mentioned above.

To propagate this state θ_e in time, its derivative w.r.t time is found θ'_e by:

$$\theta'_e = \widetilde{\omega}^s \times \theta_e - be \tag{17}$$

Discretizing [45][49] it we get,

$$\theta_{e,n+1} = (I_3 + dt * \widetilde{\omega}_s + \frac{dt^2}{2} * \widetilde{\omega}^2_s) \times \theta_{e,n} + (-dt * I_3 - \frac{dt^2}{2} * \widetilde{\omega_s}) \times be_n \tag{18}$$

3) Position and Velocity propagation: The position and velocity in the global frame (p^g, v^g) are propagated based on the motion equations. Here, the acceleration in the global frame is used as the control input. The propagation equation for position is:

$$p^g_{n+1} = p^g_n + dt * v^g_n + \widehat{a}^g_n * \frac{dt^2}{2} \tag{19}$$

Similarly for velocity,

$$v^g_{n+1} = v^g_n + \widehat{a}^g_n * dt \tag{20}$$

Where $\widehat{a}^g_n$ is the acceleration estimate in the global frame. The acceleration is rotated into the global frame by utilizing the rotation from the sensor frame to the global R_{gs}.

$$\widehat{a}^g = R_{gs} \times a^s \tag{21}$$

$$\widehat{a}^g = R_{gs}(y^s_{acc} + g^s \tag{22}$$

$$\widehat{a}^g = \widehat{R}_{gs} \times y^s_{acc} + \widehat{R}_{gs} \times (\widetilde{y}^s_{acc} \times \theta_e) + g_s \tag{23}$$

4) Range bias propagation: From the curve obtained via a linear fit of the range bias, the polynomial can be written as (equation 91) :

$$rb = 0.355 - 0.251 * r$$

The propagation equation for the range bias (w.r.t time) is derived as:

$$\frac{drb}{dt} = \frac{drb}{dr} * \frac{dr}{dt} \tag{24}$$

Where the range r is a function of the position of the left and right feet (p_l, p_r) and must be linearized by taking its Jacobian[49].

Further, discretization using Taylor series approximation yields:

$$rb_{n+1} = rb_n + (\frac{drb}{dr_n} * \frac{dr_n}{dt}) * dt \tag{25}$$

Differentiating all the propagation equations with respect to the state variables we get the state matrix F_n denoted as:

$$\begin{bmatrix} I_3 & dt & \frac{dt^2}{2} * (R_{gs} \times \widetilde{y}^s_{acc}) & 0_{3\times3} & 0_{3\times1} \\ 0_{3\times3} & I_3 & dt * (R_{gs} \times \widetilde{y}^s_{acc}) & 0_{3\times3} & 0_{3\times1} \\ 0_{3\times3} & 0_{3\times3} & I_3 + dt * \widetilde{\omega}_s + \frac{dt^2}{2} * \widetilde{\omega}^2_s & -dt * I_3 - \frac{dt^2}{2} * \widetilde{\omega}^2_s & 0_{3\times1} \\ 0_{3\times3} & 0_{3\times3} & 0_{3\times3} & I_3 & 0_{3\times1} \\ \frac{drb_{n+1}}{dpl} & \frac{drb_{n+1}}{dvl} & 0_{1\times3} & 0_{1\times3} & 1 \end{bmatrix} \tag{26}$$

The equations and derivation of the range bias equations due to its prodigiosity is omitted from this report. In case it is required, it can be furnished by the authors.

The process noise Q is set in accordance to [50][49]

F. Inputs

The input u is described as :

$$u_{pr} = \frac{dt^2}{2} * (\widehat{R}_{gs,r} \times y^s_{acc,r} + g) \tag{27}$$

$$u_{pl} = \frac{dt^2}{2} * (\widehat{R}_{gs,l} \times y^s_{acc,l} + g) \tag{28}$$

$$u_{vr} = dt^2 * (\widehat{R}_{gs,r} \times y^s_{acc,r} + g) \tag{29}$$

$$u_{vl} = dt^2 * (\widehat{R}_{gs,l} \times y^s_{acc,l} + g) \tag{30}$$

The corresponding B matrix is an $I_{12\times12}$

All other inputs are considered to be 0, thereby giving rise to:

$$u_n = \begin{bmatrix} u_{pl} \\ u_{pr} \\ u_{vl} \\ u_{vr} \\ 0_{19\times1} \end{bmatrix} \tag{31}$$

G. Update and correction

After prediction, whenever a measurement is available, the update and correct step are performed.

The traditional equations for EKFs update are given by:

$$P_{inn} = ((H \times P^-) \times H^T) + R) \tag{32}$$

$$K = (P^- \times H^T) \times ((P^-_{inn})^{-1}) \tag{33}$$

$$\overline{z} = z - (H \times x_{prior}) \tag{34}$$

$$x_{updated} = x^- + (K \times \overline{z}) \tag{35}$$

$$P_{updated} = P^- - ((K \times H) \times P^-) \tag{36}$$

$$nis = \overline{z}^T \times P^{-1}_{inn} \times \overline{z} \tag{37}$$

$$\lambda = \frac{1}{|2 * \pi * P^{-1}_{inn}|^{0.5}} * nis \tag{38}$$

An outlier rejection based on the Mahanalobis distance/normalized innovations squared (NIS) [51][49] is implemented, where a threshold (based on a distribution such as χ is implemented, and readings above the threshold are considered outliers. where,

P_{inn} - Innovations co-variance.
H - measurement matrix used to convert the state variables into the measurements.
P_{prior} - the predicted value for that instance before updating.
R - is the measurement noise co-variance.
K - the Kalman gain.
$\overline{z}$ - the innovation.
z - the measurement.
x_{prior} - the predicted state variables before updating.
$x_{updated}$ - the updated state variables.
$P_{updated}$ - the updated state co-variance.
nis - the normalized innovations square (square of the Mahanalobis distance).
λ - the likelihood.

Each measurement update and correction used is listed below:

1) Zero Velocity update and height update: From the ZUPT algorithm as mentioned before [18], the instances when the foot is flat are obtained. In this stance, an assumption is that the velocity is 0 in all the axis for the flat foot. under the assumption that the foot is flat on the ground we can also assume that the height of the IMU is the same as the one it was initialized with. With both the height and ZUPT occurring simultaneously, combination of the two is possible.

NOTE: In the following section, the subscript n indicating the time instance is omitted.

For ZUPT left foot:

$$\begin{bmatrix} v_{lx} \\ v_{ly} \\ v_{lz} \end{bmatrix} = \begin{bmatrix} 0 \\ 0 \\ 0 \end{bmatrix} \tag{39}$$

The corresponding H matrix H_{zuptl} is:

$$H_{zupt,l} = \begin{bmatrix} 0_{3\times6} & I_3 & 0_{3\times15} \end{bmatrix} \tag{40}$$

Therefore the update $z_{zupt,l}$ is given by:

$$z_{zupt,l} = H_{zupt,l} \times x + w_{zupt,l} \tag{41}$$

The height update is:

$$p_{lz} = p_{lzinit} \tag{42}$$

The corresponding H matrix is :

$$H_{height,l} = \begin{bmatrix} 0_{1\times2} & 1 & 0_{1\times21} \end{bmatrix} \tag{43}$$

The height update is given by $z_{heightl}$

$$z_{height,l} = Hheight, l \times x + w_{height,l} \tag{44}$$

For ZUPT right foot:

$$\begin{bmatrix} v_{rx} \\ v_{ry} \\ v_{rz} \end{bmatrix} = \begin{bmatrix} 0 \\ 0 \\ 0 \end{bmatrix} \tag{45}$$

The corresponding H matrix $H_{zupt,r}$ is:

$$H_{zupt,r} = \begin{bmatrix} 0_{3\times9} & I_3 & 0_{3\times12} \end{bmatrix} \tag{46}$$

Therefore the update $z_{zupt,r}$ is given by

$$z_{zupt,r} = H_{zupt,r} \times x + w_{zupt,r} \tag{47}$$

The height update is:

$$p_{rz} = p_{rzinit} \tag{48}$$

The corresponding H matrix is :

$$H_{height,r} = \begin{bmatrix} 0_{1\times5} & 1 & 0_{1\times18} \end{bmatrix} \tag{49}$$

The height update is given by $z_{heightr}$

$$z_{height,r} = Hheight, r \times x + w_{height,r} \tag{50}$$

where,

w - corresponds to the white Gaussian noise associated with a measurement.
x - is the state variable matrix.

2) Range update: The measurement in the case of the UWB range update is the distance between the feet provided by the UWB sensor. Since the state variables corresponding to the position are tracked in the global frame, there is a necessity to transform the range measurement from the UWB sensors frame to the global frame. Since the UWB sensors and the IMUs are not located in the same position, translation vectors are described as δ_l^s and, δ_r^s which is the distance between the UWB sensors and IMU in 3 dimensions in the sensor frame. Using the orientation matrix R_{gs}, we rotate the translation vectors from the sensor frame to the global:

$$\delta_l^g = R_{gs,l} \times \delta_{ls} \tag{51}$$

$$\delta_r^g = R_{gs,r} \times \delta_r^s \tag{52}$$

Mathematically, the range can be described as:

$$r = ||p_{movft} + \delta_{movft} - p_{statft} - \delta_{statft}||_2 \tag{53}$$

Since the measurements of the range from the UWB are biased to minimize the innovation between the measurements and the calculated range, the range is calculated as.

$$z_{uwb,r} = r - rb + w_{uwb,r} \tag{54}$$

where,

1) $||\ ||_2$ - is the L2 norm.
2) mov ft- moving foot.
3) stat ft - stationary foot.
4) $w_{uwb,r}$ - is the white noise associated with the UWB range measurements.

The moving and stationary feet are determined by using the ZUPT algorithm, whereby the foot currently at the foot flat position is the stationary one and the other is the moving one. Since this is a non-linear equation, it is linearized by differentiating it as using the corresponding Jacobian as our H matrix, given by:

$$\frac{dr}{dp_{lx}} = \frac{p_{lx} + \delta_{lg} - p_{rx} - \delta r_g}{||p_l - p_r||_2} \tag{55}$$

Similarly, the derivatives for other variables can be obtained. The H matrix is given as :

$$H_r = \begin{bmatrix} \frac{dr}{dp_{lx}} & \frac{dr}{dp_{ly}} & \frac{dr}{dp_{lz}}, \frac{dr}{dp_{rx}} & \frac{dr}{dp_{ry}} & \frac{dr}{dp_{rz}}, 0_{1\times18} & -1 \end{bmatrix} \tag{56}$$

In case of using the external model (eq 93, denoted as function f) to compensate for the range bias,

$$z_{uwb,r} = r + f(r) + w_{uwb,r} \tag{57}$$

The corresponding range updates H matrix is:

$$H_r = \begin{bmatrix} \frac{dr}{dp_{lx}} & \frac{dr}{dp_{ly}} & \frac{dr}{dp_{lz}}, \frac{dr}{dp_{rx}} & \frac{dr}{dp_{ry}} & \frac{dr}{dp_{rz}}, 0_{1\times18} \end{bmatrix} \tag{58}$$

3) AoA update : To incorporate the AoA measurements, the following models have been tested :

1) AoA model 1- Decomposing the range measurement into its axial components using the measured AoA and updating the corresponding state position variables. This model uses the AoA to decompose the range into its X and Z components (sensor frames). The decomposed X and Z values, after rotating into the global frame are used to update the corresponding position state vectors. In this model, the range measurements and AoA measurements are substituted with the X and Z measurement updates instead. This method required minimal amount linearization, since the measurement acquired after decomposition were the positions directly.
2) AoA model 2- Using the AoA computed from the state variables with thresholds to eliminate AoA measurements in the presence of a significant elevation angle.
3) AoA model 3- Using the AoA computed from the state variables and with elevation angle bias compensation. The elevation angle bias is compensated using the state variables from the filters output.
4) AoA model 4- Using the magnitude of the AoA measurements with the elevation angle bias compensation to minimize the influence of the elevation angle as well as the phase flipping due to gait based errors.
5) AoA model 5- Computing the cos(AoA) using the sensor Z axis (cos(AoA)= $\frac{p^s_{lz}-p^s_{rz}}{range}$), which is impervious to the elevation bias rather than the sensor X axis.

Of these, models 2 and 3 were deemed to perform better based on the results and are discussed below. In the scenario where the angle of arrival is used, we use the AoA computed from the state estimates with (eq 106) and without bias compensation. To compute the innovations in the AoA measurement updates, a modulus operator (mod $\frac{\pi}{2}$) was used since the AoA measurements are in the polar coordinate frame. Example: The innovation for an AoA measurement of $\frac{\pi}{2}$ and a filters estimated value of $-\frac{\pi}{2}$ is 0 and not π radians. Since the AoA is computed in the sensor's frame of reference, the variables in the global frame are rotated into the sensor frame of the right foot using the rotation matrix $R_{sg,r}$ given by,

$$R_{sg,r} = R^T_{gs,r} \tag{59}$$

The rotation of the sensor with respect to the global frame in the X, Y and Z axis as Euler angles are considered to be $\theta_x, \theta_y, \theta_z$ and the angle of arrival is considered as θ_{aoa} and the elevation angle as psi. The elevation angle is computed as per the equation 101. As defined in the beginning of the sensor fusion section, the global Z axis is parallel to the gravity vector and points upwards, and in our scenario, the global X axis is along the length of the foot, and the global Y is along its width.

The AoA measurement z_{AoA} is obtained from equation 106 by :

$$z_{AoA} = sin^{-1}\frac{p^s_{l,x} - p^s_{r,x}}{range} + \omega_p \tag{60}$$

The operation being performed on the pdoa from the decawave kit is given by equation 4. By cancelling the $sin{-}1$ from eq 60 and eq 4 to minimize the linearization required, the following equation is obtained

$$(pdoa + pb + w_p) * \frac{c * pi}{2 * 180 * f * dist} = \frac{p^s_{l,x} - p^s_{r,x}}{range} \tag{61}$$

The rotation of the position state vectors from the global to the sensor frame can be written as (the variables are assumed to be in the global frame unless explicitly mentioned,

$$p^s_{lx} = R_{sg,l}[0,0] * p^g_{lx} + R_{sg,l}[0,1] * p^g_{ly} + R_{sg,l}[0,2] * p^g_{lz} \tag{62}$$

$$p^s_{ly} = R_{sg,l}[1,0] * p^g_{lx} + R_{sg,l}[1,1] * p^g_{ly} + R_{sg,l}[1,2] * p^g_{lz} \tag{63}$$

$$p^s_{lz} = R_{sg,l}[2,0] * p^g_{lx} + R_{sg,l}[2,1] * p^g_{ly} + R_{sg,l}[2,2] * p^g_{lz} \tag{64}$$

Therefore, the H matrix is:

$$H_{AoA} = \begin{bmatrix} \frac{R_{sg,l}[0,0]}{range} \\ \frac{R_{sg,l}[0,1]}{range} \\ \frac{R_{sg,l}[0,2]}{range} \\ \frac{-R_{sg,r}[0,0]}{range} \\ \frac{-R_{sg,r}[0,1]}{range} \\ \frac{-R_{sg,r}[0,2]}{range} \\ 0_{1\times 19} \end{bmatrix} .T \tag{65}$$

In case of elevation angle bias compensation, similar to eq 61, we get

$$z_{AoA} = \frac{((p^s_{l,x} - p^s_{r,x})^2 + (p^s_{l,z} - p^s_{r,y})^2)^{0.5} * cos(phi)}{range} \tag{66}$$

The corresponding linearization is.

$$H_{AoA,l} = R^T_{sg,r} \times \begin{bmatrix} \frac{dh_{aoa}}{dplx} \\ \frac{dh_{aoa}}{dply} \\ \frac{dh_{aoa}}{dplz} \end{bmatrix} \tag{67}$$

$$H_{AoA,r} = R^T_{sg,r} \times \begin{bmatrix} \frac{dh_{aoa}}{dprx} \\ \frac{dh_{aoa}}{dpry} \\ \frac{dh_{aoa}}{dprz} \end{bmatrix} \tag{68}$$

$$H_{AoA,bias} = \begin{bmatrix} H_{AoA,l} & H_{AoA,r} & 0_{1\times 19} & 0_{1\times 19} \end{bmatrix} .T \tag{69}$$

By analyzing the gait and its corresponding angle values, discrepancies were observed and thresholds were set based on them. The results are tabulated in the appendix (Appendix VII, Table 3), and are as follows:

1) θ_y is below 0° - Due to the location of the UWB kit on the feet, when θ_y is below zero, the angle vales are skewed by 180°. By reviewing a MVN analyze animation of the gait, it was observed that the node (right foot) pokes through the plane of the left foot/tag (i.e the stride width is negative).

2) θ_{AoA} less than 10° - This scenario is the opposite of the first one. Here the left foot is out of the right foots sight thereby occluding the node antennae.
3) θ_y is greater than 25° - This upper threshold is a byproduct of the height bias trials, where the maximum possible elevation is determined.

Whenever these thresholds are exceeded, the filter is reverted to the normal UWB ranging more of operation.

4) Gyroscope bias correction: Since in the sensor model the gyroscope bias error is described as random walk process driven by white noise, the corrected bias can be considered as:

$$be_{corrected,n} = b_n + be_n \tag{70}$$

5) Orientation error correction: The deviation in orientation can be written as :

$$\widehat{R}'_{gs} = R_{gs} \times \widetilde{\theta_e} \tag{71}$$

Thereby the change in rotation is described as an infinitesimal transformation of R_{gs} by $\widetilde{\theta_e}$ given by:

$$\widehat{R}_{gs} = R_{gs} + R'_{gs} \tag{72}$$

Methodology - Experimental setup

H. Hardware Overview

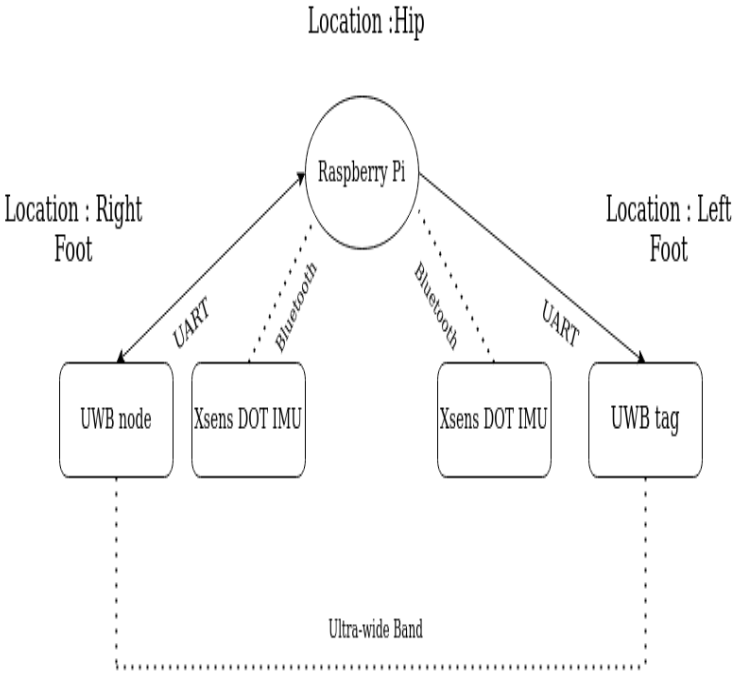

Fig. 5. The hardware setup used. Dotted lines indicate a wireless connection, while solid lines indicate physical cables. Here, the Pi SoC serves as a central hip mounted hub which is connected via wires to the UWB kit and wirelessly via bluetooth to the DOT sensors.

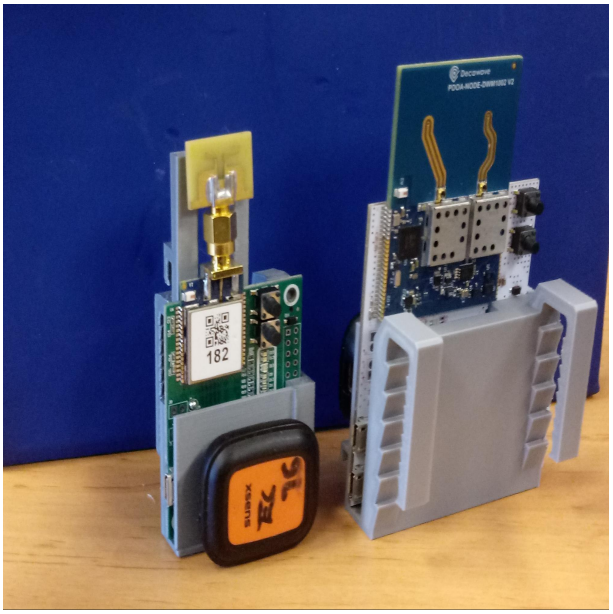

Fig. 6. The 3D printed clippable mounts for the node and the tag along with the Xsens UWB kits. The Tag holder (left), due to its longer arms, is made of PETG while the Node holder (right, facing backwards to display the clip structure) is made of PLA.

The hardware consists of two Xsens Dot IMUs sampled at 60Hz which are used along with a DecaWave UWB PDOA kit consisting of a DW1002 base station (node) and DW1003 peripheral transceiver (tag). The node and tag are mounted on a 3D printed chassis along with the dot IMU placed on the front of the chassis (Figure 7). This provides a fixed position and orientation of the DOT and UWB with respect to each other enabling the derivation of a vector connecting both positions and reference frames. The optimal location of the mount was deemed to be the inner ankle due to the stability and damping offered[52]. The node is clipped to the right foot and the tag to the left (figure 8).

The on-body setup consists of a Raspberry Pi mounted onto a waistband, and secured using a Velcro strap. The power banks for the UWB kit and the Raspberry Pi are inserted into the pant pockets of the subject. The Pi and the power sources were not mounted onto the lower extremities, due to ergonomic concerns of gait impairment/alteration as a result of their weight, and due to the trip hazards presented by the connecting cables.

Apart from our nominal setup, for validation, the Xsens Awinda system fused with the HTC Vive positioning system with two trackers and four base stations are used. The Awinda system is mounted alongside the dot sensors throughout the lower limb, and a Vive tracker is mounted as an anklet on the left tibia and the other tracker is used as the floor reference.

In case additional accuracy is required in the position of a particular segment(say, feet), the Vive trackers can be mounted on the required segment/location. Example: The trackers can be mounted on the feet.

Validation data capture and post-processing was performed

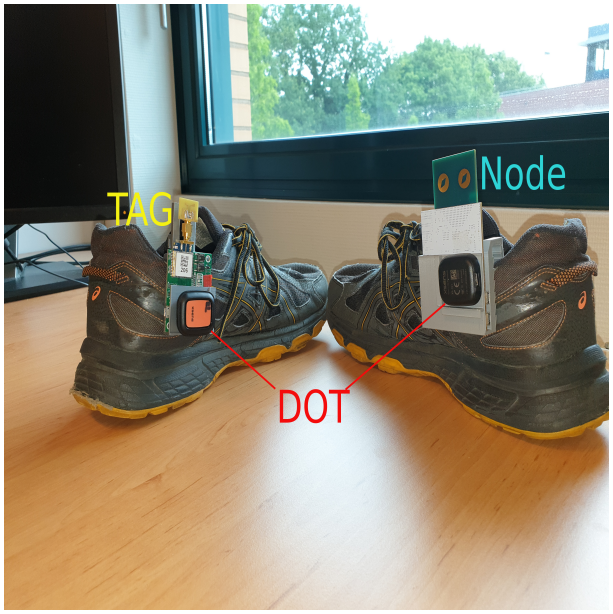

Fig. 7. The node and tag clipped onto the shoe. The tag is mounted on the left shoe and the node on the right. The mounts have a dot sensor attached to them as well.

in MVN analyze pro, using the lower limb biomechanical model.

I. Data acquisition protocol

The dataset gathered is from 4 subjects with a mean± SD height of 184cm ± 6cm comprising a total of 250 steps. The subjects were asked to cover a distance of approx 5.2 meters in an approximately straight line.

To test out the long term performance of the filter, and the performance in non-straight lines, a second experiment was conducted with 1 subject and 120 steps. This trial necessitated the subject to walk a distance of approximately 8.5 m in a curve. Sharp turns were avoided due to limitations in the validation setup.

In the initial stage, for easier validation/control, the step locations, whose locations are known, have been marked out in cellophane tape. Subject 2 was requested to walk on the cellotape markings inorder to evaluate the AoA measured from the UWB kit while walking. It was observed that the AoA acquired from the natural gait (figure 39) vs the controlled one (figure 40) had noticeable differences.

An ethical clearance was acquired from the University of Twente, Enschede, Netherlands for the aforementioned experiment.

For both the experiments, the same procedure, as listed below, was followed. The measurement is preceded and terminated by a vertical jump / kick of the left leg in order to facilitate the segmentation and extraction of the relevant part.

The detailed steps are as follows:

1) The subject is made to stand with their feet placed at the marked initial positions.
2) DOT server and UWB TWR protocol is initialized.

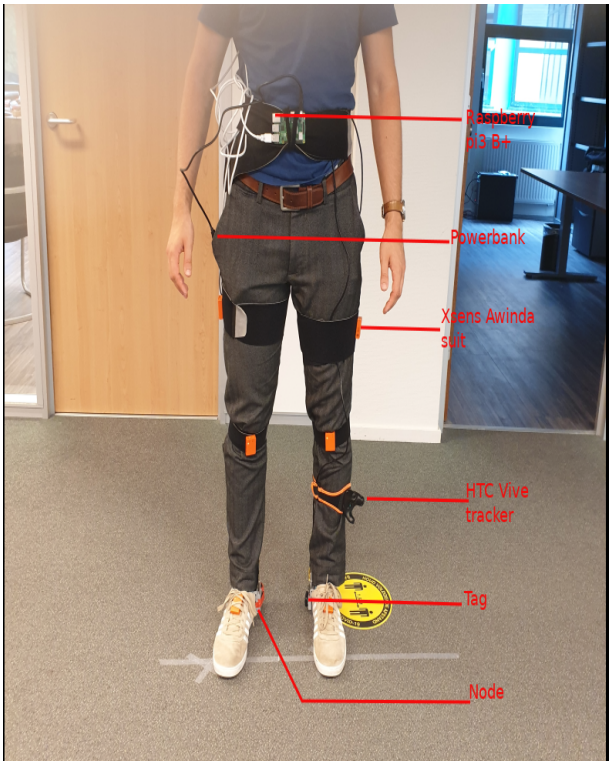

Fig. 8. The setup used for testing and validation combined. The orange sensors on the body, mounted on various straps belong to the Xsens Awinda wireless system. Our minimal sensing setup is just the tag and the node on the feet and the Raspberry Pi on the waist.

3) The DOT sensors are synchronized.
4) The subject is made to stand still for at least 5 seconds. This is to provide a reference acceleration signal exclusively exhibiting the acceleration due to gravity. This is used for further rotation and re-orientation of the signal. In addition, the gyroscope bias is calculated during this instance as well.
5) The subject is requested to make a vertical jump, preferably with the retraction of the feet towards the pelvis. This is to ensure a large peak which demarcates the start of the trial. In case the subject cannot jump, a swift kick with the left leg(with the tag) is also permissible.
6) The subject is subjected to a distance of 5.2 m or 8.5 m depending on the trial.
7) At the final feet positions, the subject is requested to stand still for 5 seconds and make a second jump similar to the one in step 5.
8) The observer terminates the programme and the data is further processed.

METHODOLOGY -VALIDATION

This section covers computation of the stride parameters using the variables from the filter and its subsequent comparison with a ground truth. A validation setup based on MVN analyze and HTC vive is used. Although conventional gold standard validation setups such as vicon have not been used in

our experiment, the utilization of Xsens MVN as a reference standard has been studied in literature[53][54]. In addition, apart from the MVN Awinda IMU motion capture setup, we utilize the HTC Vive system as well. The HTC vive system is capable of milli-meter level accuracy [55]. A fusion of the MVN awinda and the HTC vive system would provide the necessary level of accuracy needed for this project.

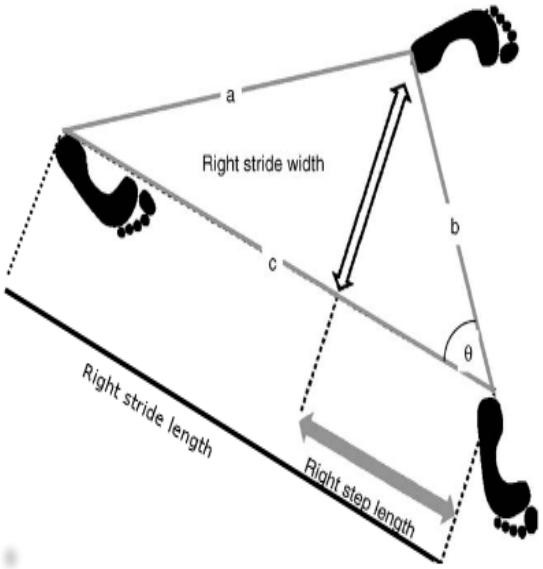

Fig. 9. The stride parameters to be computed described for the right foot as mentioned in [56]

J. Stride parameters and their estimation

The focus of this report being the accurate estimation of the stride parameters, necessitates the calculation of those parameters from the state variables. Although the subjects are requested to walk in a straight line for the 5m walk, it was observed that the idiosyncrasies of a different subject's gait's required the calculation of the stride parameters under the assumption that the gait falls under nonlinear walking. This is due to the observation that the feet are collinear, or at times, the right foot is further left than the left foot, which is closer to non-linear walking rather than in a straight line. For the 2nd experiment, since a curved path was taken, it is considered to be non-linear walking[56].

As per traditional literature on stride parameters estimation, and due to the placement of our sensors, the stride parameters are calculated at the heel. In addition, the ground truth position acquired is the foot segment position from MVN Analyse. The documentation of MVN Analyze states that the position of each segment is calculated at the point in the segment closest to the body - which, for the foot - is the heel/ankle. Since it is the comparison of the magnitudes/ distances, the frame of the segment position becomes irrelevant.

The validation parameter being used are the RMSE and its subsequent standard deviation. The error calculated in cm, is normalized with the height of the subject, thereby resulting in a percentage. This is done to account for the differences in the stride of a subject, which is a function of the height.

The stride parameters being calculated, apart from having clinical relevance, are selected such that they would enable the quantitative comparison of the filter's performance in terms of drift. The reasoning is expounded in the discussion section of the paper.

The stride parameters being estimated are:

1) Step length - The distance between the left and right feet computed between successive foot flat positions of the left and right feet and in the direction of walking (Global X frame).
   It is formulated as

$$RightSteplength(RSL) = \frac{b^2 + c^2 - a^2}{2c} \tag{73}$$

2) Step width - The distance between the left and right feet computed between successive foot flat positions of the left and right feet and the direction perpendicular to the direction of walking (global Y axis).

$$RightStepWidth(RSW) = (b^2 - RSL^2)^0.5 \tag{74}$$

3) Stride length (left and right) - the distance covered by the left or the right foot over successive foot flat positions.

$$Rightstridelength(RSTRL) = c \tag{75}$$

4) Overall - This calculates the difference between the relative foot position estimates from the filter output and ground truth at every single sample.

$$Overall = \Sigma_{n=0}^{k} r_{true,n} - \Sigma_{n=0}^{k} r_{filter,n} \tag{76}$$

5) Pearson correlation - Finds the Pearson correlation between the computed range and the true range.
   In terms of filter states,

$$a = ||pr_{ff,r,i} - pl_{ff,l,i}||_2 \tag{77}$$

$$b = ||pr_{ff,r,i+1} - pl_{ff,l,0}||_2 \tag{78}$$

$$c = ||pr_{ff,r,i+1} - pr_{ff,l,i}||_2 \tag{79}$$

where,

pr, pl - position of the right and left feet in 3D global frame.

$_{ff,r,i}$ - is the i^{th} right foot's foot flat events index (sample number).

$_{ff,l,i}$ - is the i^{th} left foot's foot flat events index (sample number).

r_{filter} - is the range computed from the filters states.

r_{true} - is the range obtained from the ground truth system.

k - is the total length of the trial (samples).

III. Results

The Results section gives and empirical overview of the output from the filters. As mentioned before, the main aim of this paper is to estimate the efficacy of stride parameter estimation algorithms which incorporate UWB data. In order to do so, a comparison of the parameters estimated by the filter without UWB data and with UWB data is warranted.

The filter outputs are used to compute the distance between the feet at every single sample and are used to represent the performance of the filter rather than the state variables directly. This is mostly due to the fact that the distance between the feet would be able to enunciate any issues/gains in the performance of the filter The five filter modes being implemented and compared are:

1) Filter 1- EKF with IMU.
2) Filter 2- EKF with IMU and UWB range measurements (with external bias compensation model- eq 93).
3) Filter 3- EKF with IMU and UWB range measurements (with the in-filter bias estimation/compensation model).
4) Filter 4- EKF with IMU and UWB range measurements and AoA measurements without elevation angle bias compensation. (with the in filter range bias estimation/compensation model).
5) Filter 5- EKF with IMU and UWB range measurements and AoA measurements with elevation angle bias compensation. (with the in filter range bias estimation/compensation model).

Based on a linear fit of the RMSE in range (computed via normal integration of the acceleration and ZUPT) with the samples, datasets are classified as those with low (slope ¡ 1cm/s), moderate (1cm/s ¡ slope ¡10cm/s) and heavy drift (slope ¿ 10cm/s). According to the thresholds, 20 % of the data had mild amount of drift, 40% with moderate and another 40% with a high amount of drift.

A. Filter 1-EKF with IMU

In the filter with just the IMUs and its related updates (filter 1), the UWB measurements updates (range and AoA) and the range bias estimation are disabled. Therefore, the filter operates solely on the zero velocity and height updates.

Figure 10 is the output of Filter 1 on a dataset with a minimal amount of drift. Since purely IMU based solutions are prone to drift, the output of this filter on a dataset with drift is depicted in figure 11. A majority of the datasets collected (approx 80%) provided results similar to the 11, with range RMSE of the final step exceeding 1 m. In this filter, in datasets with a mild amount of drift (approx 20 % of the datasets), the filter produces good results with the pearson correlation of 0.85 ± 0.06, which closer to the UWB based filters than when compared to the pearson correlation acquired from datasets with drift (0.46 ± 0.25). In addition, the stride parameters computed are on par with the results from the UWB based filters in cases without drift. In addition, the overall RMSE parameter indicated that approx 10% of the computed range estimates were outliers.

In case of the long duration measurements, the results were worse due to the drift. The correlation showed a mean value around 0.02. This drastic reduction is attributed to the cumulative drift, disfiguring the measurements (as seen in table 2 and figure12). The other stride parameters showed significant deterioration as well.

This model performed the worst of all the five investigated in all parameters except the stride length parameters. The stride length parameters, in comparison to the other stride parameters, were much closer to the UWB based filters parameter estimates. Of note, is the stride length estimate of the left foot, which is the best among all filters. In case of the long duration experiments, both stride length estimates of filter 1 were the best. In addition, the stride length estimates for both the feet are almost the same in the long duration experiments

B. Filter 2- EKF with UWB range measurements (with external range bias compensation model)

In this filter, the compensation for the range bias is by using an external polynomial model as mentioned in the Range bias compensation section.When compensated using an external mode, the RMSE ($\pm$SD) of the ground truth range vs the measured range with compensation is 0.218 ± 0.24 m. The results of using this range in the filter is shown in the graphs below. The only updates performed in this stage are the IMUs updates and the range update. This method provides slightly better step width estimates than the in-filter range bias model. While the overall RMSE of this method (3.5%) is higher than the model with the in filter bias compensation (Filter 3), the pearson correlations are mostly the same.

In case of the long term experiment, it can be observed that the stride parameter estimates acquired are similar to the short duration experiments. An exception to this trend is the stride width, which is 1.5% worse. In contrast, the step length parameter estimates for both feet are better than the short duration experiments. In comparison with other filters, the external range bias one posted the best overall RMSE and step length RMSE. Although, it should be taken into consideration that the number of outliers were also 3 times higher than the other UWB based filters. The corresponding graphs are in Figure 33 for the bias compensation and 13

C. Filter 3- EKF with UWB range measurements (with the in filter range bias estimation/compensation model)

In this mode of operation, the range bias is computed as a state variable and is used to compensate for the bias observed in the UWB measurements. When the range bias is compensated for using the internal range bias estimates, the resultant RMSE ($\pm$SD) of the ground truth range vs the measured range with compensation is 0.21 ± 0.231. The corresponding graphs are in Figure 34 for the bias compensation and 14. The results from this model outperformed the external model slightly in all regards, except for the stride width, which differed by a small margin of 0.2%.

In the long term experiments scenario, the internal model performed worse than the external model in all evaluated

metrics, excluding the step width estimates. It was also noted that this filter had a 3 times smaller number of outliers than the internal model.

D. Filter 4 -EKF with UWB range measurements and AoA measurements without elevation angle bias compensation. (with the infilter range bias estimation/compensation model)

In this mode of operation, the range bias is computed as a state variable and is used to estimate the stride parameters. The method involves the computation of the AoA alongside the range from the state variable and using them as measurement updates. The scenarios where a bias in the measured AoA due to the presence of an elevation is eliminated by using a threshold, wherein the filer reverts to the range measurements. The corresponding filter output is figure 15. This filter provides the best output among all the filters, with the exception for the stride length -left feet. The action of this filter on the data pertinent to 10 is depicted in figure45.

E. Filter 5- EKF with UWB range measurements and AoA measurements with elevation angle bias compensation. (with the infilter range bias estimation/compensation model)

This EKF uses the AoA measurements and well as the range measurements which have been bias compensated. The AoA thresholds used to eliminate errors in periphery and the gait dependent ones are still enforced. The corresponding filter output is figure 15. This model performs on par with the internal filter bias model, and falls short of the filter 5's performance.

In the long distance studies conducted, this filter performed similar to its short duration counterpart in all parameters apart from the step width, where the performance was worse. Apart from the stride width, when compared to the Filter 2, the parameters are improved, indicating that AoA does improve the readings.

F. Long duration experiment - Filter 4

A key distinction for Filter 4 in the long duration experiments, is the utilization of the external range bias compensation model. Although the difference in the performance was just slight between the range bias models, the utilization of the external range bias model provided the best possible model. This has been retained for the sake of providing the best possible solution to our problem statement.

As with the short term experiments, while not decisive, this model performed better (approx 1.5%) than other models in terms of step width estimation and correlation. The stride parameters were worse than normal IMU based EKF, but on par with the UWB based filters. The other parameters are quite close to the other filters.

The performance with the in filter range bias model was similar, but the overall RMSE was slightly better (0.6 %) for the external range bias model. This was not the case with the shorter duration measurements, where the in filter model provided the better results when fused with the AoA. A side effect of using the external model was a 2.5 times increase in the number of outlier measurements.

G. Comparison of the Accuracy of multiple models

This section involves the comparison of the stride parameters from the four different models being investigated. The results depicted in the form of bars are the RMSEs and the whiskers indicate the standard deviation of the errors. The corresponding figure is the box graph in 18. The numerical values are listed in Table I. From Table I, it is apparent that the best performing model is filter 4 - with internal range bias compensation and without AoA bias compensation. This model resulted in a pearson correlation of 0.89, almost twice as high as that from filter1. In addition, the most significant improvement is noticed in the step width measurements, with an observed approx 4 fold improvement compared to filter 1, and a 0.6% improvement over the 2nd best performing model in the step width category. On the other hand, the step length parameter shows a two fold improvement over filter 1, and a minimal improvement over other models. The stride length, on the other hand performs worse for the models with UWB measurements included. In general, the UWB measurements improve the stride parameter estimation significantly, with the AoA measurements providing a slight improvement. It is also observed that the increase in the drift compensation came at the cost of stride length estimation, with the IMU model (filter 1) performing slightly better or on par with the UWB based measurements.

In addition, it was also noted that the stride lengths were estimated on par or better by the UWB based filters when compared to filter 1, in datasets with mild drift. In datasets with a minimal amount of drift, it was observed that the overall pearson correlation was $0.85\% \pm 0.06\%$ for filter 1, while for filter 4 it as $0.93\% \pm 0.007\%$, indicating that the utilization of UWB is still beneficial.

In the long duration experiment, the filters performed similarly in most aspects. From figure 19 and table 2, all the UWB filter performed similarly. The deciding factor in favour of Filter 4 was its 1.5% improvement in the stride width estimates over the 2nd closest model.

H. Drift in the measurements

While conducting our walking experiments, a 5 m walk in an approximately straight line resulted in a large drift in the IMUs position estimates. The drift could potentially be due to either a drift in position due to noisy accelerometer data or due to a drift in orientation. The comparison of a walk of approx 5 m in a straight line comprising 9 steps of approx 0.6 m distance between successive steps in a dataset with minimal reading versus a dataset with a moderate drift is shown in the Figure20.

The drift was observed to be random, with certain trials producing a minimal amount of drift (RMSE overall : 3 cm or 1.5%, Pearson correlation with the ground truth: 0.93) versus certain trials with a significant amount of drift (RMSE overall : 47 cm or 24 %, Pearson correlation with the ground truth: 0.31). The incorporation of UWB measurements were able to compensate for this drift resulting in an improvement in the

results (RMSE overall : 8.7 or 4.3% cm, Pearson correlation with the ground truth: 0.84).

A similar drift was also observed in the long duration measurements.

IV. Discussion

The discussions consist of the analysis of the results and methodologies from the previous sections. A cursory review of the results indicate an improvement in the estimation of the stride parameters with the incorporation of UWB sensors data, thus validating our hypothesis that UWB measurements would aid in drift compensation and stride parameter estimation. The marked increase in the accuracy indicates that a combination of UWB and IMU sensors can be used for a portable gait analysis. The extent of its usage, using from the results, indicate that it can be used for normal walking analysis, or the analysis of parameters which donot required precision less than 5cms. For the analysis of diseased gait, such as classifying the different Parkinsonian stages based on stride parameters, the underlying system needs further improvement. Notably, a better IMU can aid in the precision. In terms of drift compensation, it was observed that all methods incorporating UWB data had a slope of less than 0.5cm/s when linear curve fit was performed on the overall error. In addition, the UWB based filters perform consistently across the short and long experiments. As mentioned further down in the discussions, the performance of Filter 1 is attributed to the poor quality, uncalibrated IMUs. This can be compensated by using better quality IMUs. Hence, the short duration measurements are primarily discussed.

A. Comparison of the bias models

The first part of the filter involved the incorporation of the range data from the UWB kit. Although the data was marred by a bias, methods were devised to compensate for it. From a glance at the figure with the uncompensated range 32, it is apparent that it cannot be used without further processing. The most explicit difference is the presence of an offset. The compensation for the bias by using a simple constant value added to it is similar to the range bias compensation method implemented by decawave, and is not very effective.

The first method is the utilization of an external range bias model to compensate for the range bias. Due to the bias being estimated externally from the filter, the stability and tuning of the parameter need not be considered. This results in a robust UWB measurement which is unaltered by any issues in the filter and can serve as a method which is impervious to the drift in the IMUs. In addition, another advantage of this system is its scalability in terms of complexity. Apart from not being linearized and incorporated into the filter, the bias can be modelled using much more complex methods such as generalized additive models based (GAM)[57] on penalized b-splines or with simple methods akin to the linear polynomial model used in this paper. This allows us to utilize an on-board/embedded compensation system, which allows the incorporation of the UWB device into multiple real time scenarios. In addition, this model can be improved to account for other factors, such as the incorporation of multi-path based corrections, in case of non line of sight due to occlusion by the human body - compensation for delay in transmission caused by the human body, etc. This method is also useful in the initialization stage of the filter, with the model being used to compensate for the range measurements from the UWB sensor, which again, is used to set the initial distance between the feet in the Y direction.

The second method is the computation of the range bias using an in filter model. This model, in contrast to the previous external one, requires tuning of the process noises and the measurement noises of the UWB system. On one hand, the increase in tune-able parameters allows us to tailor the estimated range bias for our application, and on the other hand, it was observed that the filter could become unstable due to bad estimates or errors in another part of the filter. The underlying reason is that the range bias, by the chain rule, is a function of the position of the left and right feet. Any erroneous changes in these variables would result in invalid estimates of the bias. To minimize this, the outlier rejection as mentioned in the methodologies is performed. A consequence of using the position, which was observed in the estimated range bias, is that, any drift in the position estimates resulted in a proportional change in the estimated range bias thereby effectively reducing the total drift in the system. This is apparent in the tail end of the figures 34 and 14 and is discussed further in the subsequent paragraphs.

A visual appraisal of the graphs depicting the calculated range from the filters (Figures 14 vs 13) whose measurements are compensated by the two different models, provides cues on the underlying working mechanism of the models. From the figures, it is clear that the in filter model performs better, closely conforming to the peaks. As the drift increases towards the end of the system, it is observed that the in-filter model performs better, with the peaks closely conforming to the ground truth. In contrast, the external model does not exhibit the same behavior.The better performance is attributed to the tuning and the drift compensation capabilities of the filter based model.

Although both the bias compensation models perform similarly in terms of RMSE, when fused with the IMUs using the filter, the differences are apparent. It can be seen that, on the whole, the filter using the internal range bias estimates performs slightly better than the one using external range bias estimates based on the overall RMSE. This is attributed to the variation of the range bias with the drift, which can be considered as a mild- self adjustment/tuning effect. This of course, cannot be replicated by the external model since it is not affected by the filter states. If the quantification of the drift is possible, then it is possible to decrease the measurement uncertainty in proportion to the drift. When comparing the stride parameters, it can be seen that the step length and step width parameters have the same or slightly less error for the internal bias model. This indicates that both models perform similarly, while the internal model is slightly better

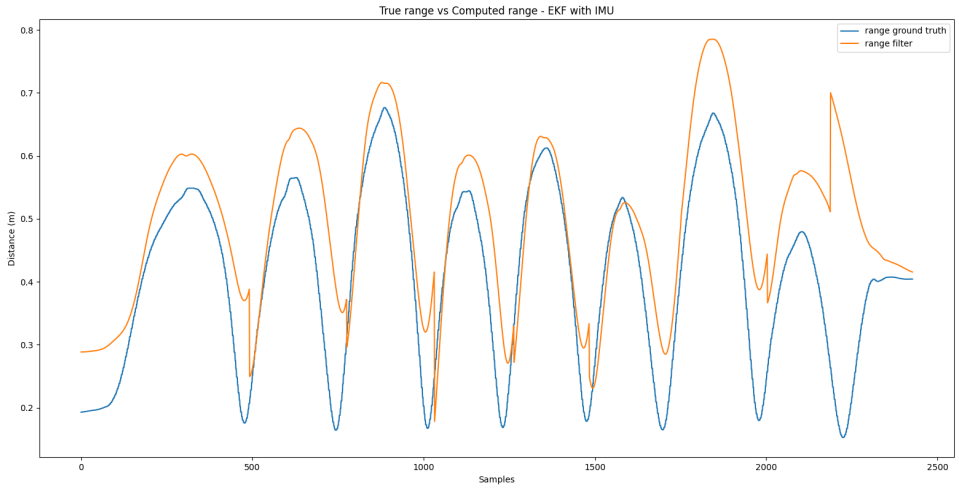

Fig. 10. Range computed from Filter 1 using IMU data on a dataset with a minimal amount of drift: An overlay of the range computed from the filter's estimates versus the ground truth. This data contained a minimal amount of drift in the system. This kind of drift can be expected from 20% of the measurements. The pearson correlation of this measurement was 0.8.

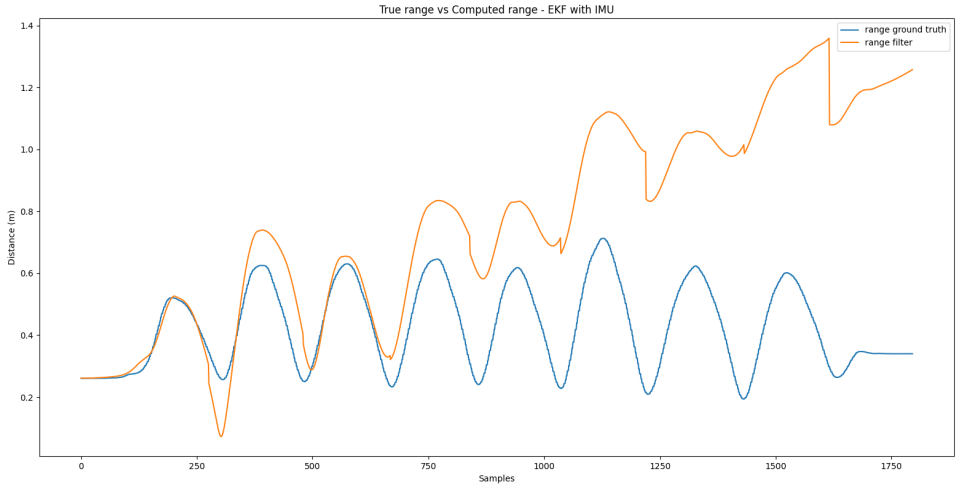

Fig. 11. Range computed from Filter 1 using IMU data on a dataset with significant drift: An overlay of the range computed from the filter's estimates versus the ground truth. The filter shows a noticeable amount of drift in the range computed. This drift persists despite implementing orientation error estimates as well as gyroscope bias error. The normalized RMSE (%) of : stride length, left foot is 2.45±1.9, stride length, right foot 3.1±3,1. step length 8.97±8.77, stride width 24±27, overall 24.6±27, Pearson correlation 0.32.

Filters/Parameters RMSE (Mean±SD)	Step length (%)	Step width (%)	Stride length - right (%)	Stride length - left (%)	Overall (%)	Pearson correlation
EKF with IMU	5.6 ± 3.2	12.8±13.6	3.7±3.1	3.1±2.1	10.6±10.5	0.46±0.25
EKF with ranging (External range bias compensation)	3.2 ±2.0	3.5±3.2	3.2±3.1	3.8±2.9	3.5±2.6	0.87±0.05
EKF with ranging (In-filter range bias compensation)	3.0±1.8	3.7±3.4	3.2±2.9	3.8±2.9	3.0±2.3	0.87±0.047
EKF with ranging + AoA (without elevation bias compensation)	2.9±2	2.9±2.3	3.5±3.0	4.1±3.1	2.9±2.2	0.89±0.038
EKF with ranging + AoA (with elevation bias compensation)	2.9±1.9	3.6±3.2	3.4±3.1	3.8±3.1	3.1±2.3	0.87±0.046

TABLE I

TABLE 1- SHORT DURATION EXPERIMENT RESULT : THE NUMERICAL TABULATION OF THE RMSE'S (%) OF THE FIVE FILTER MODELS FOR THE SIX STRIDE PARAMETERS. THE RANGE MEASUREMENTS IN BOTH THE AOA MODELS ARE COMPENSATED USING THE IN-FILTER RANGE BIAS COMPENSATION MODEL.

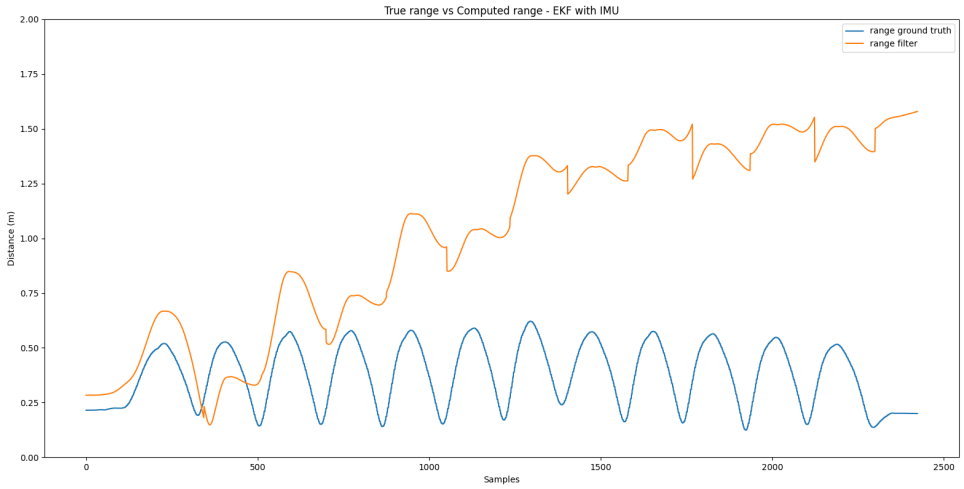

Fig. 12. Range computed from Filter 1 using IMU data for longer measurements.An overlay of the range computed from the filter's estimates versus the ground truth. The filter shows a noticeable amount of drift in the range computed. The normalized RMSE (%) of : stride length, left foot is 2.3±2.9, stride length, right foot 2.1±2.5. step length 7.77±7.57, stride width 44.2±38, overall 41.6±39, Pearson correlation 0.08. Due to the longer duration of the measurements, this model performs worse.

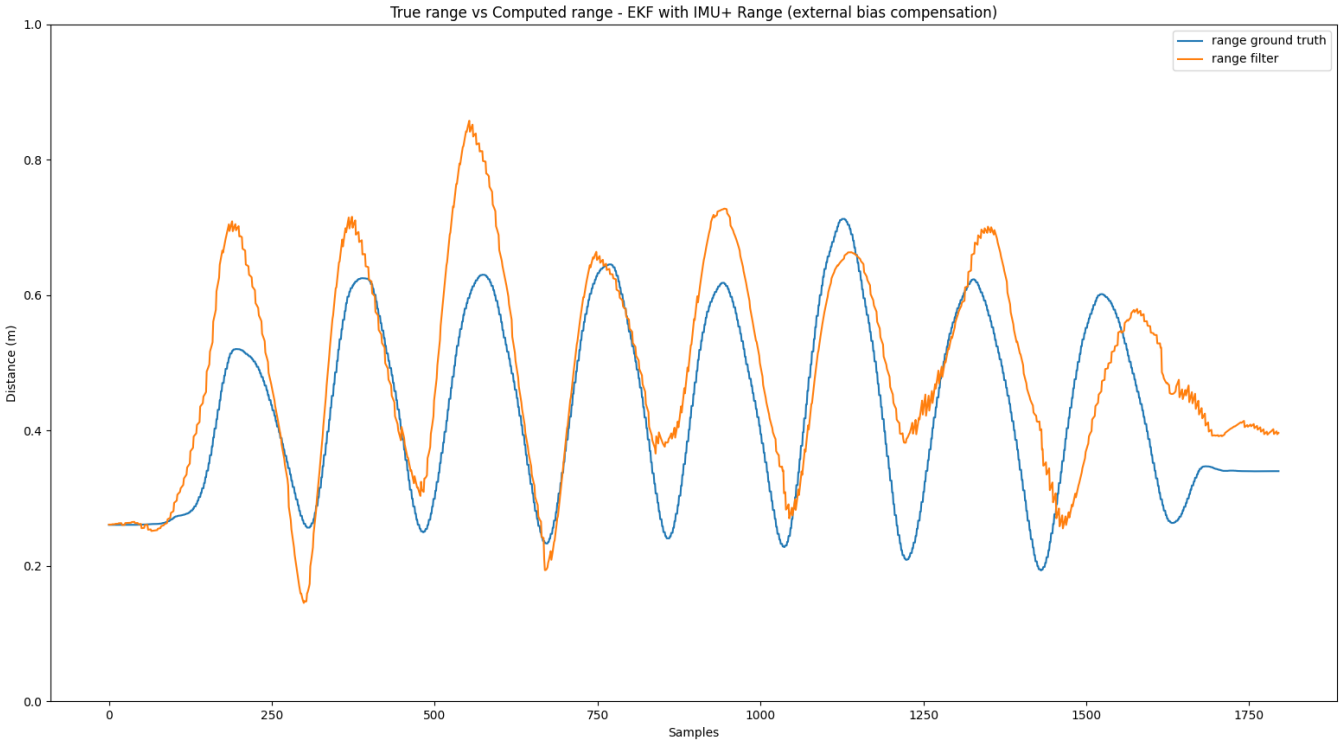

Fig. 13. Range computed from Filter 2 using UWB range data and IMU data : An overlay of the range computed from the filter estimates with the incorporation of the UWB sensors range measurements (with external model bias compensation) and IMU, against the ground truth). The normalized RMSE (%) of : stride length, left foot is 2.21±1.47, stride length, right foot 2.16±1.91. step length 3.12±2.8, stride width 6.0±7.23, overall 5.7±6.24, Pearson correlation 0.82

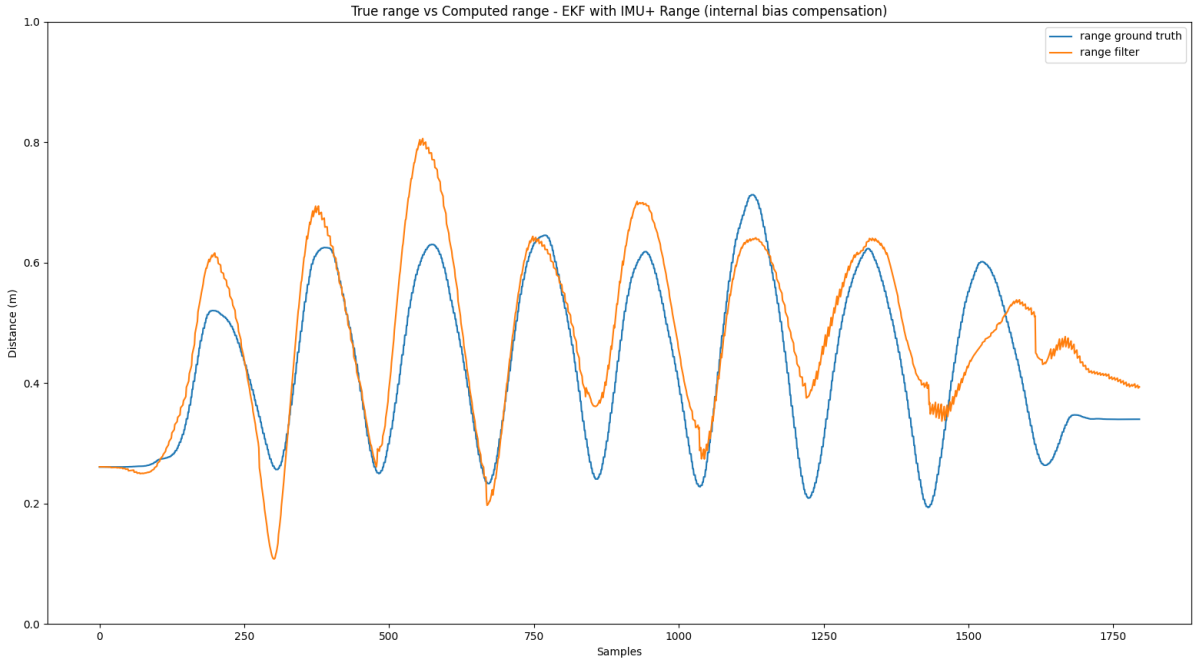

Fig. 14. Range computed from Filter 3 using UWB range data and IMU data: An overlay of the range computed from the filters estimates which is augmented using the UWB sensors range measurements and the internal range bias model, against the ground truth). The normalized RMSE (%) of : stride length, left foot is 2.35±1.24, stride length, right foot 1.94±1.57. step length 2.85±2.57, stride width 5.72±7.01, overall 4.65±5.21, Pearson correlation 0.88.

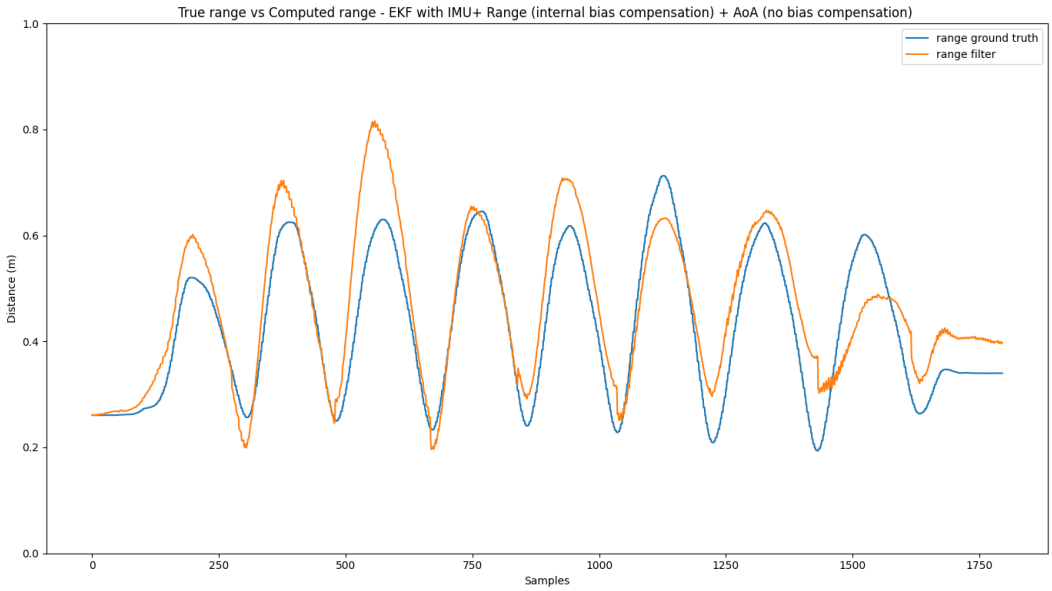

Fig. 15. Range computed from Filter 4 using UWB range data + AoA and IMU data: An overlay of the range computed from the filter's estimates versus the ground truth. The filter shows a drastic reduction in amount of drift in the range computed when compared to the filter's result from 11. This drift persists despite implementing orientation error estimates as well as gyroscope bias error. The normalized RMSE (%) of : stride length, left foot is 2.87±2.24, stride length, right foot 3.47±3,31. step length 2.75±2.78, stride width 3.1±3.03, overall 3.92±4.67, Pearson correlation 0.91

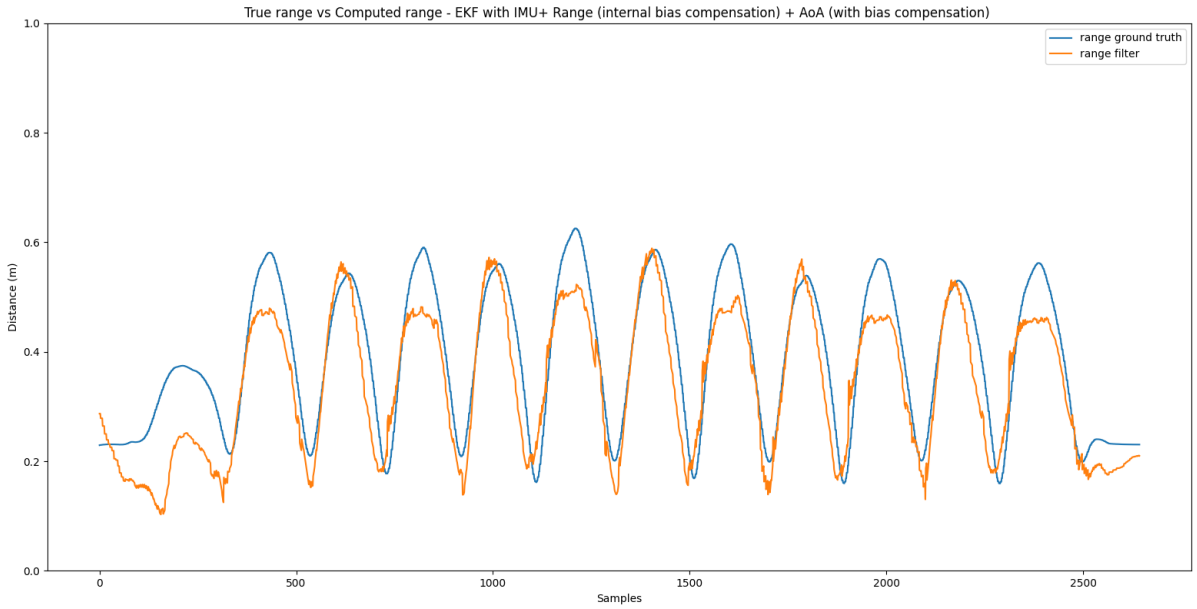

Fig. 16. Range computed from Filter 4 using UWB range data + AoA and IMU data on the longer trials: An overlay of the range computed from the filter's estimates versus the ground truth. The filter shows a drastic reduction in amount of drift in the range computed when compared to the filter's result from 12. This drift persists despite implementing orientation error estimates as well as gyroscope bias error. The normalized RMSE (%) of : stride length, left foot is 1.99±1.97, stride length, right foot 3.07±3.24. step length 4.49±4.32, stride width 4.25±3.99, overall 4.15±4.75, Pearson correlation 0.85

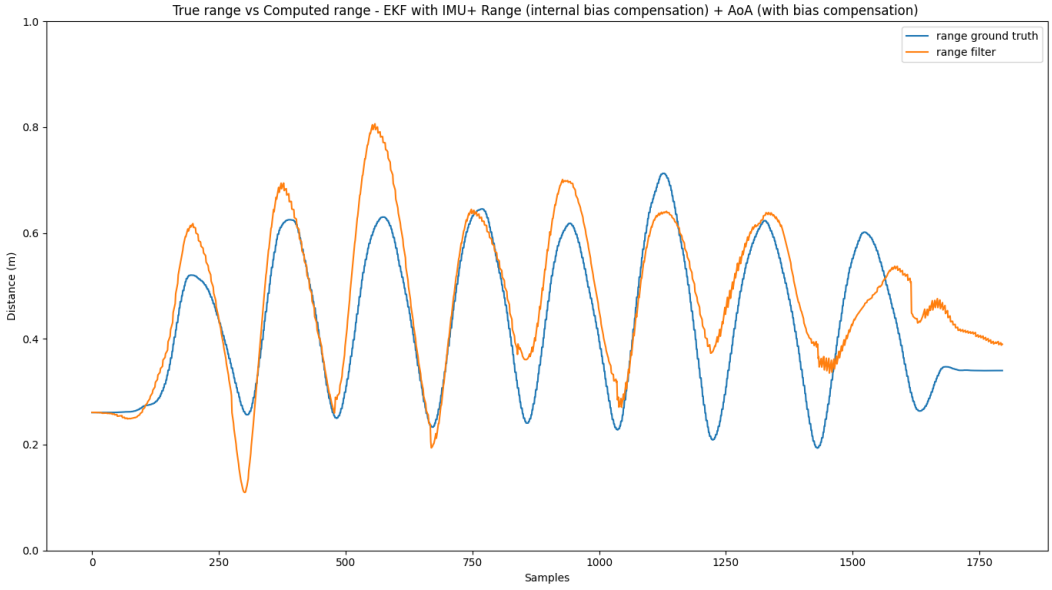

Fig. 17. Range computed from Filter 5 using UWB range, AoA measurements and IMU data: An overlay of the range computed from the filters estimates which is augmented using the UWB sensors range measurements(in-filter range bias model), and the AoA measurements (with bias compensation), against the ground truth). The normalized RMSE (%) of : stride length, left foot is 2.47±1.45, stride length, right foot 1.95±1.55. step length 2.87±2.54, stride width 5.27±6.83, overall 4.62±5.10, Pearson correlation 0.88

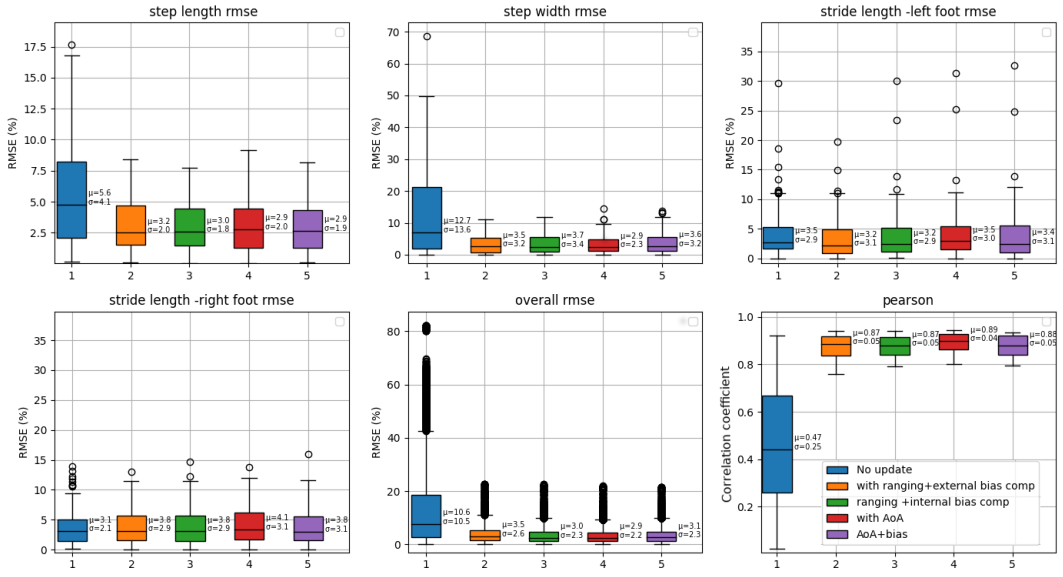

Fig. 18. A comparison of the RMSE of the six stride parameters being estimated by five different types of filters for the short trials. The blue boxes represent filter 1 (with just IMU readings), orange for filter 2 (IMU + UWB range updates (with external range bias compensation)), green for filter 3 (IMU + UWB range updates (with internal range bias compensation)), red representing filter 4 (IMU + UWB range updates (with internal range bias compensation) + AoA measurements (without elevation bias compensation) and purple representing (IMU + UWB range updates (with internal range bias compensation) + AoA measurements (with elevation bias compensation). The RMSEs are normalized with the height of the subject, resulting in %. The pearson correlation is the correlation coefficient between the filter output and the ground truth. The dots beyond the whiskers are considered outliers in accordance to the interquartile range, and the black line in the middle of the boxes is the median

Filters/Parameters RMSE (Mean±SD)	Step length (%)	Step width (%)	Stride length - right (%)	Stride length - left (%)	Overall (%)	Pearson correlation
EKF with IMU	39 ± 42	44±44	1.8±1.4	1.8±1.5	54±57	0.02±0.02
EKF with ranging (External range bias compensation)	2.9 ±1.9	5.1±2.9	2.2±1.7	2.3±1.7	2.8±2.1	0.86±0.05
EKF with ranging (In-filter range bias compensation)	3.6±2.5	3.8±2.4	2.8±2.2	2.8±2.0	3.8±2.6	0.86±0.05
EKF with ranging + AoA (without elevation bias compensation)	3.1±2.2	3.6±2.7	2.5±1.8	3.2±1.9	3.0±2.2	0.86±0.06
EKF with ranging + AoA (with elevation bias compensation)	3.3±1.6	5.6±3.5	2.7±1.9	2.9±2.1	3.2±2.4	0.86±0.05

TABLE II

TABLE II - RESULTS FOR THE LONGER TRIAL: THE NUMERICAL TABULATION OF THE RMSE'S (%) OF THE FIVE FILTER MODELS FOR THE SIX STRIDE PARAMETERS. THE RANGE MEASUREMENTS IN BOTH THE AOA MODELS ARE COMPENSATED USING THE EXTERNAL RANGE BIAS MODEL.

at compensating for the drift in the reference frames, which is usually the source of error in the step length and width.

In case of the longer duration experiment, the in filter model performs worse, in particular, the step length (0.7% worse and overall 1% worse). While these values are significant, an important distinction is the number of outliers. The number of outliers in the overall RMSE was three times smaller for the in filter range bias model, indicating that it was able to explain most of the variation in the dataset (i.e. it can handle drift based scenarios better). In addition, there is a 1.3% improvement in the step width estimates over the external model based filter. As an intermediate solution, the external and internal models can be fused together by using the bias estimates from the external model as measurement updates for the range bias state variable.

B. Comparison of filter with and without ranging data

This section compares the filter with just IMU measurements (filter 1) against the filter with the IMU and UWB ranging data. Since the performance of both the internal and external range bias compensation methodologies are similar, we are proceeding with the comparisons considering the filter with the internal bias compensation model's performance (filter 3).

From the plots (Figures 11 vs 13), it is clear that there is a significant improvement while incorporating the range data from the filter. Since the Figure 11 is explicitly worse, the figure 10 is considered for this part of the discussion, since it enunciates the underlying problems of Filter 1. Both figures depict trials in which the subject followed the same path. In case of 10 (dataset with a mild amount of drift) In the last two steps of the filter without UWB data, there appears to be a significant drift from the ground truth. In

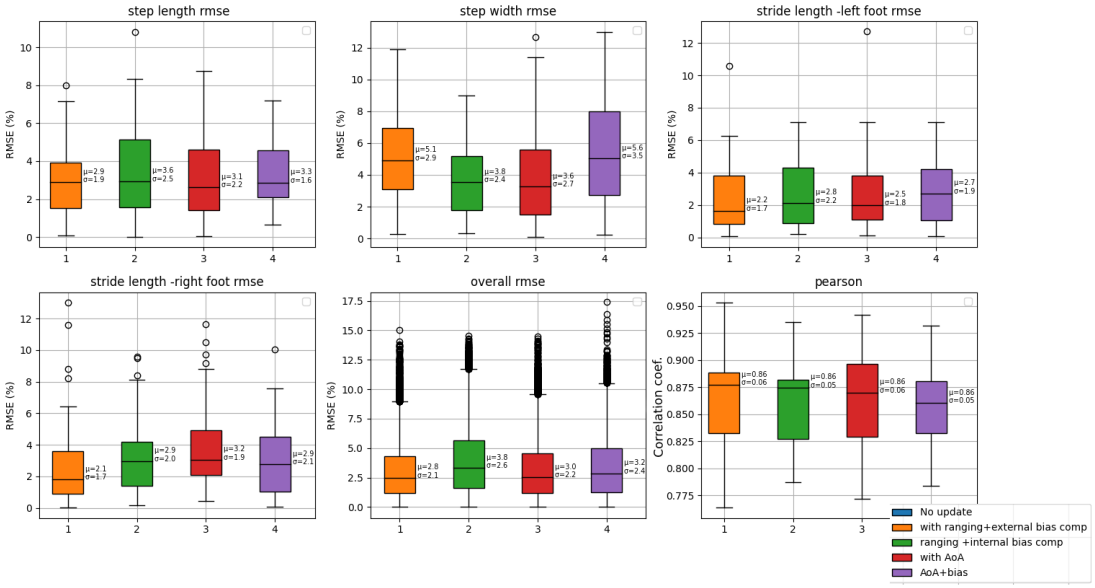

Fig. 19. A comparison of the RMSE of the six stride parameters being estimated by four different types of filters for the longer trials. The Orange boxes represent the results for filter 2 (IMU + UWB range updates (with external range bias compensation)), green for filter 3 (IMU + UWB range updates (with internal range bias compensation)), red representing filter 4 (IMU + UWB range updates (with external range bias compensation) + AoA measurements (without elevation bias compensation) and purple representing (IMU + UWB range updates (with external range bias compensation) + AoA measurements (with elevation bias compensation). Filter 1's result is excluded due to the high amount of error affecting the plots clarity. The numerics can be found in table 2. The RMSEs are normalized with the height of the subject, resulting in %. The pearson correlation is the correlation coefficient between the filter output and the ground truth. The dots beyond the whiskers are considered outliers in accordance to the interquartile range, and the black line in the middle of the boxes is the median.

particular, throughout the graph, there is a slight upward inflection followed by a significant downward dip in the measured range. Since the filter, due to the relation between the position and orientation error, minimizes any drift, the assumption is that the downward dip is the filter correcting the orientation of the feet. The orientation drift compensation is discussed further in the subsequent sections. In contrast, there is very little observed drift in both the mentioned cases when using the UWB range update. There is some mild over and undershooting of the maximum distance estimated, and the sudden dips in the valleys are minimal or imperceptible.

Numerically, the filter with range updates provides a three-fold decrement in the overall error of the system (3.1% with range vs 10.6% without) and an almost five-fold decrement in the calculated standard deviation. This can be interpreted as a minimization of the drift in the system as the estimated ranges conform to the ground truth over time, and the decrease in the standard deviation indicates that this conformity is consistent. The improvement in the standard deviation can be attributed to the number of outliers present in each filters estimates. The filter without UWB measurements had an 10% of its readings in the outliers, while the filter with UWB measurements had just 2%. The significant decrease in the standard deviation and outliers of the parameters, is an indication that the external noises/biases/drift in the system have been accounted for and are dampened. This is mirrored by the Pearson correlation, which indicates how similar the filter outputs and the ground truths are.

Another significant gain can be noticed in the step width (3.1% with range vs 12.6% without). The step width and step length, being byproducts of the accuracy in the estimation of the position in the X and Y global frame, are more sensitive to orientation drifts when compared to the stride length parameter where it is just the distance covered by the same foot. Since the walking is conducted in a straight line, the step width corresponds to changes in the global Y axis and the step length to the changes in the global X axis. From the drift comparison figure 20, it is observed that the global Y position, in relation to the total distance covered in that particular axis, has a significant amount of drift, while the X axis does not. This is reflected in the RMSE of the step lenght. While the step width had an accuracy of 12.6% with just the IMU, the step length has an error of 5.6%, which is attributed to the relatively minor drift if the X axis. With the UWB measurements, the step length estimates with UWB range updates are approximately twice as accurate.

Regarding the step length parameters, there is a worsening of the estimated step length by a factor of 0.5 % and 1% for the left and right feet respectively. This is observed across all filters incorporating UWB measurements. This worsening is attributed to the dependence of the orientation error computation to the UWB sensors updates. Since the UWB updates try to minimize the orientation drift between the both the IMUs, there is a change in the orientations computed. In

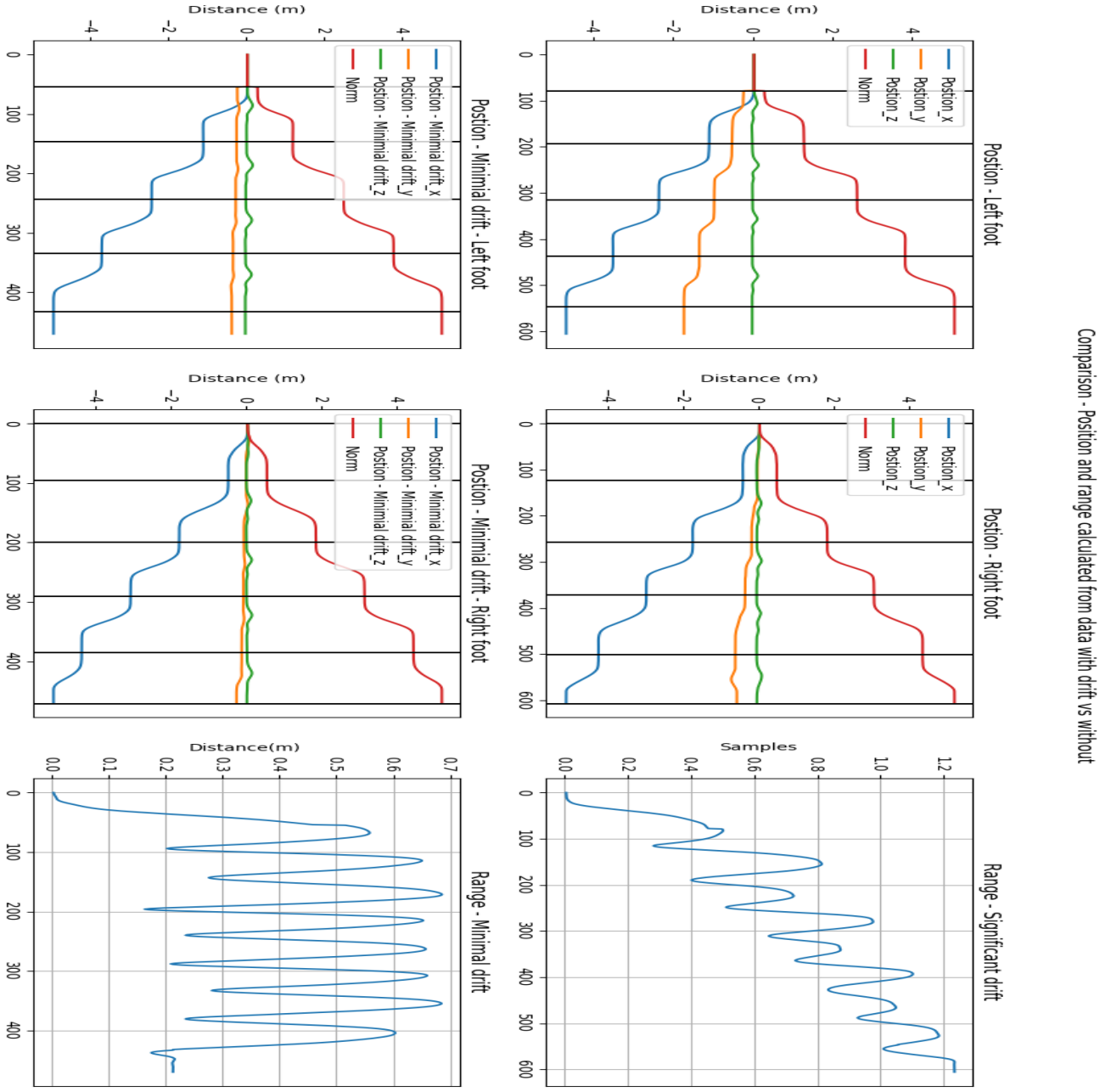

Fig. 20. The topmost row consists of the output positions and range for a dataset with a significant amount of drift. In comparison, the bottom row consists of the same parameters, but for a dataset without drift. The black bars on the estimated positions indicate the instances where the Foot Flat event occurs.

contrast, the filter with IMU based propagation does not try to maintain the relative frames of references of both the IMUs.

This leads to better stride length estimates since the stride length is independent of the relative orientations. In addition, of clinical significance are the stride length and stride width.

Apart from the above comparison, we additionally tested out:

1) Decreasing the sampling rate of the UWB sensors - This caused a decrease in the overall accuracy indicating that the UWB sensors were actively reinforcing the filter's estimation capabilities. A sampling rate of 10Hz resulted in an increase in the error (overall) by 2 cm and the stride parameters by 1 cm, whereas a sampling rate of 5Hz caused the overall error to increase by 3 cm and the stride parameters error by 2 cm.
2) From the comparison of the range bias compensation models (Figure 14) to the ground truth, it can be observed that the estimates at sub 0.2 m are skewed. An increase of the uncertainty in those measurements resulted in a minimal detriment in the overall accuracy of the system.

From this we can conclude that the incorporation of range data from the UWB sensors is beneficial for the determination of stride parameters and drift compensation in IMU based gait analysis system.

In addition, from the longer duration measurements, it is very apparent that the UWB measurements consistently provide similar or same results, while the IMU exclusive filters estimates deteriorate.

C. Assessment of the Angle of arrival model

Five models to incorporate AoA measurements in the filter were developed in this paper. Of these, the best performing one was the AoA model without any bias compensation (AoA model 2), and the AoA model with elevation angle bias compensation (AoA model 3) was included in the discussion since it can be fine-tuned to perform better. The 5 models are discussed as follows:

D. AoA model 1 - Decomposition of the range into its axial components

The main advantage of this model is the minimization of the linearization required, since the position components are being updated directly. The main disadvantage of this method is the instability. It is speculated that the combination of the AoA and UWB measurements resulted in an uncertainty which is non-gaussian. In addition, the X and Y measurements would be correlated, leading to unstable filtration.

E. AoA model 2 - Using the AoA and range measurements as separate updates - without elevation angle bias compensation

In AoA model 2, the AoA measured is used alongside the range measurements (in-filter bias compensation). Here the AoA is computed from the state variables and is used to compute the innovation. This method proved to be the best performing AoA model of the five.

In this model, the AoA measurements are used exclusively when the elevation angle is small and there is no phase reversal in the AoA measurements due to the gait. From Table I, apart from the stride length parameters, AoA model out performs other models. The decrease in the accuracy, as before, is attributed to the relative frames being maintained. In particular, the stride width parameters shows a 0.7 % increase, while the other parameters show a 0.4% increase on average. The Pearson correlation coefficient is the highest, at 89.2, almost twice as good as the 46.5 provided by the filter with just the IMU model. In addition, the standard deviation shows approx a 7-fold decrease, indicating that the filter with AoA measurements can be deployed in scenarios which have a heavy amount of drift. It was also observed that this model has the highest immunity to drift, providing the same RMSEs as those in figure 18. In contrast, the RMSEs of other UWB based models deteriorated slightly. To corroborate its performance under significant drift, this model (albeit with an external range bias compensation model) was the best performing model in the loner duration experiments with curves as well.

F. AoA model 3 - Using the AoA and range measurements as separate updates - with elevation angle bias compensation

AoA model 3 works in the same way as the previous model, with the exception that the bias in the measured AoA due to the presence of an elevation angle is compensated for using the derivation leading to equation 106. This model performs similarly, but falls slightly behind the AoA model 2. The reason for the deterioration in the performance is attributed to the utilization of the state variables to compensate for the bias. Since the bias estimation cannot be incorporated into the filter due to linearization issues, the bias variables are treated as constants, thereby neglecting its evolution. This leads to worse performance in case of drift. This is one of the scenarios which could be improved by using better linearization methods (discussed further in the limitations and future works section). In the dataset with minimal amount of drift, it was observed that this model performed on par with the AoA model 3, or in certain parameters, even better. In the longer trials, this method performed slightly worse than the other UWB based models. Despite it performing slightly worse, it does improve on the in filter range compensation model upon which it is built, indicating that AoA does improve stride parameter estimation. An exception, is the stride width estimates, which are the worst among the long duration measurements. This can be attributed to the curved path taken, and since this method is heavily dependent on the rotation matrices estimates and the state estimates, any disturbances caused by the curved route will be reflected in the parameters.

In this section, the thresholds to eliminate AoA measurements influenced by elevation angle are removed.

G. AoA model 4 - Using the magnitude AoA and range measurements as separate updates - with elevation angle bias compensation

This model build on the previous one by using the magnitude of the AoA measurements instead of the normal using the $\pm$ signs as well. Whenever the leftmost foot is the right

foot, the AoA measurements get flipped in their sign. Since these phase reversals have the same magnitude but have flipped symbols, the usage of just the magnitude eliminates the need to compute the signals. In this scenario, the thresholds in place due to remove phase reversed AoA measurements are removed.

This method performed slightly worse than the previous method. This decrease is probably due to the loss of the sign of the AoA, which raises an additional ambiguity in the position of the feet. An additional factor to this methods detriment, is the additional attenuation/ occlusion caused by the leg and shoe present between the node and the tag. Textile/rubber/human flesh, although transparent to RF signals, do cause attenuation resulting in erroneous values.

H. AoA model 5 - Using the cos(AoA)

The AoA model 5 utilizes the ratio between the sensor Z axis distance and range of the feet to compute the AoA. This model is the 2nd best performing AoA model. Since the elevation angle does not influence the sensor Z distance, this method is impervious to any elevation angle. In addition, since the sensor Z position is usually not negative, the magnitude is used, thereby eliminating the need for elevation angle bias compensation as well as phase reversal thresholds. This method ensures the maximal utilization of the AoA measurements.

While this method can use the phase reversed parts, it was observed that the model performed better if those erroneous AoA measurements were ignored. This model has potential, since it doesnot depend on utilizing state variables to compensate for biases, thereby being more error proof.

From Table 1, it can be inferred that the AoA model 2 (Filter model 4) performs better than models incorporating just the range measurements for gait analysis. For conventional localization purposes, where gait related errors like phase reversals donot exist, we expect the improvements to be more significant. In addition, AoA model 2 didnot show a deterioration in the RMSEs when used on a dataset with a significant amount of drift as well as in the longer duration dataset, thereby despicting its robustness against drift.

I. Drift in the IMU measurements - Origin and effects

The drift observed in the filters estimates is of two types - The drift in position due to the integration of the noises in the IMU, and the drift in the orientation. The drift is the orientation is primarily due to the cumulative integration errors from integrating the accelerometer signals. In addition, Due to strap down navigation and the utilization of the orientation to compute the free acceleration on which the position is dependant on, a drift in the position could also source from improper free acceleration computation.

In case of the orientation, the propagation is based on the integration of the gyroscope measures. Hence, the any biases in the gyroscope affect the orientation drift. The drift in the orientation is further divided into 2, the drift in the orientation of a sensor, and the drift in the frames of reference between sensors. The latter is quite egregious and causes a significant loss in the accuracy of the estimations.

The plots in the results section comparing a dataset with minimal amount of drift and one with a drift representative of the average measurement (20) provides an idea of the magnitude of the drift. On the left side is the dataset which drift which is experienced commonly, and on the right is the data from a set of readings which had a minimal amount of drift. Note that the axis mentioned is in the global frame. The tri-axial positions computed in the graphs are from the double integration of the accelerometer signal between the detected Foot Flat positions, which are used for zero velocity updates as well. To mitigate the drift in the velocity due to integration, a linear model of the drift is used assuming zero velocity during the foot flat positions. Similar results were obtained from the computation of the range using the EKF with just the IMU measurements in case of the dataset with and without drift.

Of interest in these computed values are the drifts in position in the Y axis. It can be seen that even if the X and Z axis position computations remain relatively drift free, the Y axis measurements are afflicted severely by a drift. In the minimal drift case, our walk in a straight line is blatant, since the movement in the Y direction for walking in a straight line is minimal. On the other hand, the dataset with drift shows a significant deviation in both the left and right foot. While the deviation between the minimal drift and with drift sets can be attributed to differences while calibration, the drift between the left and right foot Y positions of the set with drift indicates a divergence in the frames of references of the left and right feet.

To corroborate that the drift is due to the divergence in the frames of references, the norms of both the sets are compared and are found to be the same. This indicates that while the overall distance is accurately measured, the orientation does not. In addition, the distance between the feet is being estimated, any position drift (when assumed to be equal in all axis due to the same sampling rate and IMU) would not result in a continuous decrease in the estimated range as shown in the last subplot of figure 20. The range from the dataset with drift shows a continuous increase in the overall distance while progressively damping the estimated range. This along with the same norm is a symptom of the divergence in the frames of reference. Considering the calculated norm to be accurate, the remaining possibility is the drift in the orientation of the feet.

Considering that the drift observed is most likely due to the orientation drift, the incorporation of the accelerometer bias estimates is likely redundant. Another possible source of drift might be an internal misalignment of the accelerometer's axis, which might result in erroneous axial measurements. Since the latter is a physical property and its compensation is out of scope of this project, the orientation drift is minimized by computing the error states of the bias in the gyroscope measurements as well as the orientation's. Despite their incorporation, the filter fails to perform well.

A rough calculation indicated that for an orientation drift of

5°, at a distance of 5m was $tan(5 * \frac{pi}{180}) * 5$ was 0.44m and for 10m, it would be 0.88m. This is for a single IMU. since we are dealing with 2 IMUs, it is possible that drifts exceeding 1m can be observed easily. The strap down navigation using the orientation also contributes to this error further.

Although unused in our filter, there is a possibility that the magnetometer inside the IMU might influence the output of the IMU. A possible, albeit unlikely explanation for the drift is the possibility of the magnetometer inside the IMU being influenced by the surroundings, and if this magnetometer is used to process the raw accelerometer data, it would result in the tainting of the acceleration data being used.

It has been observed that the Xsens DOT is exceptionally sensitive to the presence of ferromagnetic materials in its surroundings. The device is sensitive enough to be affected by the ferromagnetic material in RC flooring. This might lead the filter inside the IMU to converge onto an erroneous state leading to distorted readings from the IMU.

J. Drift compensation by the incorporation of UWB data

The incorporation of UWB data mends the drift in position as well as the orientation. The orientation error correction is due to the ranging update being linked with the orientation error calculation. While the IMU based filter performs better than conventional ZUPT based integration, it is not able to compensate for a large amount of drift. In [20], it was mentioned that for longer measurements (9 m) a drift of 31cm + was observed while just using the IMU based updates. However, in our scenario, as depicted in Figure 11 and Figure 12 it is observed that the drift exceeded 1 m. This is attributed to the quality of the IMU used. The incorporation of the UWB data (AoA model 2) was able to reduce the drift in the system and produce the result as seen in Figure 15, it is observed that the drift is effectively eliminated. The incorporation of UWB data improved the Overall RMSE parameter from 24% to 3.92% - a six-fold increase. Corroborating this is the Pearson correlation score of 32 for the filter with just the IMU and 91 for the AoA model 2, indicating that the filter incorporating UWB measurements produces a range estimate much closer to the ground truth (i.e. the drift is almost eliminated). A linear fit of the overall RMSE resulted in a measured drift of 0.31cm/s. This kind of attenuation inf the drift was observed in the longer duration experiments as well. Under the assumption that the errors are due to drifts in the IMU, an investigation into the efficacy of the filters in combating the drift is conducted. The assessment is via the comparison and interpretation of the stride parameters being computed. Under the assumption that the drift is due to poor quality IMUs, and since smaller drift has been observed in contemporary literature using better IMUs ([20] uses Xsens Awinda, which is calibrated unlike the Xsens DOTs), we consider the shorter walk for the sake of this discussion. Pertaining to the efficacy of the UWB measurements drift compensation capacity, the tables 1 and 2 can be inspected. It can be observed that the UWB system performs similarly in both cases, thereby lending credibility to the fact that it compensates the drift present in the system. The interpretation of the parameters used in terms of the drift performance is discussed below:

1) Stride length - The stride length for the left and right feet are computed using the position estimates of the same foot. Since it is not reliant on the orientation estimates of the other foot, any error in the stride length parameter is an indicator of the drift in orientation or position. In the box plot (Figure 18), it is observed that, for the filter without any UWB sensor updates, the least error is provided by the stride length estimates of the left and right feet. Additionally, the error measured is almost on par with the error computed using filters incorporating the UWB data. This indicates that the performance deterioration of the range estimates is due to the drift in the relative orientation between the feet. Corollary, due to the relative orientations between the two IMUs being accounted for in the UWB sensor updates, there is a slight deterioration in the stride length estimates (approx. 0.5% and approx. 1% worse for the right and left feet respectively) vis-à-vis the plain IMU filter. From the box plots(Figure 18), it is apparent that the accuracy of one foot is less than the other. While tuning, a paradigm shift in the foot with better estimates was observed. Although both feet are initialized with the same parameters, it is possible that due to our limited dataset, a variation in the gait of one foot vs the other (example:a limp in one foot) for a subject would not be balanced out by normal gaits from other subjects. Hence, it is possible that the filter tends to converge on one foot leading to more erroneous estimates for the parameters of the other foot. It is also possible that the orientation estimation of one foot is worse than the other and the filter is attuned to one foot's error than the others. This theory is lent credence by the analysis of the drift in the Y axis (figure 20) where the Right foot sensor has significantly more drift that the left. This is further corroborated by the observation that the long term measurements on one healthy subject resulted in stride length estimates which are very similar for both feet.
2) Step length - The step length is the distance between the left and right feet in the axis of walking, which in our case is the sensor X axis(global X for a straight line walk). Since the error due to the position drift is not that significant as indicated by the stride length, the error in the step length can be attributed predominantly to be from the difference in the frames of reference between the two IMUs. In case of step length, we can attribute the error due to a performance degradation in the direction of walking. From the graph (18), the step length performance of all the filters are on-par, with the worst performing filter without any ranging updates. Since the step length estimate is direction dependent, the ranging update would have a minimal impact since it does not involve the decomposition of the measurement into the individual axes. The AoA update on the other

hand, is axis dependent since the range component is split into the step width and length is a good indicator of the performance of the AoA update step. The best performing model provides a twofold increment in the step length accuracy from 5.6% with just the IMU to 2.9% with AoA measurements (Table 1).

From the graphs overlaying the estimated range from the filters with the ground truth, the performance in terms of step length is deciphered by analysing the peaks, since the peaks are when the feet are far apart from each other which would result in minimal step width.

3) Step width - The step width is the distance between the left and right feet in the direction perpendicular to the direction of walking and the gravitational vector, the Y direction for a straight line walk). Given a minimal error due to the position drift, the step with is a healthy indicator of the divergence of the frames of reference between both feet. In contrast to the step length, the step width indicates the validity of the Y orientation. From the box plot (Figure 18), the best step width estimates are obtained for filters using the UWB data, in particular the filter using AoA updates. This indicates that the decomposition of the range into its respective axis aids in the localization performance. The inclusion of AoA measurements results in a 4 fold improvement in the step width estimates, indicating that the orientation drift is being compensated for.

   In contrast to the step length, the step width RMSE for the filter without any UWB measurements is almost twice as high. This stipulates that there is a significant divergence of the rotation frames between these two sensors.

   As with step length, in the plots representing the ground truth vs filter estimated range, the valleys indicate the step width performance since the feet are parallel to each other. From the graphs, it is obvious that the performance of the step widths would suffer. In case of the filter sans UWB data (Figure 10), it is in these valleys there is a significant error. The filter estimates produce a slight upward curve followed by a steep dip in the estimated range. As mentioned before, the downward inflection is attributed to the relation between the orientation error and the position estimates. This downward inflection in the valleys is minimized in case of filters incorporating range updates (Figure 14), which is reflected in the performance statistics.
4) Pearson correlation - The pearson correlation coefficient is calculated between the ground truth range and the one computed from the filters estimates. The correlation coefficient describes the similarity between the true value and the measured one. A high correlation indicates that the filter estimates are very close to the ground truth. From Table 1, the best performing model is the model using AoA measurements without bias compensation, while the worst performing one, as expected, is the one without UWB measurements. All the models using UWB measurements provide a 2 fold increase in the correlation coefficient (from 46.5 to 89.2) and a 7-fold decrease in its standard deviation. The high standard deviation of the filter using just the IMU measurements is due to the mixture of trials with a significant amount of drift (correlation coefficient approx .0.32), vs those with a minimal amount of drift (correlation coefficient approx. 83). This variation indicates that the IMU measurements are extremely prone to drift in the orientation. The low standard deviations in the filters incorporating UWB measurements highlights the drift cancelling capacity of the UWB sensors updates.
5) Overall RMSE - The overall parameter computes the RMSE between every sample of the ground truth range and the computed one. This parameter, has a function similar to the Pearson correlation. It monitors the amount of drift - both position and orientation, present in the output. A low overall RMSE indicates a high conformity to the ground truth. From Table 1, it can be seen that there is a 4-fold improvement in the overall parameter when comparing the best performing UWB based model and the IMU based one. In addition, the number of outliers for the normal measurements were around 10% of the total sample points - an indicator that the filter is not able to explain / compensate for the drift in the system. in comparison, only 2.6 % of the samples were outliers in case of the UWB models, indicating that most of the outliers in case of the filter just using IMU (i.e the drift), have been compensate for.

   The decrease in the error observed in the curated parameters strongly indicates that the orientation drift is being minimized.

K. Viability - indoor gait analysis/navigation

One of the larger challenges is the tracking of the gait indoors, where there isn't a pre-setup system for analysing the gait. This includes optical setups, NIR(Near InfraRed) based ones and even UWB base station based tracking setups. This constricts the gait analysis to a pre-setup lab or room which usually restricts the range of gaits and motions a person can exhibit. Using the completely body mounted setup devised in this paper, would allow the subject to navigate indoors without being restrained to a particular pre-setup area.

Since the antennae are mounted facing each other on the inner leg, it would be hard to encounter a situation where there is an obstacle between them causing a temporary Non line of sight(NLOS) condition. This ensures reliable readings which are not affected by environmental factors for a majority of the scenarios.

A commonplace scenario which might pose an issue is staircase climbing. While a range update might be viable, the AoA update would face certain constraints while straight climbing. The most pertinent issue would be the variation in the height of the anchor and tag which would correspond to an increase in the elevation angle from the perspective of the node. Since this scenario is similar to the one mentioned in

the tilt compensation section, the viability can be ascertained. By the Office of Health and Safety's(OSHA -USA) staircase standards [58] the average staircase depth is 24 cm and the height is 17 cm. By trigonometry, we arrive at the maximum elevation angle while the feet are placed at rest on successive stairs as 25°. While this is out of range for the Angle of arrival mode, we can subject the filter to switch over to ranging mode whenever a certain height difference threshold is reached. The ranging mode on the other hand would work reasonably in most scenarios with minimal concern of NLOS conditions as the antennae are mounted on the heel/ankle and would not be obstructed by the stair while transmission. A limitation of this would be the presence of steel staircases or any metallic content which might cause noises in the UWB measurements and the IMUs magnetometer.

Another advantage of the UWB system for indoor navigation is the minimal cross talk between UWB and other wireless modalities. Due to the low power transmissions of the UWB, it can coexist with other devices thereby giving it a clear advantage over other prevalent radiometric methods like Wi-Fi, Bluetooth etc.

L. Viability - outdoor gait analysis/navigation

In case of outdoor navigation, the main sources of interference for the UWB measurements would be the presence of metallic objects at the ground level. In outdoor scenarios, the probability of NLOS conditions goes higher, thereby reducing the performance of the device. A remedy for this might be the incorporation of UWB sensors elsewhere on the body - such as the pelvis or shank, which might be in LOS in instances where the foot mounted sensors are not. While the shank position is similar to the current one at the ankle, the distance between the shank and the ankle in the computation of the stride parameters should be taken into consideration. In case of the pelvis, the devices would be in line of sight for only half the gait cycle, when the feet are behind the body's coronal plane. In this scenario, if the current UWB sensor is used, the sensor can be rotated such that its antenna measure the elevation angle instead of the azimuth. In addition, since the UWB measurements proved to be viable at lower sampling rates as well, it is speculated that the pelvic setup would be not cause a major effect on the estimated stride parameters.

In comparison with other modalities, the UWB would still outperform conventional Wi-Fi/ Bluetooth /Radio based systems. The main disadvantage of the UWB systems when compared to Wi-Fi/Bluetooth is its constriction to short distances due to the frequency and power being used. This concern is not applicable to our use case since we measure the distances which usually fall within a meter. Against non-radio systems like ultrasound or optical methods, there is a significant advantage in the relative imperivousness towards environmental conditions like temperature, humidity and ambient brightness since electromagnetic waves are not affected significantly by the media of propagation.

A drawback of the system while used for prolonged duration (both indoor and outdoor) is the gradual accumulation of drift from the IMUs position estimates which would be transferred via the range update to the other foot. A method of circumventing this is to use a GPS system which would enable a correction of the position over longer durations.

M. Real time potential

The setup mentioned has a promising potential to be used in a real time environment. The usage of an EKF, as per its original intention, uses a linear approximation of a system resulting in easier and faster computation when compared to a system using, say, a particle filer. The current full sized filter (25 state variables) takes approx. 20s to process a walk of approx. 10s duration while operating on a single core. This process can be further streamlined by utilizing the rotations from the DOT sensors and using the external range bias compensation model. In addition, incorporation of parallel processing with GPU support would lead to a steep decrease in time required.

A major issue posed for real time operations would be the synchronization of the DOTs and the UWB kit. Currently, the synchronization is performed in post by computing the maximum cross correlation between the acceleration signals of both the sensors. In this scenario, it is possible to incorporate an initial synchronization phase where the subject is asked to walk or perform easily correlatable actions from which the lag can be discovered. An additional challenge is also posed by the lags in the transmission of UWB data over UART resulting in a skew in the samples time instances. This however, can be compensated by using a module wich incorporates all

N. Potential for analysis of impaired gait

The main end application of the filter is for the analysis of gait in a clinical environment with patients exhibiting non-ideal gait. To validate the system's performance in subjects with diseased gait, we recruited healthy subjects and conducted experiments where a limp was mimicked. To ensure an improved authenticity in the simulated limp, we added a constraint where the subject has to walk with a stiff left leg with minimal ankle flexion. Our system's performance was similar to the performance from a standard walk in case of range updates. In terms of AoA updates, we had to review the walk and the measured AoA and had to vary our thresholds in accordance.

In clinical grade gait analysis/ classification, the filter models are not viable at its current state (Ex: Classification of parkinsons stages using the stride parameters). However, improved hardware can potentially make it viable. In addition, the usage of AoA measurements for gait analysis is highly gait specific. Any variations in the gait due to a disease or disorder has to be taken into consideration before using AoA updates. This necessitates the utilization of different thresholds.

V. Limitations and Future Work

A. Limitations in the experimental protocol

The main identifiable limitation of this report is that the walking experiments involved walking for short distances

(approx 8m) and without any sharp turns. In real life scenarios walking usually consists of random turns and movements. Our algorithm exploits the peculiarities of walking and uses those for setting its thresholds and constraints. For walking involving complex or atypical patterns, the AoA measurement's thresholds should be modified in accordance. While the short duration trials had 4 different subjects, the longer duration one just had 1. The results should be extended with multiple subjects as well in the future for a conclusive idea.

In addition, due to constraints in the validation setup, the walking trials conducted covered a relatively short distance (5 to 9 m) and a short span of time as well (˜15 to 30 sec of walking per trial). While the drift encountered in these 30s was still palpable (Pearson correlation of filter output using just IMU and the ground truth is 8), experiments have to be done to quantify the performance over longer periods of time. For the current distances, drift over 10cm/s were encountered and compensated for, but the filters stability and performance over longer distances should also be assessed.

B. Limitations due to the hardware

The results, although good, still fall short of the results produced by some of the other linked papers. With the UWB measurements. This can be attributed to the difference in the IMUs quality and the evaluation setups used. It was observed that the stride length parameters in datasets with a nominal amount of drift are on par or better than the contemporary work, but due to the dearth of such datasets, it still needs further assessment before drawing any conclusion.

Due to the UWB kit and the IMU being 2 separate modules, a clock offset/drift is present in between the readings. This offset and drift manifests as a lag in the measurement output, leading to errors in the stride parameter estimates. This skew in the clock between the UWB range measurements and the ground truth was observable in the long duration experiments, leading to worse results. The issue with the current system is the synchronization of 3 different systems - Xsens Awinda, the UWB kit and the dot sensors - each operating at a different sampling frequency,

In addition, the IMU used - the Xsens DOT, is uncalibrated. The lack of calibration leads to worse filter outputs. Better IMUs such as the Xsens Awinda can be used as well. Since, the Awinda was used as the validation setup, an extension of this work can be the utilization of the Awinda data to estimate the stride parameters.

C. Limitations due to the validation setup

An additional reasoning on the error in the parameters could be the validation setup used. Since MVN analyze is being used to compute the position of the feet, the points at which MVN analyze computes the ground truth might be different from the points where the filter estimates the position. Since the error being dealt with is of the magnitude of a few cm, minor differences in the points of calculation would be magnified.

Apart from the previously mentioned error, it was also observed that the system performs worse at its periphery, out of the HTC vive systems sight. There are jumps, jitters and spasms observed in the GUI display of Xsens MVN Analyse. Although HD processing mitigated most of these errors, the validity of the long term measurements at the borders are of suspect. This is one of the major reasons on talking a curved path rather than sharp turns within the experimental space.

D. Improvements in the range measurements

In its current state, the UWB sensor's range measurement with range bias compensation portrays a RMSE(SD) 21 cm $\pm$23 on an average when compared to the ground truth while walking and an RMSE(SD) of 36 cm $\pm$44 cm from the characterization setup. This is on par with external experiments conducted with the UWB sensors ranging measurement[59][35].

From the figures depicting the ranging performance at different angles, it can be gathered that the angle has an influence on the bias experienced. The current solution of using a single model to compensate for the bias could further be expanded by using more advanced models to compensate for the bias in the range measurements.

It has been observed that certain AoA's and certain ranges (in particular a range band from 25 to 35 cm) have some issues. Towards the periphery (sub 30°) a sidewards inflection was noticed. The reason for the inflection is currently unknown but could be either the method of parsing data or the antenna parameters. An in depth analysis of the errors in the UWB system would improve the measurement's accuracy, thereby leading to better performance while fusion. A possible reason/solution could be by tweaking the hardware thresholds and limits.Currently, the UWB system detects the received signal by using a threshold based methodology. Due to the general use-cases of the DecaWave kit (at distances larger than 50 cm and typically in the order of a few meters), the threshold might be set lower, to compensate for the attenuation a signal would face at larger distances. In addition, the DecaWave kit also has thresholds for the detection of first path peaks and amplitudes which reinforce the measurements against any possible multipath. It is possible to adapt the threshold for our particular application, leading to more robust measurements.

An alternate method which was briefly investigated, is the utilization of predictor models/ Machine learning models to model and compensate for the errors in the UWB measurements. The incorporation of ML models would enable the modelling of the underlying error sources which influence the system and would result in its compensation. In the appendix(Appendix XI - Range bias-Old) section of the paper, the utilization of a Generalized Adaptive Model (GAM)[57] to compensate the range bias is discussed. Other features based regression/prediction models like the GAM using multiple sources of information, like the RSS, the First Path amplitudes and the measured distance, could potentially be used to compensate for any disturbances in the measurements.

E. Improvements in the AoA measurements

The AoA measurements use the phase difference to calculate the angle by trigonometric approximations. Improvements

in the AoA measurement algorithm could be by the application of Maximum Likelihood methods (ESPIRIT)[38][60] and subspace decomposition based methods(MUSIC)[38] on the CIR data. These have been implemented on UWB based devices, to varying degrees of success depending on the hardware used. A constraint while using algorithms like MUSIC is the number of antennas being deployed in the array. Due to the subspace decomposition methods, the number of signals which can be detected is given by N-1, where N is the number of antenna elements in the array. In our case, we have two antenna elements, and therefore are limited to 1 signal. Although the theoretical maximum is N-1, performance right at the theoretical maximum has proven to be poor. A possible method to circumvent this is the utilization of antenna interpolation/virtual antenna techniques which might artificially augment the number of array elements. In addition, the antenna characteristics need to be known for an effective deployment of these methods. A debatably simpler method of ascertaining the AoA is the utilization of a simple Neural Network to ascertain the AoA. This method, as deployed in [61] uses just 13 samples from each antenna's CIR to ascertain the AoA with an error of 2.9°. This method could potentially be less computationally expensive than the other advanced AoA methods mentioned above and could be deployed in real time conditions.

An add-on to the current setup would be the upgradation to a URA (Unifrom rectangular array consisting of four antennas in a square configuration -2x2) from the current ULA setup (uniform linear array). If there are problems in antenna design such as coupling and mutual inductance, it might also be possible to use an L shaped configuration comprising 3 antennae. The inclusion additional antenna in the vertical direction would enable the measurement of the elevation angle, thereby allowing us to localize the object in 3 dimensions. The deployment of the advanced AoA algorithms in this configuration would also minimize the bias due to height since those algorithms usually involve the modelling of the antenna array manifold matrix (essentially modeling the behaviour signals arriving in a square grid comprising angles of from 0 to 180 in the elevation and azimuth).

In addition, if the AoA measurements are to be used for a large portion of the gait cycle, the precise estimation of the AoA is a must. This to minimize the probability of getting erroneous measurements. A slight variation in the AoA, might translate to a large variation in the positions, since AoA essentially measures ratios. Ex: An error of 0.1 rads in the AoA measured, at a range of 60cm translates to approx 6cm of error. This error is quite significant in the clinical gait analysis domain. A small error/bias in the ratio can be caused by a multitude of factors such as propagation of the UWB signals though a thicker medium, occlusion, elevation angle etc.

F. Improvements in the filter

While the filters using UWB measurements depict a significant improvement in the stride parameter estimation, there are possibilities on improving the filter further.

1) Drift compensation: At its current state, the filter depends significantly on the UWB measurements to minimize the drift observed. The system, according to its initial blueprints, exploits the UWB range measurements for drift mitigation, and the IMU measurements for precision. The IMU component being on the weaker side, worsens the accuracy of the system. Any improvements in the IMU based stride parameter estimation would be transferred to the IMU + UWB based ones as well. In its current iteration, the filter corrects for the drift in orientation via compensating the angular velocity bias and the orientation error. While it is postulated that the accelerometer bias would be ineffective, there is a possibility of an oversight.

2) Improved linearization for AoA updates: The conversion from polar to Cartesian coordinates is extremely non-linear. This non-linearity is not adequately captured by the EKF system, thereby not using the AoA measurements to its utmost potential. An Unscented Kalman Filter (UKF)[62] can also be implemented, and would perform better, albeit marginally. The usage of other systems like a particle filter, although accurate, might not be viable for a real time system.

Currently, the AoA's elevation angle bias compensation is performed by computing the bias using the state variables and considering it as a constant when linearizing it for the measurement matrix $H_{AoA,bias}$. As seen with the range bias compensation, the incorporation of the bias as a state variable resulted in better performance. Similarly, the incorporation of the AoA bias internally, as a state variable, might yield better performances. Due to the non-linearity, an unscented transform might be more apt for such a state variable.

3) Range bias update for long duration measurements: One of the major limitations, due to the available measurement space, is the length of the measurements. Although the filter converges and is stable, the long term analysis of the filter is pending. This might not be of significant relevance in clinical studies, where the durations would not be more than few minutes typically, it is of concern when used in navigation systems.

The main parameter of concern is the internal range bias estimates, which are dependant on the state variables. In its current state, the range bias estimates drifts along with the state variables, but with an opposite magnitude, thereby negating the drift in the variables. For longer duration analysis, this might not be the case. In such scenarios, an additional measurement update is proposed as follows.

Using the external range bias model(equation 93), we get the measurement update z_{rb} as

$$z_{rb} = 0.29 - 0.214 * r_{UWB} + \omega_{uwb,r} \tag{80}$$

therefore the corresponding H matrix (H_{rb}) would be,

$$H_{rb} = \begin{bmatrix} 0_{1\times 24} & 1 \end{bmatrix} \tag{81}$$

Using a range bias measurement update would result in the long term stability of the filter, since the range bias

measurement from the external model is independent of the state variables.

G. Improvements in the overall hardware setup

A possible improvement in the setup to estimate the elevation would be to utilize the barometer present in certain Xsens IMUs. This would improve the performance of our system when contending with steps or with measurements involving a large elevation angle. This solution is less complicated and would be easier to implement and test (due to the existing barometer in certain Xsens IMUs) than the incorporation of additional antenna elements.

For the evaluation of a larger range of gaits, it is possible to include another UWB sensor or IMU in the pelvic region or any other region of the body. Doing so would enable a more accurate calculation of the lower limb bio-mechanics rather than just the foot parameters.

As mentioned in the previous section, for long term navigation, the inclusion of a GPS tracker would enable the development of a navigation system while maintaining the on-body/portable theme.

Most of all, one of the most important setup changes which could be implemented is the utilization of a smartphone in our setup[21]. Due to the ubiquitousness of the smartphone, it is reasonable to assume that any user who can avail a portable gait system, would also have access to a smartphone. Contemporary smartphones have the following advantages:

1) On board barometers, IMUs and GPS sensors - Most smartphones released in the past decade include a barometer, an IMU and a GPS system. The exploitation of these sensors would minimize the hardware costs and design requirements which would be needed to otherwise incorporate those sensors on the feet.
2) On board UWB device - A major push by most smartphone manufacturers in the current decade is the incorporation of UWB technology in their devices for the purpose of localization and interaction with smart devices. The UWB sensor used in mobile devices can serve as an additional reference point for the UWB sensors on the feet, thereby improving the accuracy of the measurements.
3) On board computation power - Most modern smartphones have more computation power available at their disposal. This computation power, in combination with rapidly advancing cloud computing would far exceed the processing power available in our current system (Raspberry Pi 3b+), thereby enabling the deployment of advanced and the full-fledged filter rather than a stripped down version.

The combination of a readily available sensor array in addition to the computational power ensures that the combination of our setup with the modern day smartphone would result in a complete lower body navigation and gait analysis system which can operate without any fixed setup.

VI. Conclusion

From the results and discussion, it is clear that the system developed is capable of the accurate estimation of stride parameters. The characterization and modelling of the UWB system's operation in sub 50 cm range, and its implementation, was also successful. The results portray that the UWB system can boost the performance of the IMUs and successfully mitigate the drift in it, with lower limb stride parameters being estimated with an average accuracy of approx 3.1 %. In addition, the inclusion of Angle of arrival for stride parameter estimation has shown to improve the estimates in comparison to plain UWB range based models, albeit by a small percentage (approx 0.6% on an average). It was also observed that the Filter 4, which included the AoA measurements, was the least impacted when tested on a dataset with a significant amount of drift as well as on the longer duration trials. While the given setup can be used for normal walking analysis, for clinical/disease analysis, it needs to be improved further. Furthermore, the setup used is completely on-body and works without any stationary fixtures allowing the analysis in a wide variety of environments. The rapid proliferation of UWB technology in mobile phones boosts the viability of advancing the current prototype into a full-fledged lower limb gait analysis/navigation system.

References

[1] Walter Pirker and Regina Katzenschlager. "Gait disorders in adults and the elderly". In: *Wiener Klinische Wochenschrift* 129.3 (2017), pp. 81–95.

[2] Bayram Kaymak and Abdullah Ruhi Soylu. "Fundamentals of Quantitative Gait Analysis". In: *Musculoskeletal Research and Basic Science*. Springer, 2016, pp. 93–106.

[3] Lars Donath et al. "Validity and reliability of a portable gait analysis system for measuring spatiotemporal gait characteristics: comparison to an instrumented treadmill". In: *Journal of neuroengineering and rehabilitation* 13.1 (2016), pp. 1–9.

[4] Valentina Agostini et al. "Surface electromyography applied to gait analysis: how to improve its impact in clinics?" In: *Frontiers in Neurology* 11 (2020), p. 994.

[5] Stacy J Morris Bamberg et al. "Gait analysis using a shoe-integrated wireless sensor system". In: *IEEE transactions on information technology in biomedicine* 12.4 (2008), pp. 413–423.

[6] Andrew L McDonough et al. "The validity and reliability of the GAITRite system's measurements: A preliminary evaluation". In: *Archives of physical medicine and rehabilitation* 82.3 (2001), pp. 419–425.

[7] P Chinmilli et al. "A review on wearable inertial tracking based human gait analysis and control strategies of lower-limb exoskeletons". In: *Int. Robot. Autom. J* 3.7 (2017), p. 00080.

[8] Stephanie Studenski et al. "Gait speed and survival in older adults". In: *Jama* 305.1 (2011), pp. 50–58.

[9] Jennifer S Brach et al. "Too much or too little step width variability is associated with a fall history in older persons who walk at or near normal gait speed". In: *Journal of neuroengineering and rehabilitation* 2.1 (2005), pp. 1–8.

[10] Alvaro Muro-De-La-Herran, Begonya Garcia-Zapirain, and Amaia Mendez-Zorrilla. "Gait analysis methods: An overview of wearable and non-wearable systems, highlighting clinical applications". In: *Sensors* 14.2 (2014), pp. 3362–3394.

[11] Joseph Jankovic. "Parkinson's disease: clinical features and diagnosis". In: *Journal of neurology, neurosurgery & psychiatry* 79.4 (2008), pp. 368–376.

[12] Yanshun Zhang et al. "The height-adaptive parameterized step length measurement method and experiment based on motion parameters". In: *Sensors* 18.4 (2018), p. 1039.

[13] Benoit Sijobert et al. "Implementation and validation of a stride length estimation algorithm, using a single basic inertial sensor on healthy subjects and patients suffering from Parkinson's disease". In: *ElectronicHealthcare* (2015), pp. 704–714.

[14] *MDS-Unified Parkinson's Disease Rating Scale (MDS-UPDRS). (2019). Movement Disorders*. URL: https://www.movementdisorders.org/MDS/MDS-Rating-Scales/MDS-Unified-Parkinsons-Disease-Rating-Scale-MDS-UPDRS.htm.

[15] Johannes CM Schlachetzki et al. "Wearable sensors objectively measure gait parameters in Parkinson's disease". In: *PloS one* 12.10 (2017), e0183989.

[16] Anat Mirelman, Nir Giladi, and Jeffrey M Hausdorff. "Body-fixed sensors for Parkinson disease". In: *Jama* 314.9 (2015), pp. 873–874.

[17] Alienor Vienne et al. "Inertial sensors to assess gait quality in patients with neurological disorders: a systematic review of technical and analytical challenges". In: *Frontiers in psychology* 8 (2017), p. 817.

[18] Isaac Skog et al. "Zero-velocity detection—An algorithm evaluation". In: *IEEE transactions on biomedical engineering* 57.11 (2010), pp. 2657–2666.

[19] Alberto Ferrari et al. "A mobile Kalman-filter based solution for the real-time estimation of spatio-temporal gait parameters". In: *IEEE transactions on neural systems and rehabilitation engineering* 24.7 (2015), pp. 764–773.

[20] Dirk Weenk et al. "Ambulatory estimation of relative foot positions by fusing ultrasound and inertial sensor data". In: *IEEE transactions on neural systems and rehabilitation engineering* 23.5 (2014), pp. 817–826.

[21] Chenshu Wu and KJ Ray Liu. "Accurate Stride Length Estimation via Fused Radio and Inertial Sensing". In: *2020 IEEE 6th World Forum on Internet of Things (WF-IoT)*. IEEE. 2020, pp. 1–6.

[22] Wang Guosheng et al. "UWB and IMU system fusion for indoor navigation". In: *2018 37th Chinese Control Conference (CCC)*. IEEE. 2018, pp. 4946–4950.

[23] Chenshu Wu et al. "RF-based inertial measurement". In: *Proceedings of the ACM Special Interest Group on Data Communication*. 2019, pp. 117–129.

[24] Pratham Singh et al. "Measuring Gait Velocity and Stride Length with an Ultrawide Bandwidth Local Positioning System and an Inertial Measurement Unit". In: *Sensors* 21.9 (2021), p. 2896.

[25] Paul K Yoon et al. "Robust biomechanical model-based 3-D indoor localization and tracking method using UWB and IMU". In: *IEEE Sensors Journal* 17.4 (2016), pp. 1084–1096.

[26] Juan Antonio Corrales, FA Candelas, and Fernando Torres. "Hybrid tracking of human operators using IMU/UWB data fusion by a Kalman filter". In: *2008 3rd ACM/IEEE International Conference on Human-Robot Interaction (HRI)*. IEEE. 2008, pp. 193–200.

[27] Xin Li, Yan Wang, and Kourosh Khoshelham. "UWB/PDR tightly coupled navigation with robust extended Kalman filter for NLOS environments". In: *Mobile Information Systems* 2018 (2018).

[28] Yan Wang and Xin Li. "The IMU/UWB fusion positioning algorithm based on a particle filter". In: *ISPRS International Journal of Geo-Information* 6.8 (2017), p. 235.

[29] Boyd Anderson et al. "Mobile gait analysis using foot-mounted UWB sensors". In: *Proceedings of the ACM on Interactive, Mobile, Wearable and Ubiquitous Technologies* 3.3 (2019), pp. 1–22.

[30] Henk J Luinge and Peter H Veltink. "Measuring orientation of human body segments using miniature gyroscopes and accelerometers". In: *Medical and Biological Engineering and computing* 43.2 (2005), pp. 273–282.

[31] *APH007 -Application note Antenna Selection/Design guide for DW1000*. Tech. rep. 2014. URL: https://thetoolchain.com/mirror/dw1000/aph0007_dw1000_antenna_selection.pdf.

[32] *DW1000 USER MANUAL*. Tech. rep. 2017. URL: https://www.decawave.com/sites/default/files/resources/dw1000_user_manual_2.11.pdf.

[33] Decawave ". *APPLICATION NOTE: APS016*. Tech. rep. 2015. URL: https://www.decawave.com/sites/default/files/aps016_moving_from_trek1000_to_a_product.pdf.

[34] Decawave. *APPLICATION NOTE: APS011 SOURCES OF ERROR IN DW1000 BASED TWO-WAY RANGING (TWR) SCHEMES*. Tech. rep. 2015. URL: https://www.decawave.com/sites/default/files/resources/aps011_sources_of_error_in_twr.pdf.

[35] Vincenzo Di Pietra et al. "Evaluation of positioning and ranging errors for UWB indoor applications." In: *IPIN (Short Papers/Work-in-Progress Papers)*. 2019, pp. 227–234.

[36] *PDOA Primer Calculating position directly from range and phase difference of arrival at two antenna*. Tech. rep. 2018.

[37] Igor Dotlic. *Angle of Arrival Estimation Using Decawave DW1000 Integrated Circuits*. Tech. rep. 2018.

URL: https://www.decawave.com/sites/default/files/angle_of_arrival_estimation_using_dw1000_online.pdf.

[38] Constantine A Balanis and Panayiotis I Ioannides. "Introduction to smart antennas". In: *Synthesis Lectures on Antennas* 2.1 (2007), pp. 1–175.

[39] Rudolph Emil Kalman. "A new approach to linear filtering and prediction problems". In: (1960).

[40] Greg Welch. "" An Introduction to the Kalman Filter", Univ. of North Carolina". In: *http://www. cs. unc. edu/˜ welch/media/pdf/kalman_intro. pdf* (2006).

[41] Bruce A. McElhoe. "An Assessment of the Navigation and Course Corrections for a Manned Flyby of Mars or Venus". In: *IEEE Transactions on Aerospace and Electronic Systems* AES-2.4 (1966), pp. 613–623. DOI: 10.1109/TAES.1966.4501892.

[42] H Martin Schepers, Daniel Roetenberg, and Peter H Veltink. "Ambulatory human motion tracking by fusion of inertial and magnetic sensing with adaptive actuation". In: *Medical & biological engineering & computing* 48.1 (2010), pp. 27–37.

[43] Daniel Roetenberg et al. "Compensation of magnetic disturbances improves inertial and magnetic sensing of human body segment orientation". In: *IEEE Transactions on neural systems and rehabilitation engineering* 13.3 (2005), pp. 395–405.

[44] Adriano Solimeno. "Low-cost INS/GPS data fusion with extended Kalman filter for airborne applications". In: *Masters of Science, Universidade Technica de Lisboa* (2007).

[45] Joan Sola. "Quaternion kinematics for the error-state Kalman filter". In: *arXiv preprint arXiv:1711.02508* (2017).

[46] Sven Ronnback. *Developement of a INS/GPS navigation loop for an UAV*. 2000.

[47] Nikolas Trawny and Stergios I Roumeliotis. "Indirect Kalman filter for 3D attitude estimation". In: *University of Minnesota, Dept. of Comp. Sci. & Eng., Tech. Rep* 2 (2005), p. 2005.

[48] Martin A Skoglund, Zoran Sjanic, and Manon Kok. "On orientation estimation using iterative methods in Euclidean space". In: *2017 20th International Conference on Information Fusion (Fusion)*. IEEE. 2017, pp. 1–8.

[49] F. Gustafsson. *Statistical Sensor Fusion*. Studentlitteratur, 2010. ISBN: 9789144054896. URL: https://books.google.nl/books?id=yd%5C_2SAAACAAJ.

[50] *Open IMU documentation*. URL: https://docs.openvins.com/propagation.html.

[51] Guobin Chang. "Robust Kalman filtering based on Mahalanobis distance as outlier judging criterion". In: *Journal of Geodesy* 88.4 (2014), pp. 391–401.

[52] Markus Zrenner et al. "Does the Position of Foot-Mounted IMU Sensors Influence the Accuracy of Spatio-Temporal Parameters in Endurance Running?" In: *Sensors* 20.19 (2020), p. 5705.

[53] Mohammad Al-Amri et al. "Inertial measurement units for clinical movement analysis: reliability and concurrent validity". In: *Sensors* 18.3 (2018), p. 719.

[54] Frank J Wouda et al. "On the validity of different motion capture technologies for the analysis of running". In: *2018 7th IEEE International Conference on Biomedical Robotics and Biomechatronics (Biorob)*. IEEE. 2018, pp. 1175–1180.

[55] Miguel Borges et al. "HTC vive: Analysis and accuracy improvement". In: *2018 IEEE/RSJ International Conference on Intelligent Robots and Systems (IROS)*. IEEE. 2018, pp. 2610–2615.

[56] Frances Huxham et al. "Defining spatial parameters for non-linear walking". In: *Gait & posture* 23.2 (2006), pp. 159–163.

[57] Gareth James et al. *An introduction to statistical learning*. Vol. 112. Springer, 2013.

[58] *Stairway regulations OSHA*. URL: https://www.osha.gov/laws-regs/regulations/standardnumber/1910/1910.25.

[59] Jian Wang et al. "UWB positioning algorithm and accuracy evaluation for different indoor scenes". In: *International Journal of Image and Data Fusion* (2021), pp. 1–23.

[60] Yongwei Zhang et al. "High Resolution 3-D Angle of Arrival Determination for Indoor UWB Multipath Propagation". In: *Wireless Communications, IEEE Transactions on* 7 (Sept. 2008), pp. 3047–3055. DOI: 10.1109/TWC.2008.060979.

[61] Anton Ledergerber, Michael Hamer, and Raffaello D'Andrea. "Angle of arrival estimation based on channel impulse response measurements". In: *2019 IEEE/RSJ International Conference on Intelligent Robots and Systems (IROS)*. IEEE. 2019, pp. 6686–6692.

[62] M Sanjeev Arulampalam et al. "A tutorial on particle filters for online nonlinear/non-Gaussian Bayesian tracking". In: *IEEE Transactions on signal processing* 50.2 (2002), pp. 174–188.

[63] Laura Susana Vargas-Valencia et al. "An IMU-to-body alignment method applied to human gait analysis". In: *Sensors* 16.12 (2016), p. 2090.

[64] Alfonso Gomez-Espinosa, Nancy Espinosa-Castillo, and Benjamin Valdes-Aguirre. "Foot-mounted inertial measurement units-based device for ankle rehabilitation". In: *Applied Sciences* 8.11 (2018), p. 2032.

[65] Richard Johnson, Harold Crawford, and Henry Jasik. *Antenna Engineering Handbook*. 2nd. McGraw-Hill Professional, 1993.

[66] Yanhua Ruan and Lang Hong. "Use of the interacting multiple model algorithm with multiple sensors". In: *Mathematical and computer modelling* 44.3-4 (2006), pp. 332–341.

[67] Anil Kumar Khambampati et al. "An interactive multiple model method to identify the in-vessel phenomenon of a nuclear plant during a severe accident

from the outer wall temperature of the reactor vessel". In: *Nuclear Engineering and Technology* 53.2 (2021), pp. 532–548.

[68] Karthik Gopalakrishnan. "Multi model estimators". In: *Papers on the Interacting Multi Model algorithm* 2 (), p. 3.

[69] Anthony F Genovese. "The interacting multiple model algorithm for accurate state estimation of maneuvering targets". In: *Johns Hopkins APL technical digest* 22.4 (2001), pp. 614–623.

VII. List of commonly used abbreviations and acronyms

AoA - Angle of Arrival.
approx - Approximately.
CIR - Channel Impulse Response.
EKF - Extended Kalman Filte.
ENU - East North Up.
GAM - Generalized Additive Model.
GPS - Global Positioning System.
GUI - Graphical User Interface
IMM - Interacting Multiple Model.
IMU - Interial Measurement Unit.
KF - Kalman Filter.
LOS - Line of Sight.
MSE - Mean Squared Error.
NIS - Normalized Innovations Squared.
NLOS - Non Line of Sight.
OSHA - Occupational Safety and Health Administration.
PDOA - Phase Difference of Arrival.
RC - Reinforced Concrete.
RMSE - Root Mean Square Error.
SD / std. - Standard deviation.
TA - Technical Anatomical Frame.
TDOA - Time Difference of Arrival.
TOF - Time of Flight.
TWR - Two Way Ranging.
ULA - Uniform Linear Array
URA - Uniform Rectangular array
UWB - Ultra-wide Band.
w.r.t - With respect to.
ZUPT - Zero Vlocity Update

Appendix I -DecaWave UWB kit

The UWB kit consists of a node and tag transmitting at a central frequency of 6.5GHz with a bandwidth of 500 MHz. The mode of ranging is an asymmetric Two Way Ranging (TWR) which dampens the influence of the clock drift between two devices [33]. The device is capable of accuracies in the order of 10 cm. In addition, the node module consists of two DW1000 chips connected to two UWB antennae. This enables the estimation of the angle of arrival via the path difference of the signal between the two antennas.

In addition, the module utilized - DWM1002 has an integrated 3 dimensional accelerometers, enabling the synchronization with the dot sensors. The UWB kit provides a wide range of information regarding the TWR and the communication channel. Of pertinence to our project are the Channel Impulse response (CIR), the 3-axial acceleration, the TWR result and the received signal strength.

Appendix II- DecaWave PDOA kit re-purposing

The DecaWave PDOA kit provided is a beta/developmental kit recommend and tested for distances larger than 1 meter and for comparatively slow moving objects. In-order to make it viable for walking estimation, we had to re-purpose the DecaWave kit to suit our needs.

The following modifications were implemented in the embedded programme of the DecaWave Node

A. Acquisition of the antenna parameters

The original approach for range bias compensation in the DecaWave kit involved the utilization of the received signal strength. The received signal strength is calculated from the formula

$$rss = 10 * log_{10} * (\frac{C * 2^{17}}{N^2} - A(dbm)) \tag{82}$$

and the First path RSS is given by:

$$rss_{fp} = 10 * log_{10} * (\frac{F_1^2 + F_2^2 + F_3^2}{N^2} - A(dbm)) \tag{83}$$

Where,

rss- Received signal strength (dBm)
rss_fp Received signal strength- Frist path(dBm)
C - CIR power from register 12
N - Preamble accumulation count (with symbol compensation) from register 10
F_n - n^{th} First path point amplitude from registers 12 and 15
A - constant of 121.74 for our PRF of 64MHz

The aforementioned register values are acquired via the SPI read commands and is sent via UART either at the end of the message or along with the Diagnostic mode data. In our close proximity scenario, the receiver faces a premature preamble detection leading to the saturation the RXPACC register culminating in erroneous RSS calculations. For a PRF of 64MHz, the corresponding SFD symbols are −−−−−−+−+−−−−−−+−−+−+−−+−−+−−+−−−++−−−+++−+−+−+−−−+−−+−−−−++00 corresponding to a preamble length adjustment of -82.

B. CIR data acquisition

The CIR data encodes the channel's behaviour and is used to determine the time instances of signal arrival as well as to determine the phase difference of arrival. The CIR data is vital in the diagnosis and rectification of the algorithms working internally in the DecaWave kit.

At the received state, the CIR data was not acquirable. The data transferred from the ACCUMULATOR (register 25)which contained the CIR suffered from data loss and junk values. The enormity of the CIR data (˜4 KB) and our mode of

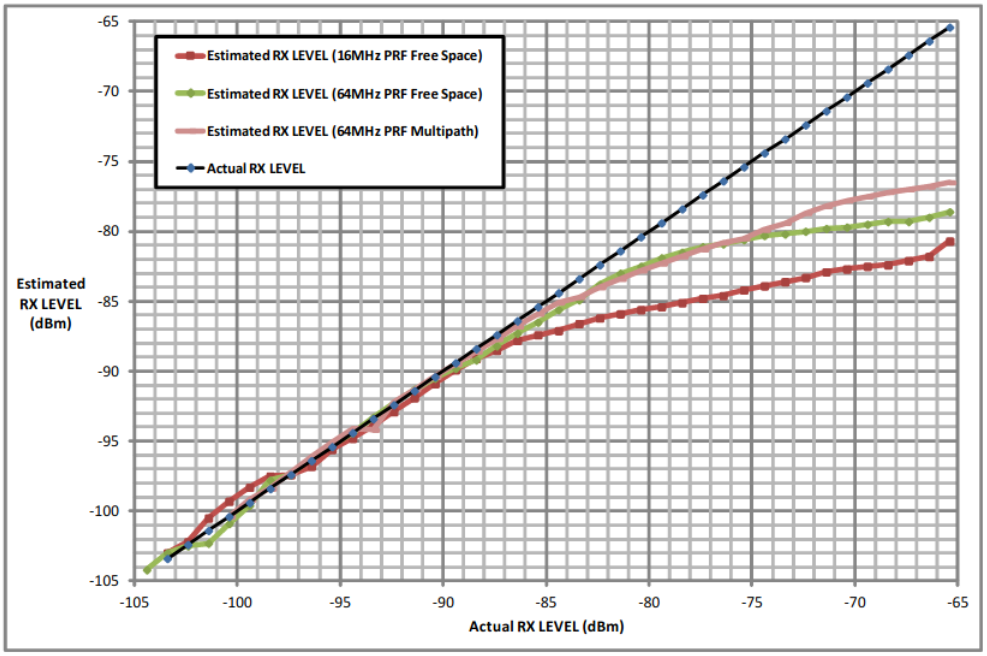

Fig. 21. The bias in the RSS from DecaWaves manual. The graph depicts the estimated RSS vs the true RSS. Of pertinence is the green dotted line which indicates the bias at 64MHz PRF and with minimal multi path.The RSS bias mentioned is restricted to -65dBm which exceeds the minimum RSS expected by our system.

communication (UART @ 115200 baud) was speculated to be the reason for this. This was confirmed after analysing the circular buffer which is used to send the data packets from the node to the PC. It was observed that an insufficient buffer size resulted in its saturation requiring multiple smaller and inefficient packets to send a single CIR reading. Due to the new incoming CIR value, the contents of register 25 (ACCUMULATOR) get replaced before it is sent completely resulting in junk/incomplete data.

The following changes were programmed to optimize the data transfer:

- Decreased the allocated serial transmission buffer size from 0x8000 to 0x400 (The original setting was too large translating to an allocation 32 KB of memory - which due to the limited inbuilt memory available, overlapped with other memory causing junk).
- Increased the size of the linear buffer to 2048, which gathers the next set packet of data.
- Increased the packet size to 2048, thereby minimizing the amount of chunks in which the data is sent.

The following changes to the code ensured a seamless transmission and acquisition of 4096 bytes of CIR data at 2 Hz.

C. Increasing the sampling frequency of the DecaWave kit

While a lower sampling rate might be suitable for fusion if the UWB kits ranign data with the IMU sensors, it would be very hard to synchronize both sensors at lower sampling rates as our synchronization is based on the correlation between the accelerometers in the tag and the dot sensors.

A normal walk cycles acceleration frequencies range from 0 to 5Hz typically necessitating a minimum sampling rate of 10Hz. While the DecaWave kit offered a sampling rate of 10Hz by default for its ranging mode, it was insufficient to synchronize both sensors due to the higher frequency peaks from jumping used for synchronization.

To increase the sampling frequency, we tried to increase the rate at which data was being sent. An increase int eh baud rate had no impact on the sampling frequency

An increase in the sampling frequency to 50Hz was achieved by decreasing the MAX_KNOWN_TAGs and MAX_KNOWN_TAGS_LIST to 1 and 2, thereby decreasing the time the DecaWaves TWR algorithm waits for any other connected tags to respond. Apart from this, we decreased the time for each super frame (a superframe can be considered as the structured data being sent at each iteration of TWR) to 10ms, thereby increasing the sampling frequency to 50 Hz.

This resulted in an accelerometer signal comprising all the peaks and points of interest in the walking signal, resulting in a much better synchronization via correlation.

APPENDIX III -XSENS DOT

The Xsens DOT is an IMU sensor consisting of a tri-axial accelerometer and a tri axial gyroscope sampled at 60Hz. The communication to our Raspberry Pi server is conducted via Bluetooth - with the transmitted packets comprising Free Acceleration, Euler orientation and Angular velocity in the East North Up frame (ENU). The DOT boasts of a synchronization capability, which enables multiple dot sensors to sample in sync with each other. In addition, it provides a heading reset

Fig. 22. The sensor frame of reference. The X axis is along the long edge, the Y axis along the short edge and the Z axis points outward.

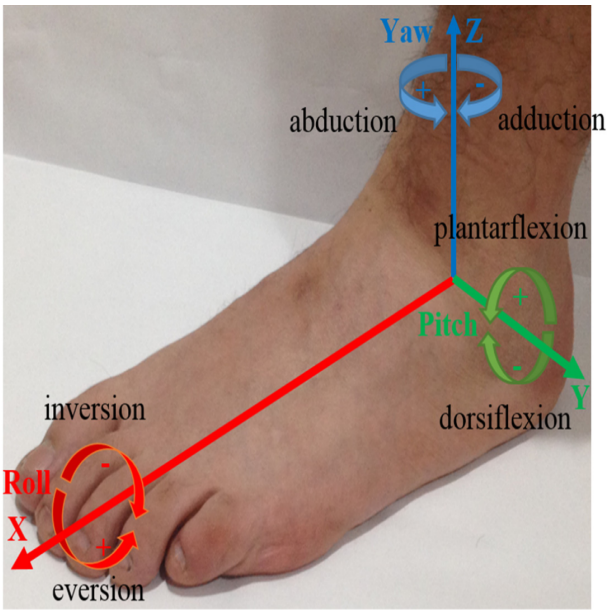

Fig. 23. The technical anatomical frame (X, Y, Z) from [64]

ability, wherein the heading of the sensor is aligned with the body segment (in our case, along the foot).

D. DOT Frames of reference

Currently, the Free Acceleration obtained is in the ENU frame. To ensure that our frame of reference is in the segment frame, we are rotating the acceleration in accordance to the technical anatomical (TA) frame of the foot [63].

The sensor's frame of reference is aligned to the TA frame by orienting the X axis along the heading and parallel to the ground, the Z axis parallel to gravity and the Y axis mutually perpendicular to both, pointing left.

To align the sensor to the TA frame, we exploit the assumption that in the foot flat position, the sensor's acceleration is exclusively the gravitational one. Another assumption (as a result of the sensors being mounted on a chassis) is that the sensor frames heading is parallel to the heading of the foot. Hence, a quaternion linking the acceleration vector in the sensor frame at foot flat and the gravitational vector would align the sensor frame to the TA frame.

A multiplication of the quaternion linking the ENU frame to the sensor frame and the sensor frame to the TA frame results in a quaternion linking the ENU frame to the TA frame. This is used to rotate all the subsequent Free Acceleration in the ENU frame to the TA frame.

For the validation of the drift, in order to zero in on the source, we used the Xsens Dot app to record the IMU data on board the DOTs and used the Acceleration signal exported from it for analysis. In addition, the Acceleration in the sensor frame is used in the filter. The TA frame is used to make the foot flat stance detection easier. In addition, the TA frame is used as an alternative to the ENU frame to set the initial orientation R_{gs}.

APPENDIX IV -DATA ACQUISITION / SYSTEM INTEGRATION

The data from the UWB and DOT sensors are acquired via a Raspberry Pi3 B+ running on the Raspbian OS. The UWB kit is interfaced with the Pi by means of UART communication at 115200 baudrate in Python3.

As a result of the delays in the TWR as well as data transmission, the sampling frequency of the UWB kit is approx. 50Hz while providing the ranging and IMU data, and approx. 7Hz while extracting the CIR data for the angle of arrival determination.

As mentioned in the prior section, the DOT sensor interfaces with the PI via Bluetooth. The Xsens DOT server for the raspberry PI3+ provides a GUI interface for connecting and acquiring the dot data. The server was tweaked to acquire the required parameters and the GUI event handling was automated via using the JavaScript interfacing library - selenium in Python 3.

The data acquisition is preceded by configuring the DOT server to sync and reset its heading.

After the server's initialization, the TWR is initialized in the DecaWave kit with the preset parameters. The synchronization between the UWB kit and the DOT sensor employs the cross correlation between the acceleration signals from the IMUs present in the DOT and the tag to find the lag. The synchronization methodology is elaborated in the signal processing algorithm part of the report.

An entire python3 based server was built to configure, debug, run and parse the UWB and DOT acquired.

APPENDIX V -SIGNAL PROCESSING

The signal processing for the sensor data comprises steps which ensure that we obtain a relatively noise free and viable

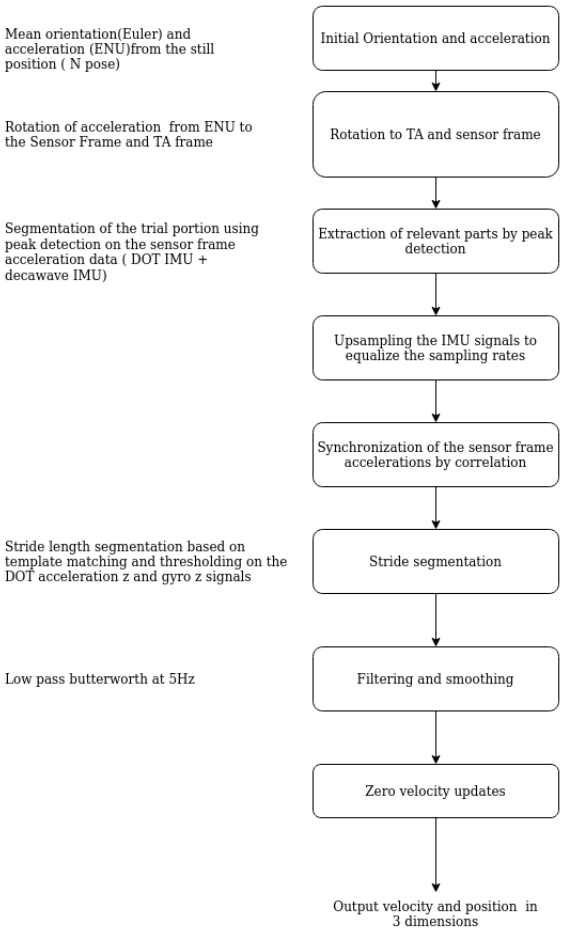

Fig. 24. An overview of the signal processing algorithm

data which consists of the required walking. This consists of a frame of reference rotation, walking segmentation, sensor synchronization and the Zero Velocity Update.

A brief overview of the signal processing steps are as follows,

1) The first 5 seconds of the data (the still period) is averaged to get the mean orientation and acceleration.
2) The acquired orientation and acceleration is aligned with the TA frame of the foot.
3) From the DOT and DecaWave acceleration norms, using peak detection we identify the jump instances and extract the enclosed walking signals.
4) The DecaWave IMU is up scaled to the sampling frequency of the DOTs using a rudimentary interpolation filter.
5) This is succeeded by synchronization of the sensors, which involves locating the point of maximum correlation between the interpolated DecaWave IMU and the DOT acceleration signals. The point of maximum correlation provides the lag, and the corresponding number of DOT samples are shifted forward or backwards by zero filling in the beginning or the end of the signal.
6) This is followed by the stride segmentation, wherein the Gyroscope velocity along the sagittal plane (Z axis in our case) and the Z axis Acceleration is used to find the foot flat regions. This in corroboration with a template matching algorithm is used to decompose the walking signal into a series of steps
7) The signal is filtered with a Butterworth 4th order low pass filter of cutoff 5Hz to eliminate any high frequency jitters which might adversely affect our calculation.
8) The zero velocity update algorithm [18] is performed on each step and the resultant position is used for further processing.

Note: Sometimes, the main synchronization is not enough to handle lags less than a 0.25 seconds. In this case, we opt to redo the lag estimation via cross correlation to the segmented walk signal.

E. Zero Velocity update

The position of the IMUs are acquired by the double integration of the accelerometer signal. The main assumption behind the Zero Velocity update [18] (ZUPT) is that during foot flat phases, the velocity of the foot is considered to be 0 and the foot is considered to be aligned parallel with the ground and gravity. To minimize drift and other possible sources of error in the orientation, at each detected foot flat position, the velocity of the foot is set to 0 and the orientation is reset to 0.

In addition, since the velocity at the termination of each FF position is 0, a linear drift function is implemented and is utilized to compensate for any possible drift in the velocity, thereby improving any drift in the calculated position.

APPENDIX VI -ANGLE OF ARRIVAL AND LOCALIZATION

Angle of arrival from the perspective of the receiver is the angle of incidence of a signal from a transmitter. In the figure shown below (Figure 25) the AoA is θ and is based on an impinging planar wave. A planar wave is a wave which propagates parallel to each other and is usually perpendicular to the direction of propagation. Any signal which propagates from the far field (for a carrier at 6.5GHz and an antenna diameter of 2.5 cm, the far field starts at 2.5 mm). Due to the spacing difference between antennae, the antenna closer to the source acquires the signal a bit earlier than the distal antenna. This difference in the time of acquisition corresponds to a wavenumber, which when expressed in distance, gives us the path difference of arrival, and in terms of phase, the phase difference of arrival (PDOA).

In the Figure 25 ,

ψ - Phase difference between successive antennas
θ - Angle of incidence of the planar wave with respect to the normal from the antennas
N - Antenna number
d - Antenna element spacing (successive antennas. In our case, 2.08 cm)
β - Wave number vector

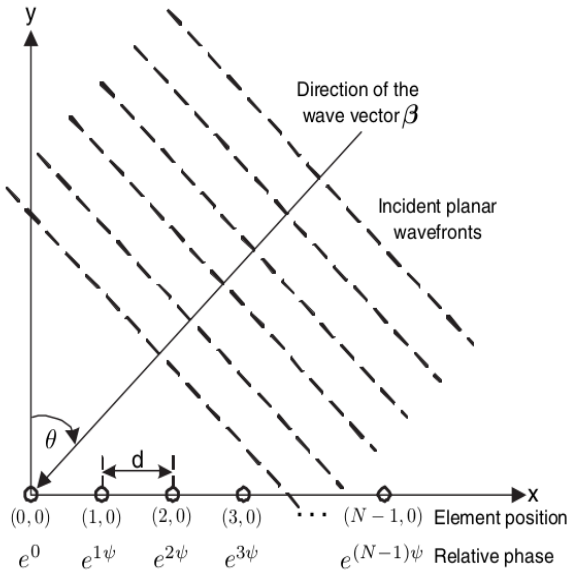

Fig. 25. The angle of arrival θ from the perspective of a receiver antenna array with N elements. Figure from [38]

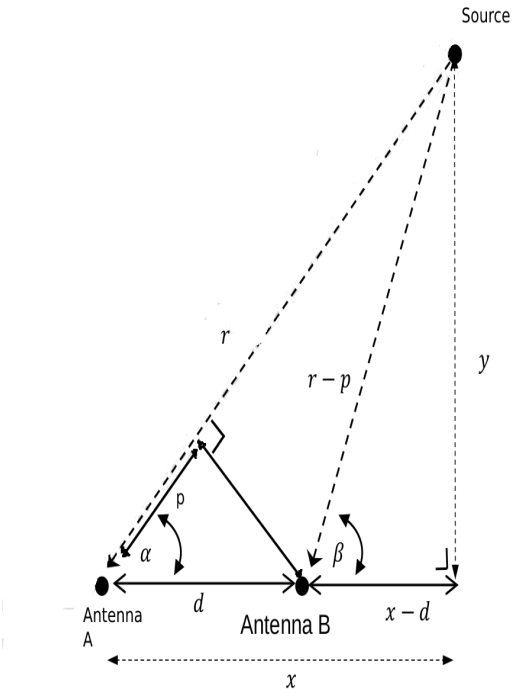

Fig. 26. The Angle of Arrival based decomposition of the range into X and Y coordinates from the DecaWave manual [36].

In our case, we know Phase difference(ψ), element spacing (d), wavelength (λ) and using the following equation, the AoA can be estimated by:

$$\psi = 2 * \pi * d * \frac{sin\theta}{\lambda} \tag{84}$$

Therefore, by rearranging we get:

$$\theta = sin^{-1}\frac{\psi * \lambda}{2 * \pi * d} \tag{85}$$

For the Decawave kit, the PODA is measured in degrees, ranging between $\pm 180°$. In terms since the UWB channels central frequency and the speed of light are known, the equation 85 can be rewritten as

$$\theta = sin^{-1}(\psi * \frac{c * pi}{2 * 180 * f * d}) \tag{86}$$

From the acquired path difference, it is possible to localize the range measured into its X and Y coordinates. This of course, is in 2D scenarios, for 3D scenarios the derivation is provided in the AoA bias compesation section of this paper.

In figure 26

r - Distance between the antenna and source (UWB ranging distance)
p - Path difference
α - Angle of arrival with respect to the antennae
x - Cartesian X distance from the antenna
y - Cartesian Y distance from the antenna

The path difference p can be calculated from the incident angle θ and the spacing d by:

$$p = d * cos\theta \tag{87}$$

From which, the y coordinate can be derived as

$$y = \pm(r - \frac{p}{2}) * (1 - (\frac{p}{d})^2) * 0.5 \tag{88}$$

And the x coordinate is

$$x = \pm(r^2 - y^2)^0.5 \tag{89}$$

VIII. Appendix VII - Bias evaluation and compensation in the UWB kit

A. Range Bias in the DecaWave Kit:

The DecaWave ranging kit has an inherent range bias which is a function of its received signal strength (RSS)[34] as shown in figure 27. At higher strengths i.e. at close proximity, we postulate that the sensors exhibit errors sourcing from the antenna design or from the thresholds and parameters in the device, causing distortions in the ranging functions of the kit. The chance of the signal being received at high RSS due to the proximity of the feet to each other while walking(approx. 20 cm to 70cm) is high. This warranted an investigation into the sensors range biases.

While the inserted figure 27 from DecaWave might portend a straight-forward solution, an additional layer of complexity is faced in the Received signal strength estimation(RSS). The estimated RSS calculated from the DecaWave kit's registers suffer from a bias at strengths more than -85dBm21. In contrast, the minimum calculated RSS for our system (at a step length of 1 m) by using the Friis formula is -63.01dBm [32].

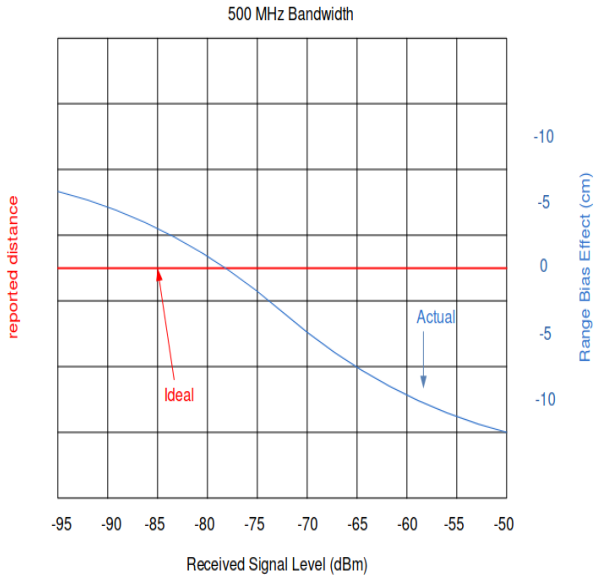

Fig. 27. The range bias as a function of the received signal strength from DecaWaves manual

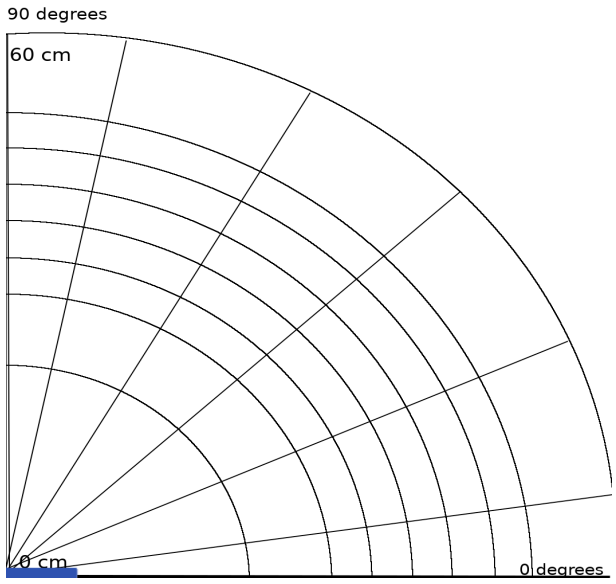

Fig. 28. The UWB characterization measurement setup. The blue line at the bottom depicts the node. The node as been aligned in a way that the 90 degree line bisects the node's antenna array. The furtherest arc depicts 60 cm and the closest one is 15 cm. Each arc (apart from the first and last) is drawn at a radius increment of 5 cm. regarding the angles, the line along the longer axis of the node depicts 0° (periphery) and the one perpendicular to it is 90°. The tag is placed at each intersection and the corresponding ranging and AoA results are acquired.

Further experimentation was conducted to estimate the range bias based on the estimated range, and the approach was discarded due to the following reasons:

- Unreliable RSS estimates (significant amount of noise).
- The RSS bias is not fully charted for RSS's smaller than -65dBm in the DecaWave kits manuals. Due to noisy RSS estimates the formulation of an experimental model using measured RSS vs ideal RSS was unsuccessful.
- The RSS estimates are more susceptible to extrinsic environmental factors than the distance estimates.

Since the RSS is a function of the distance measured (by extension of the Friis formula)[65], an alternative is to compute the range bias as a function of range. To evaluate the bias in the ranging measurement, a setup as shown in the figure 28 was devised. In order to evaluate the range bias, a manual measurement of the estimated range from 15 cm to 60 cm and at various angles from 0 degrees to 90 degrees was acquired and used to formulate the range bias model. The measurements were conducted at different angles in order to ascertain the dependence of the ranging function on the AoA. The basis of the dependence of the range on the angle is the antenna parameters (like non-uniform gain) or occlusion related issues in the periphery. The resultant graphs acquired from the evaluation setup is depicted in figure 29. Figure 29 depicts the measured range at various angles. Each angle at which the evaluation was performed is plotted as an individual subplot. The last subplot titled 'overall' is the compilation of range measurements from all the measured angles.

From the inset, it can be seen that at angles close to 90°, the slope of the measurement compared to the ground truth is minimal, while towards the periphery (10°) the slope is steeper. The last subplot depicts the overall (at all angles combines) mean and standard deviation.

The range bias is defined as the difference between the true range and the measured one from the UWB kit, formulated as:

$$rb = r - r_{UWB} \tag{90}$$

where,

r - The measured distance between the node and tag (m).
rb - the bias in the measured range at a particular range (m).
r_{UWB} - is the UWB distance measurement(m).

In addition, the measured range has been compared with the ground truth in order to compare the performance of the UWB kit while walking as depicted in figure 32.

B. Range bias compensation

DecaWave provides a rudimentary range bias compensation methodology based on the measured distance. Further assessment of DecaWaves range bias compensation methodology indicated that at distances less than 1 meter, it involved the addition of a constant offset value of 17 to the measured distance. This rudimentary mode of compensation is not suitable for applications involving a significant modicum of precision. Since the difference in the measured values vs the truth appears to be linear, we fit the measured range bias with the true range (r) using a polynomial resulting in the following model for the range bias (rb):

$$rb = 0.355 - 0.251 * r \tag{91}$$

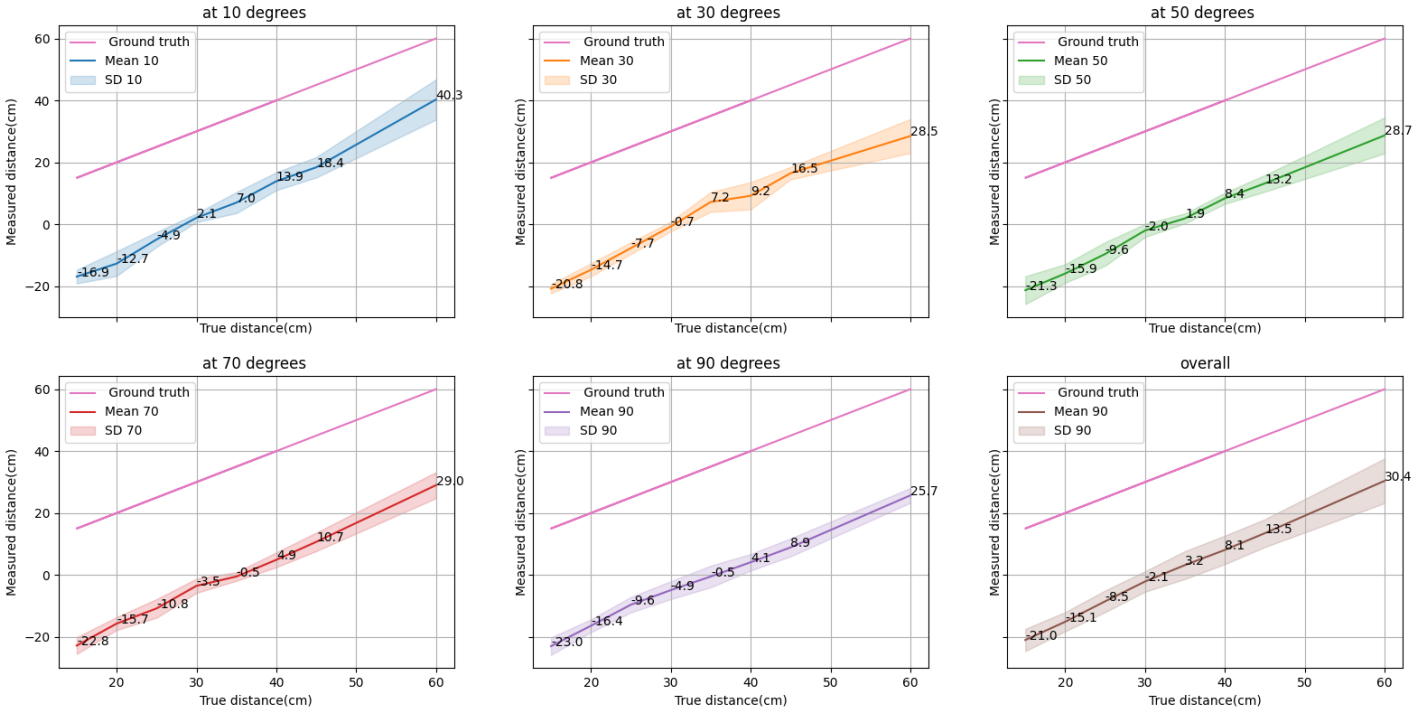

Fig. 29. The range measured at various angles. The annotations along the line depict the measured range (cm) at the ground truth ranges (Y-axis). At a fixed distance between the node and tag, the tag is moved through an arc encompassing angles from 10 to 90 degrees and is plotted against the ground truth. The last graph titled overall is the combination of the measurements from all the preceding graphs, and represents the ranging performance of the UWB kit at angles from 10 to 90 degrees .

From equation 90 and equation 91, we get:

$$r - r_{UWB} = 0.355 - 0.251 * r \tag{92}$$

The resulting fit is depicted in the figure 30, and the Root Mean Square Error (RMSE±SD) of the fit was approx 21±23cm. At any given instance, the range is estimated by the filter using the position of the feet. Availing this information would enable the development of a sensor fusion algorithm to compensate for the bias.

In addition, it is possible to fit the range bias with the measured distance, by means of a linear polynomial. The RMSE of this fit was slightly higher at 23±24cm.

$$rb = 0.29 - 0.214 * r_{UBW} \tag{93}$$

The current section involving the characterization of the UWB kit, resulted in two viable strategies to compensate for the bias in the range, namely:

1) An EKF based range bias estimation model, where the estimated range is used to find the range bias
2) A statistical polynomial model which can be used externally (without the filter) to compensate for the range bias

This paper proceeds with the in-filter range bias model due to the potential prospects for tuning and adjustments in accordance to the situation/state of the filter. In addition, for the sake of practical real time implementation and as a reference, a linear polynomial fit based external model is tested. While the incorporation of these models is explained in the methodology, the results are shown in figure 13 for the external bias compensation model and 33

C. Angle of arrival bias

The basis for the angle of arrival in a Uniform Linear Array (ULA) of antennas is explained in the Appendix section (Appendix VII- Angle of arrival and Localization) of this report. In an ideal scenario, the ULA components are assumed to have 0 coupling and to have uniform gain. However, this is not possible. To compensate for the antenna parameters, the polynomial prescribed by DecaWave [36] has been used to correct the path difference.

It is given by:

$$pd_{corr} = -14205 + 419 * pd + 4.59 * pd^2 + 0.8361 * pd^3 \tag{94}$$

where,

pd_{corr} - corrected path difference in cm.
pd - measured path difference in cm.

In this paper, the tag antenna is assumed to be omnidirectional and the errors due to its antenna parameters and ori-

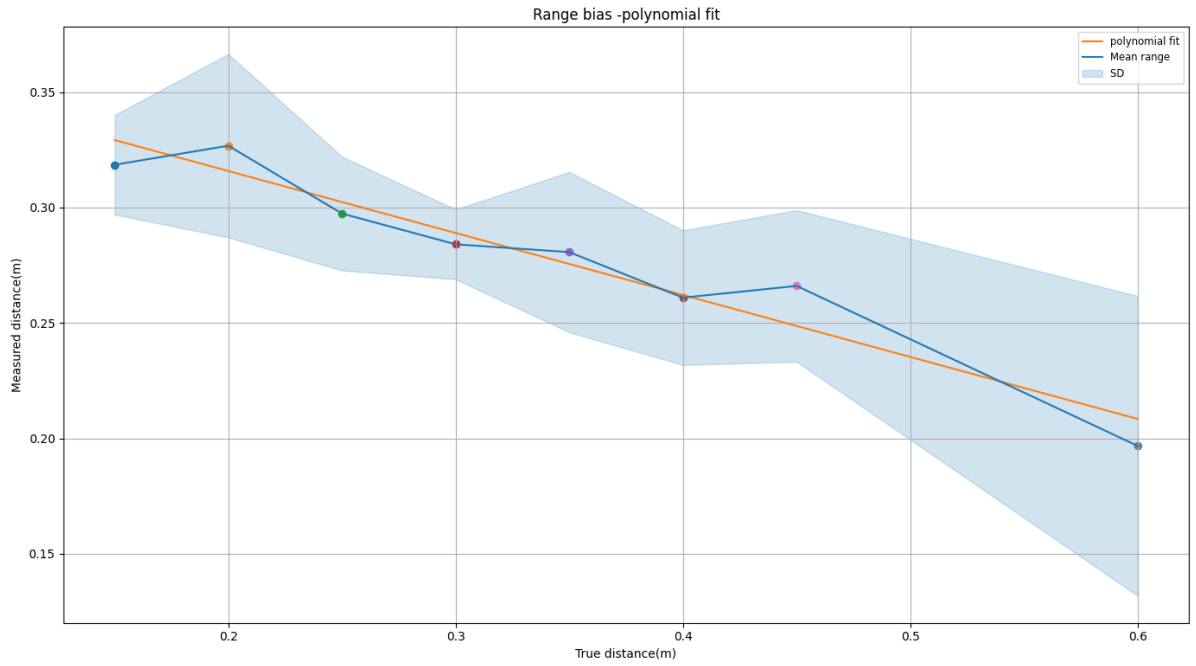

Fig. 30. The polynomial fit range (orange) plotted alongside the bias in the measurements(rb). The polynomial fits the measured range bias with the true range, thereby providing an avenue to compensate for the range bias by means of the estimated range from the filter. The RMSE(SD) of this fit is 21±23cm

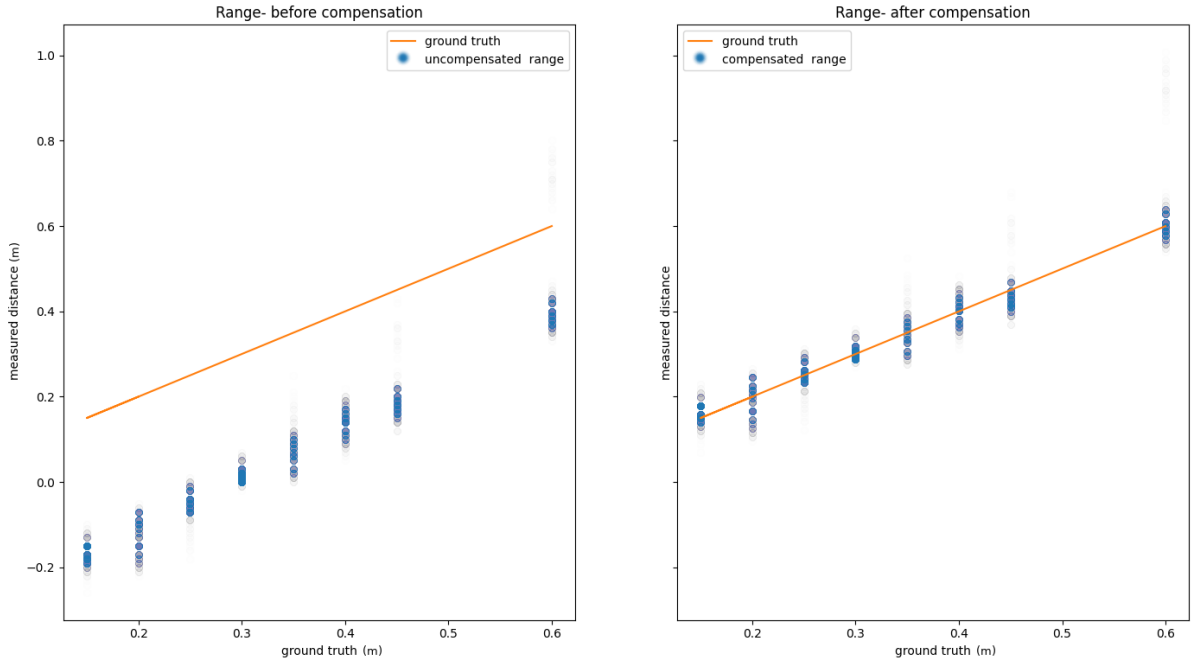

Fig. 31. The range measurements from the DecaWave kit before compensation(left) and the corrected range measurements based on the fit in Figure30. The fit for the external bias compensation model is also very similar.

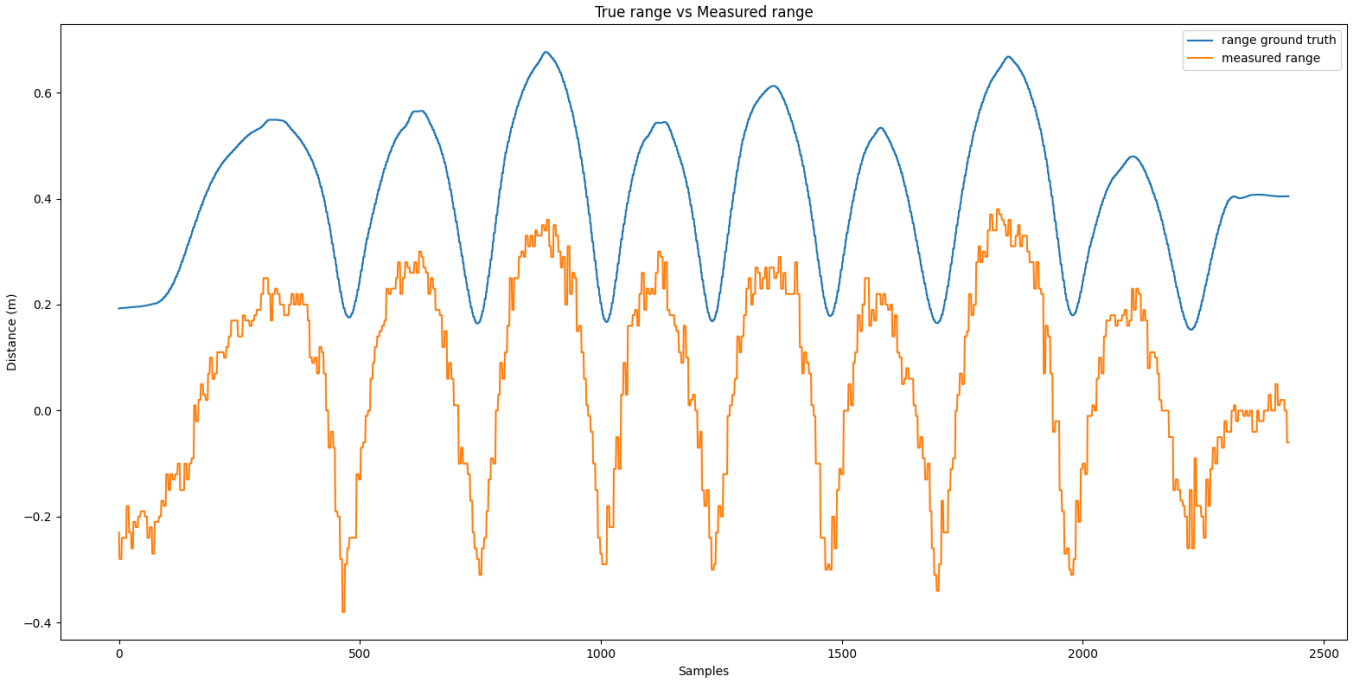

Fig. 32. The measured range (orange) plotted alongside the ground truth for a walk comprising 9 steps. Each peak represents a foot flat position of a foot, and each valley indicates the point where the feet are parallel to each other. There is a dominant offset paired with higher order terms. The effect of the polynomial components are apparent in the Foot flat and foot parallel states (minima and maxima of each step) where it appears to be stretched.

entation is considered negligible and is excluded. Conversely, the orientation of the node is considered and compensated for, since the ranging and angle of arrival is dependent on the node antenna array's orientation. The viability of the AoA measurements in different walking phases is computed, and the relevant biases and compensation mechanisms are discussed in the following sections.

Apart from the antenna parameters, we expect an ambiguity / anomalies in the AoA in the following scenarios:

1) Node and tag are collinear - i.e. When the AoA is close to 0 or 180°. This scenario would occur when the distance between the feet are maximum and while navigating corners.
2) Fluctuations/ phase difference reversals when the tag is behind the node (i.e. 3rd and 4th quadrants). This phase reversals manifest as a flip in the sign of the AoA measured. A visualization of this error is seen in figure 39. In the figure 39, using the AoA measured, the range measured is decomposed into its X and Z distances (sensor frame). Whenever the Z distance drops below 0, there is a corresponding flip in the magnitude of the X distance. The underlying reason is that the PDOA would be flipped due to the order in which the RF signal impinges on the antenna array.
3) Elevation angles - Due to the mounting method, the antennae experience tiling while walking. This tilt causes the incoming signal to have an elevation angle. Apart from the tilt, an elevation angle is also introduced due to the difference in the height between the node and the tag. Since the antennas in the UWB kit are constrained to a ULA along the azimuth, the elevation angle cannot be measured. An elevation might pose issues to the AoA estimation's efficacy. This scenario is likely during the toe off phase of the right foot (the foot with the node) when the foot has a maximum amount of tilt. The left foots (the foot with the tag) tilt is ignored under the omnidirectional antenna assumption. The orientation estimate of the right foot could be used to gauge the elevation angle, and the viability of this method is discussed in the following sections.

D. Evaluation of the AoA performance in the azimuth

In this scenario, the AoA capacities are evaluated in two dimensions (the node antenna's azimuth). The anchor is located in a center while the tag is being placed at known positions and angles. The difference between the true angle measured one is used to ascertain the bias in the AoA measurements. In the following section, in order to evaluate the AoA's accuracy, we use the ground truth distance for all computations.

Fig. 33. UWB range data after compensation using an external model: The measured range with the bias being compensated by using a polynomial model based equation 93, overlaid with the ground truth)

Fig. 34. UWB range data after compensation using the range bias estimates from the filter (Filter 3) vs ground truth: The measured range with the bias being compensated by adding the estimated range bias from the filter, overlaid with the ground truth)

To evaluate the AoA performance, we measured the AoA estimated by the UWB kit at known AoAs of 10 to 90 degrees. In addition, to model the AoA behaviour at sun 50 cm ranges, we perform the angle measurements at distances from 15 cm to 60 cm. (as in figure 28)
Barring some aberrations, the standard deviation increases as the tag moves towards the periphery (from 90 to 0°). This is mostly due to the partial occlusion of the signal from one of the receiver's antennae. We expect this scenario to occur around every Foot flat event. A standard deviation of around 15° were observed at the maximum. In addition, due to variations in the gait and during nonlinear walking and due to the location of the UWB mount, the foot with the tag has a chance to go behind the antenna's plane of measurement. This might cause erroneous range and phase measurements.

E. Evaluation of AoA performance with a variation in the distance

The following fluctuations and errors is visualized in figure 35. For reasons believed to be based on the method by which the phase difference is compensated and calibrated in the decawave kit, the measured phase difference of arrival (pdoa) and by extension the AoA faces a phase reversal (ex: an actual value of 30° is reflected as 150° at ranges below 30 cm frequently, which manifests as an increase in the standard deviation of the angle measurements at distances ranging between 25 and 35 cm (fig 35 subplot 3 titled 25 cm). In addition, there is a noticeable deviation in the measured AoA in the same band, towards the periphery. The readings at larger angles (towards 90°) tend to be more accurate. The accuracy at 90° is attributed to minimal fluctuations in the measured PDOA.

F. Evaluation of AoA performance in the presence of an elevation angle (3D evaluation)

As mentioned previously, the height difference between the node and tag presents an elevation angle. This elevation angle causes a disruption in the measured AoA in the azimuthal plane. Apart from the height difference, the inclination of the foot with the node is a factor in the perceived elevation angle. A decomposition of the geometry behind the effective elevation angle perceived by the node is depicted in figure 37.
During an average gait cycle, the IMU on the foot undergoes a rotation of around $40/degrees$ in the sagittal plane (θ_y). Under the assumption that the IMU and the node share the same sensor frame, the node gets titled through the same range of angles θ_y as well. This rotation introduces an elevation angle, which skews the AoA measured.
To evaluate the effect of the tilt (θ_y) on the measured AoA, we compute the relation between the tilt and the height difference between the tag and the node (z_{diff}) by means of basic trigonometric identities. This relation was computed since it is difficult to precisely vary the tilt of the node for testing and evaluation. A more intuitive visualization of the elevation angle from the nodes frame of reference is provided in Appendix XIII, containing figures 43 and 44. In cases where the node is not tilted and is flat on the ground like our experimental setup:

$$z_{diff} = 0 \tag{95}$$

Therefore,

$$z_{height} = sin(\theta_y) * Xdistance \tag{96}$$

where z_{height} is the height subtended by the angle 90-$theta_y$ as shown in figure 37. In the experiment conducted to measure the effect of the tilt on the measured AoA (Figure 38), the z_{height} is varied in place of $theta_y$. This experiment is further discussed below.
In a scenario where the node and the tag are on the same azimuthal plane (absence of an elevation angle), the AoA measured by the UWB kit is denoted by

$$AoA = sin^{-1}\frac{Xdistance}{range} \tag{97}$$

In the above scenario, X distance = X_{UWB} due to the lack of an elevation angel.
When there is a height difference(z_{diff}) and thereby an elevation angle (phi) between the node and tag, the measured AoA would be

$$AoA = sin^{-1}\frac{X_{UWB}}{range} \tag{98}$$

where X_{UWB} is obtained using the AoA and the elevation angle as

$$X_{UWB} = range * cos(AoA) * cos(phi) \tag{99}$$

To find the elevation angle phi, the following trigonometric decomposition is performed. Considering the right angle triangle formed with z_{diff} and a projection of the X distance onto the ground plane as the sides and the range in the XY plane (sensor frame) as the hypotenuse, we get

$$psi = atan2(\frac{X_{distance}}{range_xy}) \tag{100}$$

$$phi = \frac{\pi}{2} - psi - \theta_y \tag{101}$$

In terms of θ_y and z_{height}, by the law of sine's:

$$\frac{sin(phi)}{z_{height}} = \frac{sin(\frac{\pi}{2} - \theta_y)}{range_{xy}} \tag{102}$$

Rearranging we get,

$$phi = sin^{-1}(\frac{sin(\frac{\pi}{2} - \theta_y)}{range_{xy}}) * z_{height} \tag{103}$$

Which again is, by substitution:

$$phi = sin^{-1}(\frac{sin(\frac{\pi}{2} - \theta_y)}{range_{xy}}) * sin(\theta_y) * Xdistance \tag{104}$$

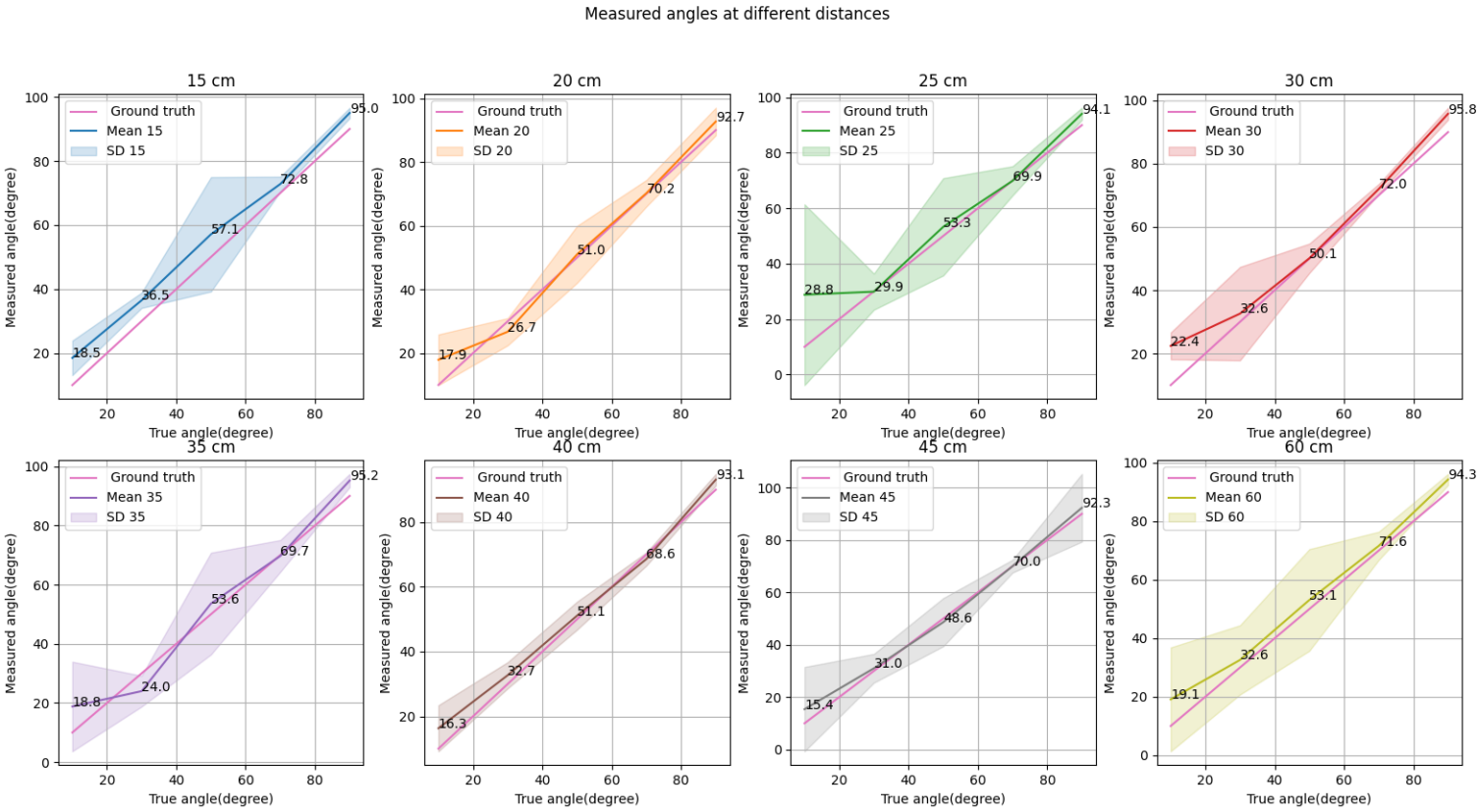

Fig. 35. The angle of arrival estimated by the DecaWave kit at various known AoAs and distances. The point of interest in these graphs is the measurements in the 25 cm to 35 cm band where the mean standard deviation is higher than normal and there is a significant deviation in the mean towards the periphery (10°). The annotations along the lines indicate the measured AoA in ° for the corresponding ground truth AoA values.

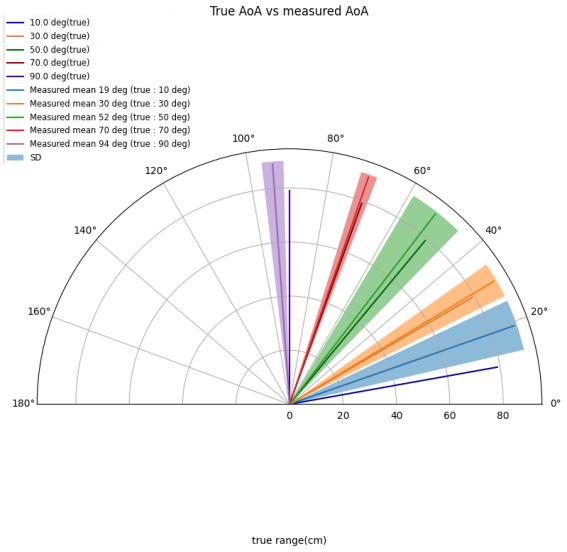

Fig. 36. The overall mean and standard deviation of angle of arrival estimated by the DecaWave kit at various known AoAs and distances in terms of a polar plot. While this figure is suitable for a generalized overview of the AoA performance, for fine-tuning and tweaking Figure 35 is referred to.

where $range_{xy}$ is the range in the XY (sensor frame) plane. Therefore, when θ_y is small, the resulting elevation angle ϕ becomes small, leading to the effect of the elevation angle being negligible.

To further improve the viability of the AoA measurements for gait analysis, using the filter state estimates (the filer would be described in the following sections), the quanta required to compensate for the bias in AoA due to the elevation angle can be computed. From the figure 37,

$$X_{UWB} = range_{xy} * cos(phi) \tag{105}$$

The corresponding bias compensated AoA measurement from the filter states would be

$$z_{AoA} = \sin^{-1} \frac{X_{UWB}}{range} \tag{106}$$

Combining eq 105 and eq 106,

$$z_{AoA} = \sin^{-1} \frac{range_{xy} * cos(phi)}{range} \tag{107}$$

Since the aforementioned bias compensation method (eq 106)uses the filter state estimates to compute the bias,

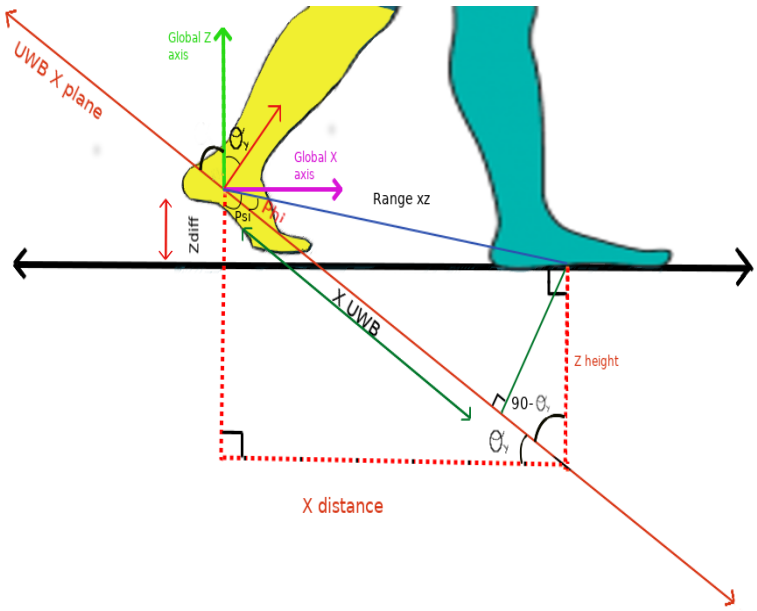

Fig. 37. The trigonometric derivation of the actual X distance between the feet and the height of the intercept between the UWB X plane and the project tag position in that plane. Using the decomposition in this figure, the elevation angle (ϕ) is determined from the tilt of the right foot (θ_y), the AoA and the measured range.

there is a possibility of erroneous bias estimates in case of trial instances with a particularly large amount of drift. In this scenario, a threshold to ignore the AoA measurements is implemented. Due to the dependence of the elevation angle (phi) on the tilt of the foot θ_y a threshold based on θ_y is utilized.

The measured azimuthal angle (AoA from the decawave kit) at various heights(z_{height}) as per the discussion preceding eq 96 is depicted in figure 38. Since the distance between the node and the tag is fixed in the horizontal plane in this experiment, any measurements made by varying the height would correspond to an increase in both the tilt and the elevation angle. As the azimuthal plane of AoA measurement is parallel to the sensor's XZ plane, the errors or biases in the AoA measurement due to the elevation angle would correspond to a particular tilt angle. For the evaluation in Figure 38, we fix the range in the global XY frame to 60 cm and vary the height ($z_{height} + z_{diff}$) from 8 cm to 32 cm. This experiment resulted in significant deviations at a height of 32 cm, rendering it unusable. The measurements at 25 cm showed significant deviations at angles less than 20°. The experiment, repeated at multiple azimuthal angles (0 to 90 °), indicated a robust estimation of the AoA in the UWBs plane till the height of 16 cm or tilt of 16°.

G. Erroneous AoA measurements due to the gait

Due to our assumption that the subjects walk non-linearly, it is prudent to analyse the effect of the gait on the measured angle. In the figure 39, the pitch of the right foot (θ_y) is plotted against the variation in the relative foot position in the sensor's X and Z axis. The X axis distance in the sensors frame represents the forward-backward motion of the foot (the swing). On the other hand, the Z axis distance in the sensors frame depicts how close the feet get to each other.

From the graphs in figures39 and 40, the instances where the X and Z distances are erroneous can be deciphered. Upon further inspection, these instances correspond to when the Z axis distance falls below 0. Intuitively, this indicates that the left foot goes behind the right foot. As we know that the AoA is constrained to the Quadrants I and II i.e. The AoA is valid only when the tag is in front of the node's antennae, any traversal beyond this plane (Quadrants III and IV) would cause errors (in this case, the angle would be flipped due to the since the antenna considered to be the distal one for computational purposes would be considered the proximal, and hence would be inflicted by a -ve multiplier).

An appraisal of the angles corresponding to this event indicates that the flipping coincides with the pitch angles of the right foot dipping below 0. i.e. This event occurs right before a foot flat event, when the right heel strikes the floor.

H. Angle of arrival bias compensation

This section describes the measures taken to combat the bias or error in the AoA measurements. The points below discuss the error observed and the action taken to combat the error.

a) Increase in uncertainty of AoA measurements towards the periphery: To compensate for the increase in the standard deviation of the measurements (i.e. the measurements are noisier), we adjust the measurement noise to be in proportion to the maximum standard deviation. Although the other less acute angles (angles between 90 ° to 20°) might be more accurate, those angles are expected only when the feet are parallel to each other.

From the measurements, it was observed that the standard deviation increased from 5 ° to 20 ° corresponding to the AoAs at angles from to 90 ° to 20°, depicting a four-fold increase in the measurement noise. This was modelled by mapping the noise values with a coefficient given by:

$$AoA_{noisemultiplier} = (|AoA| * \frac{\pi}{2} + 0.5) \quad (108)$$

The corresponding measurement noise would then be

$$R_{noise,AoA} = AoA_{noisemultiplier} * R_{noise,AoA} \quad (109)$$

where,

AoA - Angle of arrival in radian.

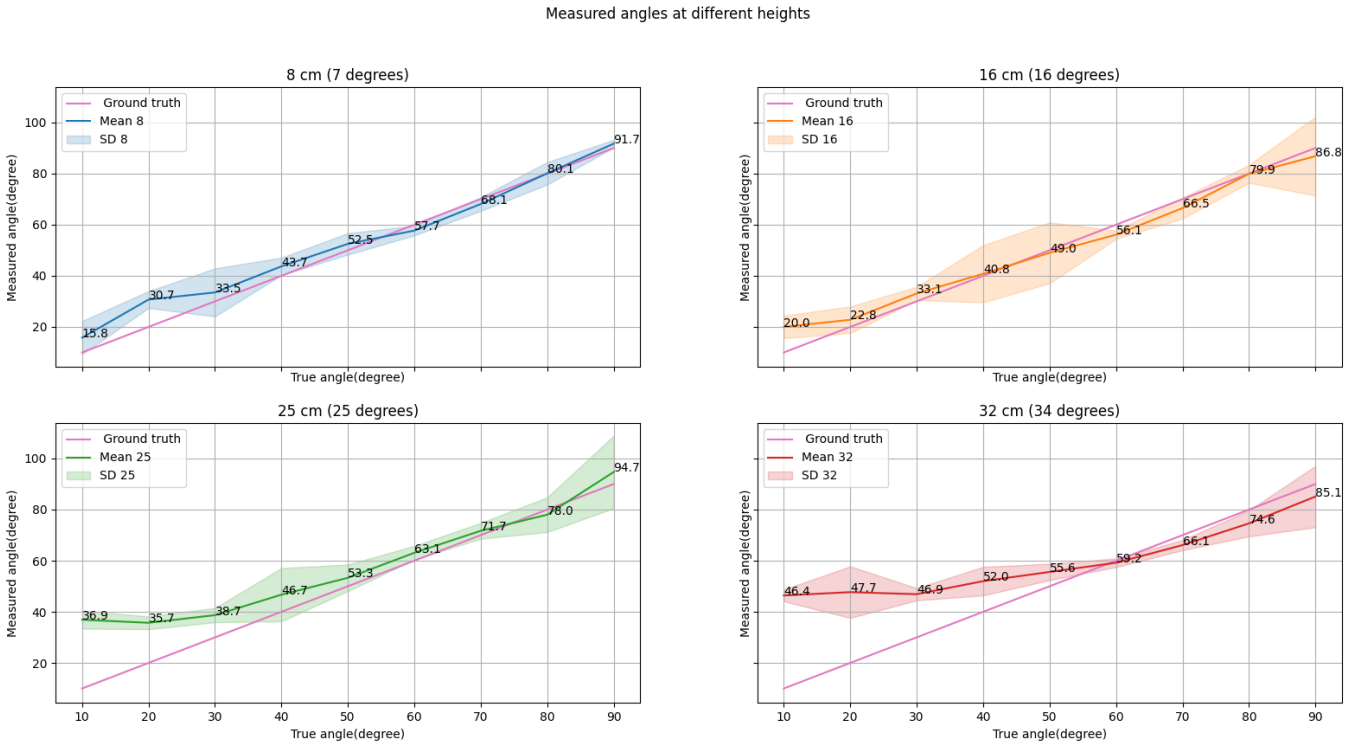

Fig. 38. The angle of arrival estimated by the UWB kit at by holding the distance in the azimuthal plane constant, and varying the height of node. The effective elevation angle corresponding to different heights can be calculated (mentioned in the brackets) to set the thresholds for operating in AoA mode).

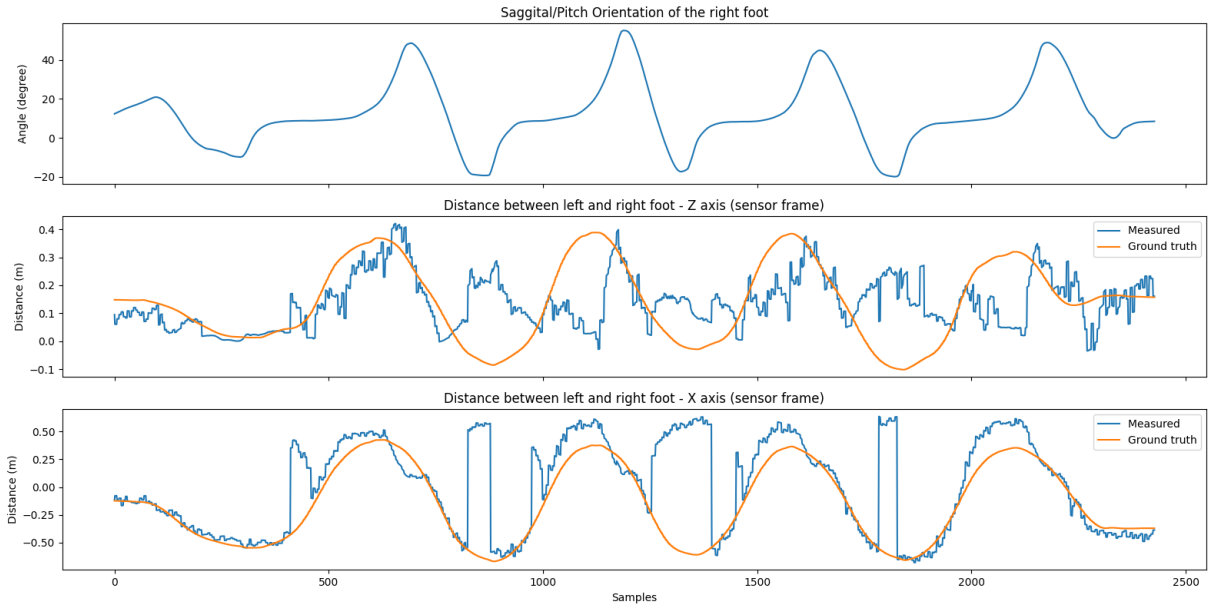

Fig. 39. The figure depicts the variation in the relative position of the feet in the X and Z axis (sensor frame), which has been calculated using the AoA and range measurements from the UWB kit. The tilt of the right foot (pitch,θ_y) is plotted on top for the identification of the onset of erroneous measurements). The pitch θ_y is calculated from the gyroscope measurements, which is further detailed in the Methodologies -Sensor Fusion section of the paper.

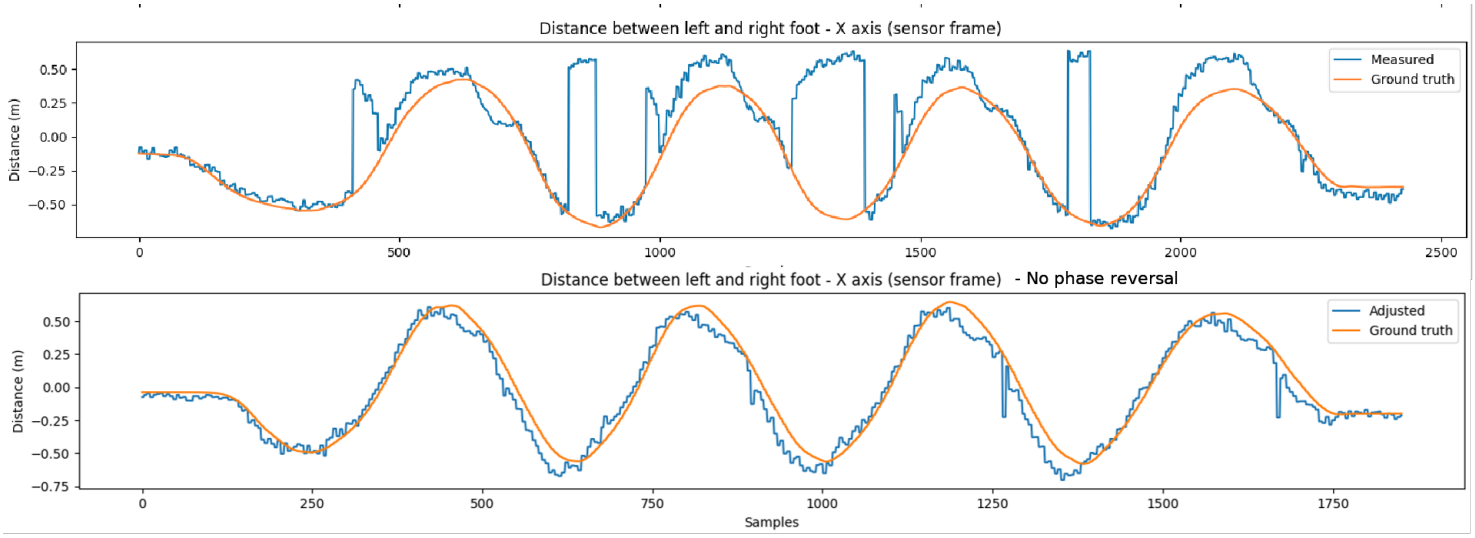

Fig. 40. This figure paints a picture on how the gait affects the AoA. Here, similar to figure 39, the range from the decawave kit is decomposed into its X axis component using the measured AoA. The subplot on top depicts a measurement where the Z distance (sensor frame) did not dip below zero. The bottom figure is extracted from a trial where the Z distance (sensor frame) was negative (i.e the leftmost foot was the right foot). The effect of this is the phase reversal in the AoA measurements.

| | - Magnitude operator.
$AoA_{noisemultiplier}$ - The coefficient for mapping.
$R_{noise,AoA}$ - Measurement noise for the AoA measurements.

In certain scenarios, increasing the measurement noise of the AoA measurements based on the AoA calculated from the filter states leads to worse results than when a constant measurement noise was used. This is attributed to the drift present in the system, which results in the computation of incorrect AoAs from the state variables. Any measurement noise for the measured AoA based on these measurements would lead to inappropriate measurement noises.

b) Distortions in the 25 to 35 cm band: Due to the non-deterministic nature of the phase measurements in the 30 to 35 cm bands, it is hard to model the bias in it. By switching to the ranging mode of operation, we still utilize the UWB data instead of discarding it. This switching is performed when the estimated range falls within a particular threshold (discussed below).

c) Elevation angle due to height differences and tilts: The bias due to the presence of an elevation angle is compensated by exploiting the estimated rotation in the sagittal plane and the UWB measurements as per equation 106. In addition, due to the possible errors in the state variables, an additional threshold based model (discussed below) is proposed.

Based on the analysis above, we erect certain thresholds within which the AoA data is used. In case of transgressions, we revert to the ranging data. The angle of arrival data is not utilized when the following conditions are satisfied:

a) AoA $< 10\& > 170°$ - This corresponds to the periphery where the chances of occlusion are high and when the difference in the height of the feet are maximum. In these scenarios, the AoA measurement is discarded.

b) $\theta_y < 0°$ or intuitively, the difference between position of left and right feet ¡0 - Corresponding to instances where the left foot is behind the right foot. As per the figure 39, whenever the inclination of the foot is below zero degrees, it indicates that the feet are in the heelstirke /pushoff phase. It is during these phases that the leftmost foot is the right foot. By implementing a threshold, the AoA measurements from the UWB kit in this stage is neglected. A θ_y based threshold is used, rather than the position of the feet, since the former does not drift as much.

c) $\theta_y > 25°$ corresponding to instances where the azimuthal AoA estimation deteriorates due to the influence of the tilt / perceived elevation. Note

Error	Error source	Threshold
Peripheral error	At the periphery, the AoA performance deteriorates due to an increase in the PDOA's uncertainty	AoA <15 & AoA >165 degrees
Phase reversal	When the leftmost foot is the right foot, due to the method by which the PDOA is calculated, phase is flipped (+ 75 becomes -75)	$\backslash\theta_y$ <0 degrees
Elevation angle bias	When an elevation angle is present (due to the tilt or height difference between the feet), the measured AoA in the azimuth has a bias.	$\backslash\theta_y$ <25 degrees or AoA bias compensation.

TABLE III

TABLE III : THE SOURCES OF ERROR AND BIASES IN THE AOA MEASUREMENTS, AND THE CORRESPONDING THRESHOLD USED TO IGNORE THE AOA MEASUREMENTS. IN THE THREE SENSORS LISTED, THE AOA MEASUREMENTS ARE IGNORED, THUS REVERTING TO THE UWB SENSORS RANGE MEASUREMENTS. IN THE 3RD SCENARIO, THE ELEVATION ANGLES CAN BE THRESHOLDED AS IN CASE OF AOA MODEL 2, OR IT CAN BE COMPENSATED FOR AS IN AOA MODEL 3.

that the threshold is higher than the 16° observed in the figure 38 due to our previous threshold on AoAs¡10° which would eliminate most of the erroneous values observed at $theta_y$ 25 °. All AoAs measured while exceeding this threshold is ignored. This is an alternate to the elevation angle bias compensation proposed in equation 106.

IX. APPENDIX VIII -2D REPRESENTATIONS OF THE AOA AND RANGE UPDATES

The figures related to this section are Figures 41 and 42. This section gives a clearer 2D view of the range updates uncertainity and the combination of the range and AoA updates uncertainities.

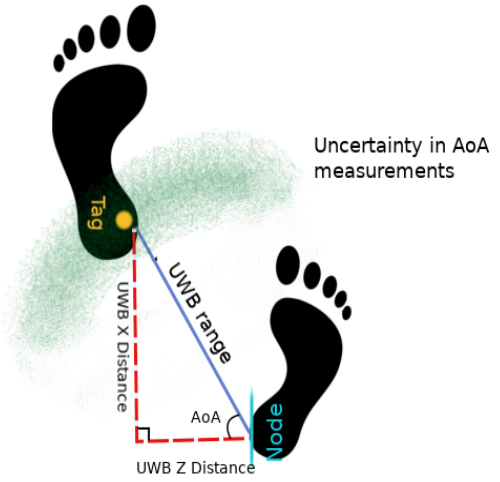

Fig. 41. A 2D representation of the uncertainty of the measured range combined with the measured AoA (hued green segmented toroid). A combination of the AoA and angle would result in the localization of the feet in a two dimensional plane.

X. APPENDIX IX - PERSPECTIVE SHIFT USING THE NODE AS THE REFERENCE FRAME

This appendix demonstrates how a tilt can be perceived as an elevation angle.Figures 44 and 43

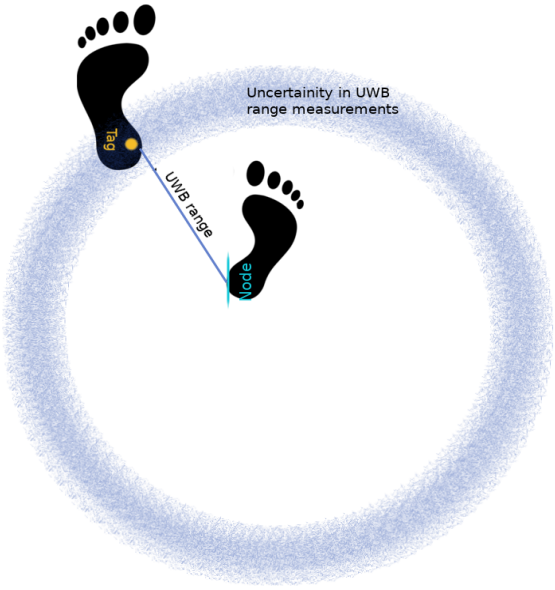

Fig. 42. A 2D representation of measured range uncertainty (Blue toroid). On a 2D plane, the uncertainty in the UWB range measurements is a toroid whose radius is the distance measured, and the uncertainty is depicted by the thinness of the toroid. While the AoA measured is in a 2D plane the range measured is 3D, leading to an additional uncertainty in the height/elevation.

XI. APPENDIX X - FILTER OUTPUT PLOTS

This section contains additional filter output plots.

A. The range computed from the filter which uses IMU, UWB range measurements (in-filter range bias compensation) and AoA measurements

This figure (fig 45 is the output acquired when the Filter 4 is run on 10

XII. APPENDIX XI - RANGE BIAS-OLD

Before the software bug was discovered, we assumed that the range bias experienced was due to an issue in the design of the hardware. This doubt was further compounded by the lack of literature discussing the utilization of the UWB device in sub 50 cm ranges.

Initially, the measured range bias showed a sharp downward inflection at ranges less than 30cms. This introduced an ambiguity in the distance measured. From Figure 46 it can

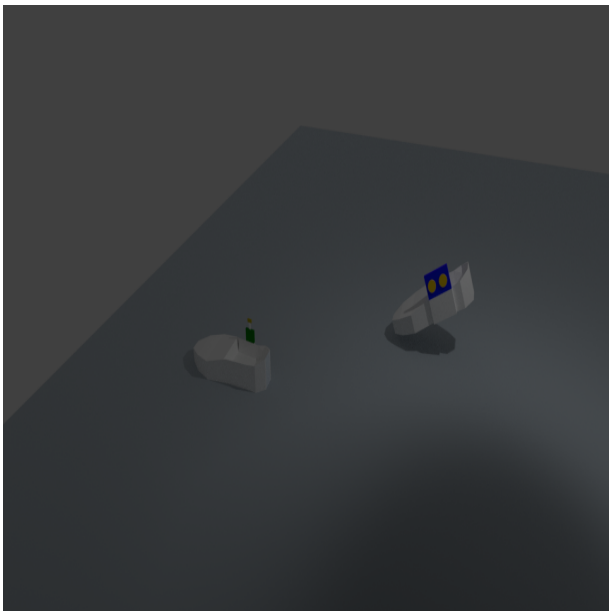

Fig. 43. Scenario:1 - A still of the gait where the node is elevated and tilted, and the tag is on the floor. Due to the tilt of the node, the node's plane of measurement would not be parallel with the plane of the ground.

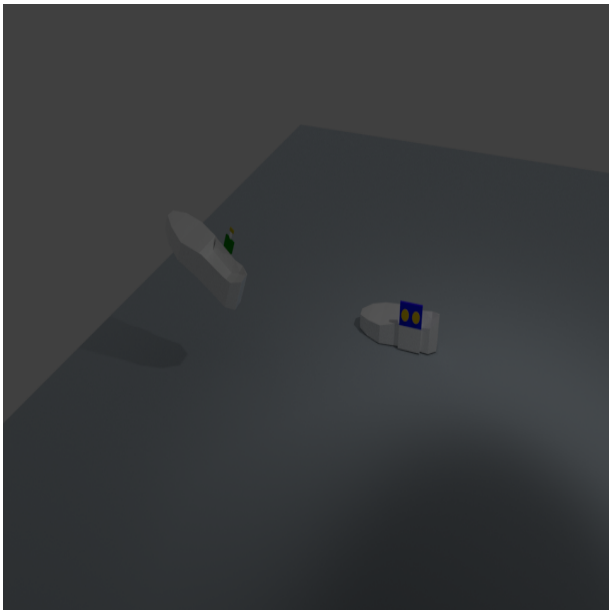

Fig. 44. Scenario 1 from the node's perspective.The same still from Figure 43, with the ground plane reoriented to make it parallel to the plane of the node in which the AoA is measured.

be inferred that for a measured distance of 20 cm the actual value could either be ˜15 cm or ˜50 cm. The measured distance could not be used further without any compensation.

This led to the devising of algorithms to tackle the nonlinearity - both internally and externally. The solutions tested out were:

1) Using the filters states to estimate the range and ignoring/ increasing the uncertainty of measurements from the UWB which were acquired below that range.
2) Using a Linear GAM model based on penalized b-splines to solve the problem.
3) Using an Interacting Multiple Model Kalman filter to tackle the issue.

A. Ignoring the sub 30cm readings

This is the simplest solution available. The V shaped inflection around 30 cm proved to be hard to compensate for. So the solution was to ignore it. This solution worked well in case of minimal drift in the IMUs. Unfortunately, as from 10, it can be seen that the IMUs are not that reliable as well for this thresholding purpose. This lead to runaway and cumulative errors in the system.

B. Using a GAM

A generalized additive model(GAM)[57] is a statistical regression model (can be used for classification as well) which utilized p-splines to perform a polynomial fit.It performs the polynomial fit of each feature used in the system and as the name suggests, it sums up all the resultant functions to model our system. In addition, there is a link function which enables it to conform to highly nonlinear curves. In case of a unity link function, the GAM model essentially becomes a linear sum of the underlying (usually)linear models.

A GAM can be described by:

$$l(E(Y)) = B + F1(x1) + F2(x2)\ldots\ldots\ldots + Fn(xn) \quad (110)$$

Where,

l = Link function (1 for a linear model)
E(Y) = Output model with to an exponential probability distribution
B = constant
F1....n = Random function with linear coefficients
X1....n= Variables

In our case, a linear model with the variables as X position and Y position calculated from the DecaWaves AoA and range was used. The model was fitted with 17 cubic b-splines. However, since the model was nonlinear, we fitted the model to the RSS calculated using the Friis formula [65] instead of the ground truth. This was then used to convert the RSS back into distance measured. The resultant was a compensation of the estimated range bias which was observed in the lower ranges, the efficacy of which is depicted by the figure48.

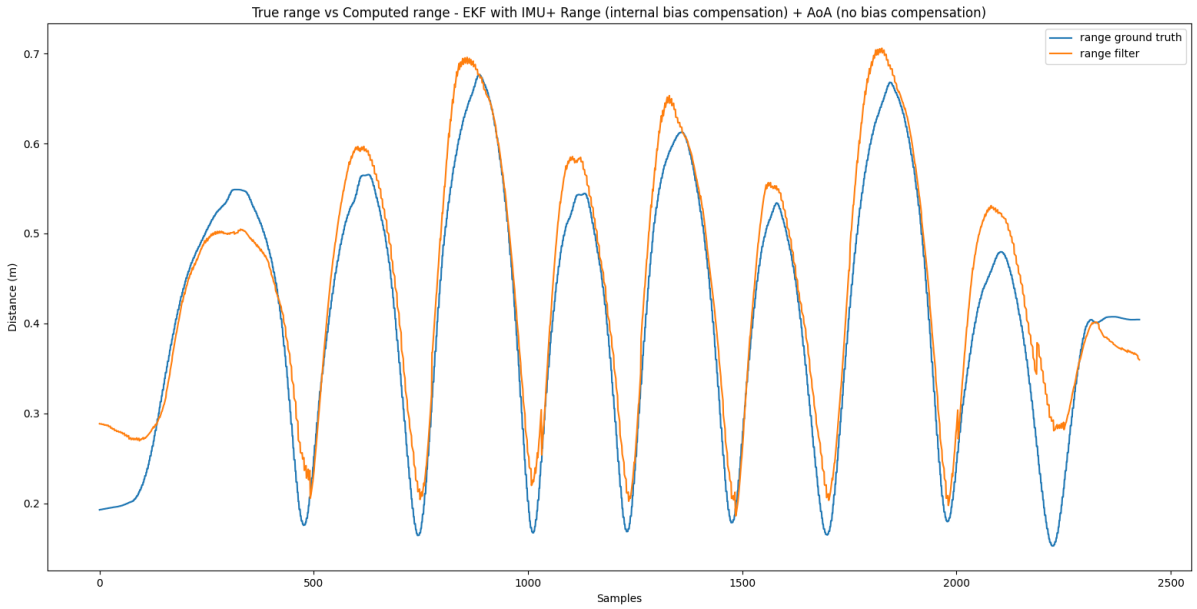

Fig. 45. Range computed from Filter 4 using UWB range, AoA measurements and IMU data: An overlay of the range computed from the filters estimates which is augmented using the UWB sensors range measurements(in-filter range bias model), and the AoA measurements (without bias compensation), against the ground truth). The pearson correlation is 0.93 for the range computed in this figure.

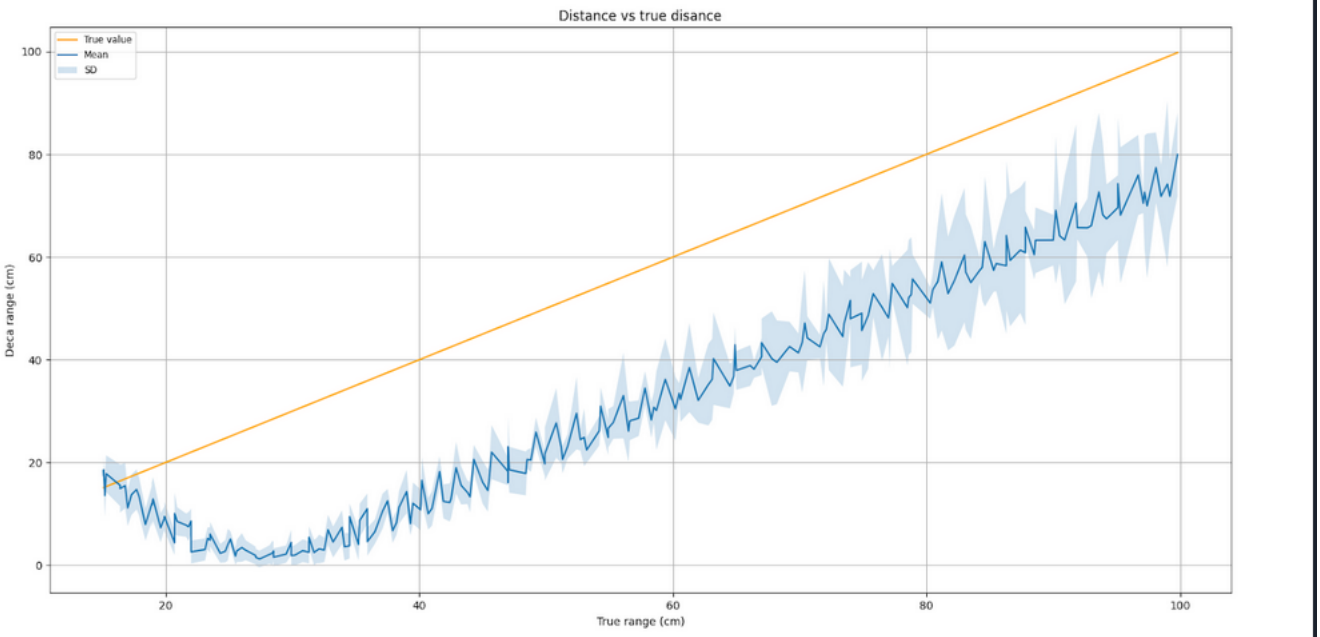

Fig. 46. The range measured by the DecaWave kit versus the ground truth. Notice the upward increment at distances below 30 cm

C. Piece-wise polynomial based

From the range bias graph shown in Figure 47 it can be observed that the range bias consist of two parts. A polynomial in the lower range (piece wise polynomial 1 - PW1) from 0 to 30 cm and a polynomial for the higher range from 30 cm to 1 m (piece wise polynomial 2 - PW2). Now the 5th degree polynomial can be further broken down into two 2^{nd} degree polynomials or a linear and a quadratic polynomial as shown

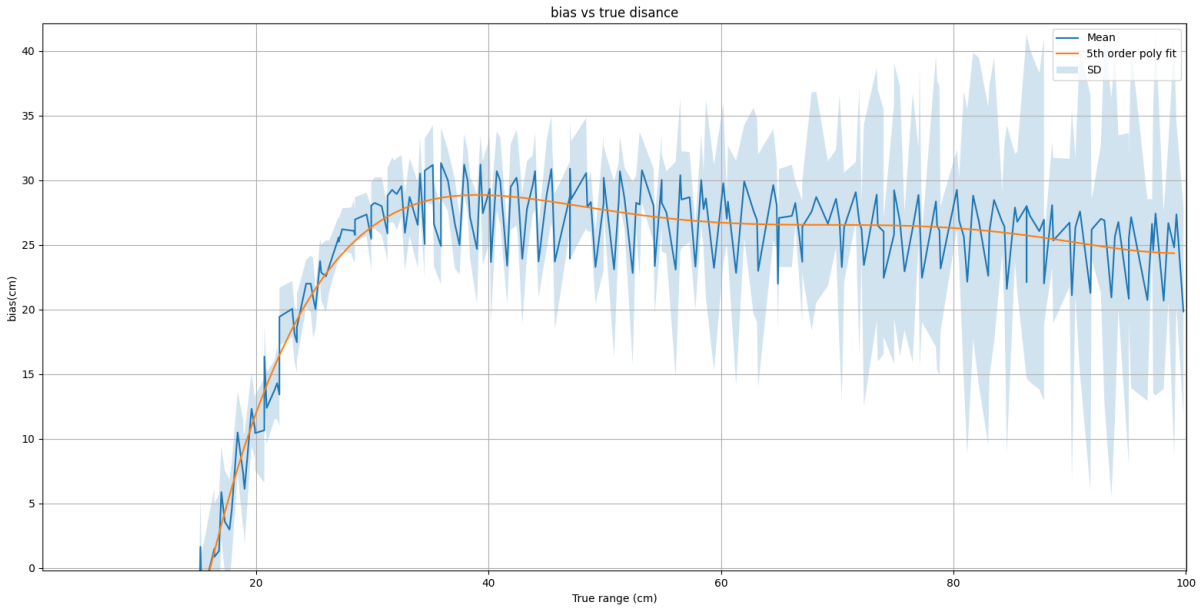

Fig. 47. The range bias previously measured using the DecWave kit. A polynomial fit of the range bias resulted in a 5th order polynomial (depicted by the orange line)

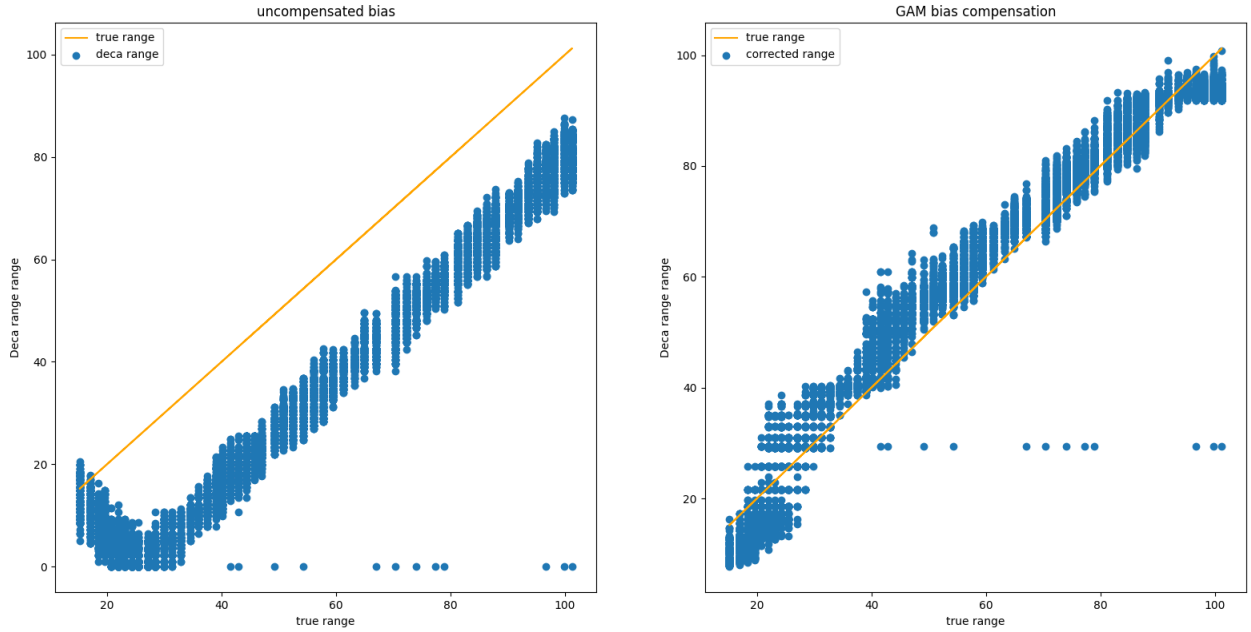

Fig. 48. The range bias before compensation with a GAM model, and after getting compensated by the GAM model as described above

in 49. These can be linearized easily and can be incorporated in the filter as a state variable.

Due to non-linearity in the propagation of the co-variances, a simple if-else statement cannot be used to switch out the state equation matrix. To circumvent this, we use two models in parallel, each running a piece-wise model to estimate the range bias. Since at each time instance, the actual model being used by the filter can change from one model to another, it

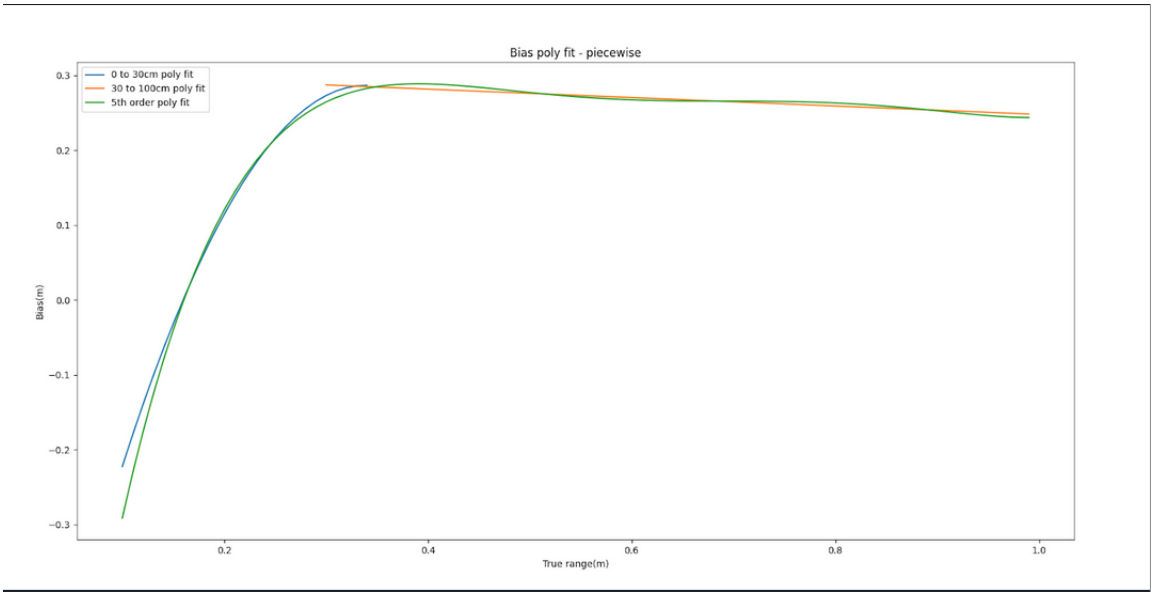

Fig. 49. The fifth order polynomial as showing in figure 47 split into 2 smaller order polynomials for the use in an IMM

would be necessary to propagate the two models from the current estimates of the two models. This leads to the branches growing exponentially, leading to an intractable solution. An alternative is to use a switching hidden state, propagated by Markov dynamics, to predict the posterior probabilities of each state occurring given the current states. Multiple possible states, based on the historical models can be fused into one using the Generalized Pesudo-Bayesian(GPB) algorithm. Using this hidden state probabilities, it is possible to find a Mixed state which is the weighted sum of the previous two states. This mixed state can now be propagated using the two models and based on the innovations and likelihood from the update section, the model probabilities can be found and can be used to weight the probability of the model being the current state. These probabilities weighted sum would give the current state estimate. This filtering approach using multiple models simultaneously is called the Interacting Multiple Model approach (IMM). Further details on the implementation and working of this model can be found in[66][67][68][69].

The workflow of this filter is charted in the following figure 50.

This filter was implemented and was successfully able to compensate for the bias. From the probability plots, it was apparent that the filter switched when the distance was sub 30 cm to the sub 30 cm model and used the supra 30 cm model in other cases. In addition, it was noticed that due to the weights being prescribed by the probability of each model, the filters output was the best possible weighted combination of each model which conforms to the observations rather than the output of the true model. Example: At 25cm, the model 1s probability, ideally should be 1 and model 2s probability should be 0. But from our observation, the assigned probabilities for each model are, say 0.85 and 0.15. While this gives a better result, we suspect that this might have potential stability issues without proper tuning in some scenarios.

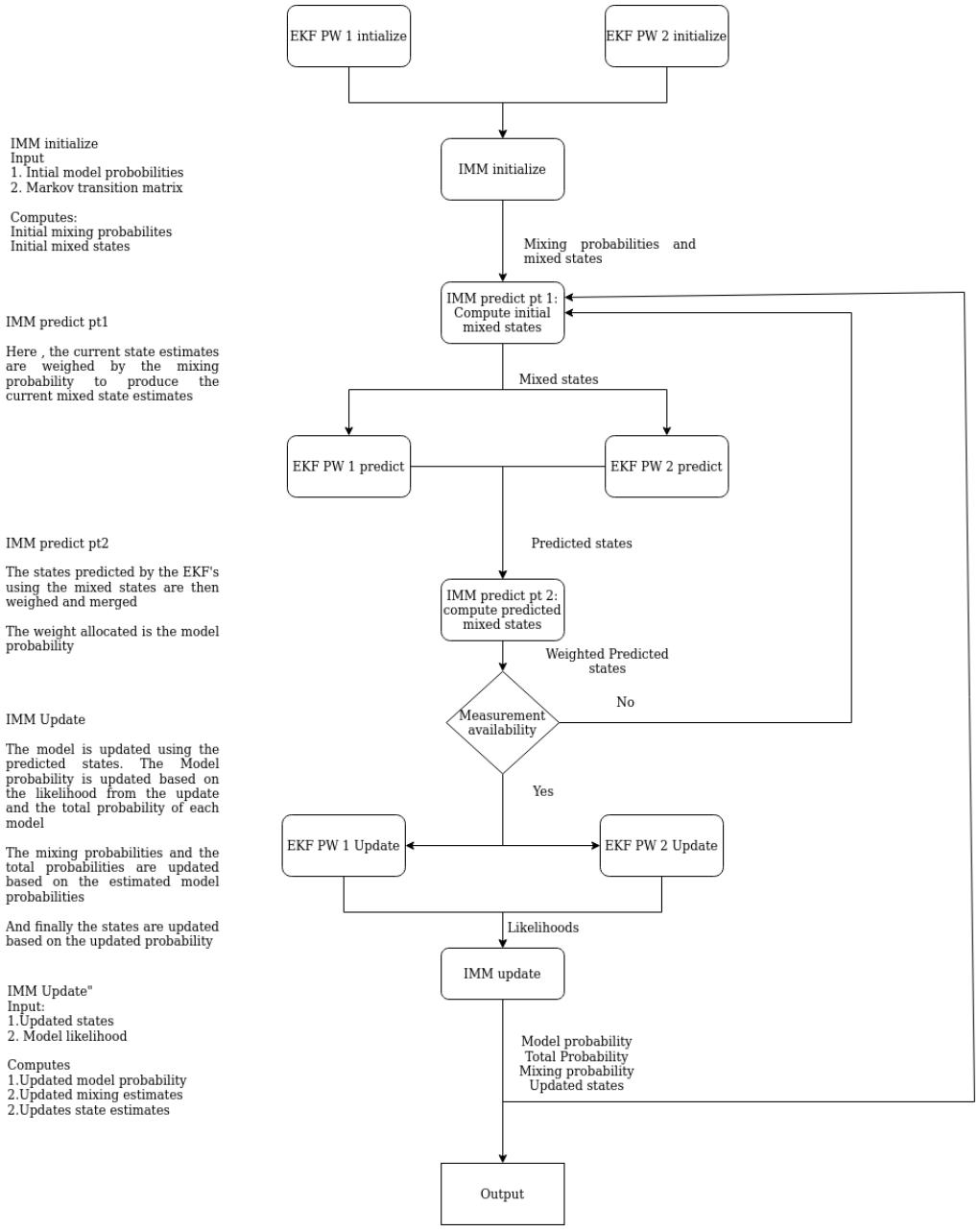

Fig. 50. The overall workflow of the IMM model.